KTH Land and Water
Resources Engineering

Analysis Of Lining Properties at Landfills Using Geophysical Methods — Case Study: Tveta (Sweden)

Michał Żywna

May 2011

TRITA-LWR Degree Project
ISSN 1651-064X
LWR-EX-11-11

Degree Project
Environmental Engineering
Department of Land and Water Resources Engineering
Royal Institute of Technology (KTH)
SE-100 44 STOCKHOLM, Sweden
Reference to this publication should be written as: Żywna, M (2011) Analysis Of Lining Properties at Landfills Using Geophysical Methods – Case Study: Tveta (Sweden) TRITA LWR Degree Project 11:11.

SUMMARY

Studieområdet är Tveta deponi i Södertälje kommun, 70 km från Stockholm. Sex prototyper med täckningsmaterial överlagrande en deponi har byggts på en sluttning med varierande lutning. Täckningsmaterialet består i allmänhet av sekundära material såsom aska från förbränningsanläggningar. Konstruktionen får inte överstiga vissa permeabilitetsgränser för att vara kommersiellt användbar. Vatteninfiltration har tidigare bestämts med lysimetrar som är monterade under ytan. Resultatet har visat en hög permeabilitet i ett av områdena (område 3). Syftet med denna studie har varit att kontrollera lysimeterresultaten, särskilt i område 3. Insamlade data avser att ge ökad information om konstruktionens täthet och uppbyggnad. Om infiltrationvägar kan identifieras ges förslag till förbättringar av konstruktionen.

Undersökningen har omfattat tre geofysiska metoder. Inducerad Polarisation (IP), DC elektriskt motstånd och markradar (GPR). Sådana mätningar är valda eftersom de är icke-förstörande, snabba och billiga att utföra. Sex områden har undersökts med totalt åtta profiler. Varje profil består av resistivitetmätning och GPR-undersökning med 250 MHz och 100 MHz antenner. Laddningsbarheten (IP-mätningar) har utförts endast längs en profil.

De geoelektriska mätningarna har bearbetats med Res2Dinv programvara. IP-mätningarna bedömdes ge god kontrast mellan avfall och täckmaterial, däremot var kontrasten mellan infiltrerat vatten och täckmaterialet dålig, varför sådana mätningar endast utfördes på en profil. GPR-data har bearbetats och filtrerats i RAMAC GroundVision programvara.

Läget av de åtta profilerna har bestämts med GPS-utrustning. Därefter är profilerna inritade på topografiska kartor från Tveta Återvinning. Höjdlägen längs profilerna har tagits från kartan inför modellering med Res2DInv. De modellerade profilerna med definierade longitud, latitud, höjd och resistivitet har därefter kombinerats till en pseudo-3-D-modell i Voxler programvara.

Infiltrationsvägar är inte synliga i IP-mätningarna troligtvis på grund av att joninnehållet i det inträngande vattnet är otillräckligt. Endast avfallshögen kan identifieras från laddningsbarhetsmätningarna. Signalerna som skickades från GPR-antennerna trängde bara några meter under markytan på grund av att den höga konduktiviteten ger en stor dämpning. Det är möjligt att med radarmätningar urskilja de olika täckskikten, korsande vägar med avvikande uppbyggnad och störande föremål såsom slangar och rör, däremot inte mindre mängder infiltrerande vatten. IP och GPR tycks således inte vara lämpliga referensmetoder för identifiering av infiltrerande vatten i denna miljö.

Generellt har vegetationsskiktet samt täta lager en högre resistivitet än täckskiktet och de dränerande lagren som är mer konduktiva. Resistiviteten sjunker genom de svårgenomträngliga lagren, vilka därmed tycks ha en god barriärfunktion. Den lägsta resistiviteten är uppmätt i område 3, vilket konfirmerar resultaten från lysimeterstudierna. Resistivitetavvikelser kan också ses i delar av områdena 4 och 6 där lysimeterstudier inte utförts. Täckningsskiktet har generellt en bra täckande funktion utom beträffande platån i område 3 där lutningen är minimal och vattenflödet litet. Dessutom finns zoner av låg resistivitet i ytlagren även nära topografiska brytningspunkter där täckningsskiktet troligtvis blivit deformerat genom masstransport neråt. Förhöjd konduktivitet kan också uppkomma lokalt i ytan där vatten ackumulerats ovan täckningslagret som har en betydligt lägre genomsläpplighet än det översta vegetationslagret.

De förbättringar av täckningsskiktet som föreslås är därför en generellt ökad tjocklek på skiktet, något flackare lutning och eventuellt en modifierad sammansättning som minskar risken för sprickbildningar och masstransport. Geoelektriska mätningar har givit god information om läckvägar och täckningsproblem varför sådana mätningar kan rekommenderas för funktionskontroll. IP-mätningar och GPR-mätningar har dock inte givit tolkningsbara resultat beträffande täckningsskiktets egenskaper.

ACKNOWLEDGEMENTS

My most profound gratitude goes to my thesis advisor Bosse Olofsson for his inspiration, guidance and consultations. Mr Olofsson provided necessary geophysical equipment and skilled me how to properly use it, process collected data and correctly interpret them. Despite numerous duties Bosse always had time to answer my questions. In this place I would like to apologize him for any inconveniences and delay in finishing this thesis.

I would like to thank David Gustafsson from KTH for the support with GPR equipment and data processing.

Special gratitude goes to Telge Återvinning staff, especially Igor Travar who provided topographic map and lysimeter records of the study area.

I am grateful to Sabrina Pearson from Technical Support of Golden Software, Inc. for online consultations. Processing of resistivity profiles in Voxler software would not be possible without her feedback.

Final thanks go to my family for their endless encouragement and support.

Gdynia, May 2011

Michał Żywna

TABLE OF CONTENT

ABBREVIATIONS AND SYMBOLS

2D	**TWO-DIMENSIONAL**
3D	**THREE-DIMENSIONAL**
AC	**ALTERNATIVE CURRENT**
BOD	**BIOLOGICAL OXYGEN DEMAND**
CLR	**CONFIDENCE LEVEL RATE**
COD	**CHEMICAL OXYGEN DEMAND**
CRU	**CENTRAL RECORDING UNIT**
CVES	**CONTINUED VERTICAL ELECTRIC SOUNDING**
DC	**DIRECT CURRENT**
EP	**ELECTRICAL PROFILING**
ERI	**ELECTRICAL RESISTIVITY IMAGING**
ERT	**ELECTRICAL RESISTIVITY TOMOGRAPHY**
EU	**EUROPEAN UNION**
GPR	**GROUND PENETRATING RADAR**
GPS	**GLOBAL POSITIONING SYSTEM**
IP	**INDUCED POLARIZATION**
pH	**POTENTIAL HYDROGEN**
RMS	**ROOT MEAN SQUARE**
SDR	**STANDARD DEVIATION RATE**
VES	**VERTICAL ELECTRIC SOUNDING**
VLF	**VERY LOW FREQUENCY**

ABSTRACT

Recently established EU environmental legislation obliged Sweden to close many landfills until year 2020. Such an operation requires a lot of inexpensive and water resistant coverage materials. Six prototypes of linings were constructed at Tveta landfill. Built coverage consisted mainly of residual products such as compost, sludge, fly and bottom ash. Between 2004 and 2007 water permeability through tested coverage was well below the maximum limit for non-hazardous waste. However, recent lysimeter records indicated increased permeability through the constructed linings. Readings of water infiltration were verified. Direct current (DC) resistivity, induced polarization (IP) and ground penetrating radar (GPR) were the methods applied in the research. The data was processed to present resistivity distribution in 2D pseudo-sections and 3D model. Resistivity measurements confirmed increased conductivity at the area with highest lysimeter readings. Unfortunately, GPR and IP output could not be used as reference information for DC resistivity readings. Constructed prototypes seemed to be suitable for coverage lining. Leakage was probably a result of minor mass transport along the slopes of the waste pile. It was recommended to prepare additional DC resistivity measurements to verify correctness of the processed 2D pseudo-sections and 3D model.

Key words: Landfill coverage; Direct current (DC) resistivity; Leachate; Ash and residue material; Waste deposit; Lysimeters.

1. INTRODUCTION

This chapter explains why landfill covering has recently become such an important issue and why coverage prototype was constructed at Tveta. Thesis background is followed by description of the study area. The next subsection, literature study, contains general information concerning landfill surveying, presentation of eight case-studies, short recapitulation of studied literature and motivation for the thesis research. Finally, investigated problem is introduced and the aim of this thesis is stated.

1.1 Background

Following EU directives, Swedish waste disposal legislation has recently become stricter. The majority of Swedish landfills do not meet the new regulations and have to be closed down by the year 2020. Therefore, there is a huge demand on a material for the final coverage (Tham et al, 2003; Travar et al, 2005; Travar et al, 2007; Tham & Andreas, 2008; Travar et al, 2009). According to Tham & Andreas (2008), 100 million tons of coverage material is required until 2020. The ideal substance should be inexpensive and abundant. Residues from waste incineration and wastewater treatment meet such requirements.

A research concerning feasibility of secondary materials for landfill covering has been performed by Telge AB in cooperation with Luleå Technical University. Six prototypes, with different structure, were tested on a four hectare area at Tveta landfill. The covers were constructed on a slope with varied steepness in order to investigate different scenarios. Water permeability through each of six tested areas was determined by ten lysimeters which were randomly located. More detailed information about this study was presented in Appendix 1 (Tham & Andreas, 2008).

1.2 Description of the study area

The study area is situated at the eastern slope of Tveta landfill which is owned by Telge Återvinning (Fig. 1) (Jernberg & Rosenqvist, 2002; Ljungberg & Rodriguez, 2006; Tham, 2006). It is located 7 km in the south-west direction from Södertalje community, Sweden. The altitude of the landfill is 40-90 meters above the sea level and its location is 500 m in the east

Fig. 1 Plane view on the landfill (Tham & Andreas, 2008).

direction from Lake Vällingen. The lake is a water protection area and serves as a water reservoir for three local communities. The landfill is built on a relatively thick layer of clay which is overlaying till and hard rock. Predominant rock types in the area are sediment-gneiss and gneiss-granite. Such rocks are characterized by low permeability (Ljungberg & Rodriguez, 2006).

Telge Återvinning accepts industrial sludge, household, business and construction waste. According to Tham & Andreas (2008), 200 000 tons of waste were brought to Tveta landfill in 2006 and 95 % of them were recycled. The household waste has been disposed at the eastern slope of the landfill until 2001 (Tham & Andreas, 2008).

The study area will be investigated in this thesis with non-invasive technology to assess water permeability of the constructed coverage.

1.3 Literature Study

Literature review contains general information about landfill surveying, followed by description of eight case studies thematically similar to problem investigated in this thesis. The last two parts contain summary to introduced publications and motivation to research performed at Tveta. Cited articles present current situation in geophysical mapping of landfills and were taken into account in selection of the thesis methodology.

1.3.1 General Information

Landfills have a heterogeneous structure due to random origins of the disposed waste. Irregular content makes waste pile a challenging target for geophysical measurements. One-dimensional surveys are insufficient to comprehensively study heterogeneous character of landfills. 2D imaging and 3D modelling is preferred (Hermozilha et al, 2010). Automation of data acquisition and development of 2D and 3D inversion software increased popularity of the geophysical methods and data visualization (Aristodemou & Thomas-Betts, 2000).

Landfill sealing often becomes fractured or eroded (Carpenter et al, 1991; Meju, 2000). Coverage cracking can lead to release of gases and formation of leachate from the infiltrated water. Periodic geophysical surveys can act as a non-invasive monitoring of the landfill cover to identify eventual discontinuities or thinned areas (Carpenter et al, 1991).

Geological properties, waste disposal and covering process are usually poorly documented (Martinho & Almeida, 2006; Hermozilha et al, 2010). Thus, inexpensive and time-saving methods such as the geophysical surveys are required to provide information about subsurface properties (Martinho & Almeida, 2006). Waste disposal is usually disordered, environmental regulations are not respected and techniques for proper landfill management are ignored (Mondelli et al, 2007; Reyes-López et al, 2008). Sweden is an example of a country where landfill protection is an important issue. Since 2002 all landfills in Sweden are obliged to prepare a plan including procedures for landfill closure or continued exploration. The document must contain solutions reducing leakage and the infiltration rate. The annual limit of water infiltration (50 mm) must be fulfilled to close a landfill (Leroux et al, 2007).

Landfill thickness generally ranges from 3 m to 20 m. However, sites even 30 m deep are known to exist. Waste in old landfills is less compacted than at modern sites. Thus, permeability is higher and propagation of the signal emitted during geophysical survey is lower (Soupios et al, 2007). Disposed matter is gradually decomposed and changes volume (Meju, 2000; Soupios et al, 2007). Older landfills also lack geological and artificial bottom barriers (Soupios et al, 2007). Fluids generated from landfills are generally acidic. The pH tends to increase with landfill age while the BOD/COD content decreases with time. Leachate transport is slow, unsteady, non-uniform and sometimes discontinuous (Meju, 2000).

Leachate is a liquid formed from decomposed waste, can contain groundwater and percolated rainwater. Ion concentration in leachate from older landfills should be lower than from modern sites due to higher permeability of a waste pile (Meju, 2000). Concentration of chloride ions is an example of indicator for leachate presence in groundwater (Ahmed & Sulaiman, 2001). Contamination problems are particularly dangerous for the landfills located in abandoned gravel pits which often are situated below groundwater table (Soupios et al, 2007).

Direct current (DC) resistivity method is preferred for inorganic pollutants which increase liquid conductivity due to presence of dissolved salts (Aristodemou & Thomas-Betts, 2000; Martinho & Almeida, 2006). Other types of pollutants, such as the hydrocarbons, can reduce leachate conductivity (Aristodemou & Thomas-Betts, 2000). Recent improvements in geophysical techniques, like spectral induced

polarization, allowed identification of organic pollutants as well (Aristodemou & Thomas-Betts, 2000; Hermozilha et al, 2010).

Electric resistivity was invented in early 1900s but has not been widely used until 1970s when computers became available to process and analyze data (Al-Tarazi et al, 2006). Geoelectrical methods are the most common geophysical techniques in conductivity measurements (Mota et al, 2004). Resistivity surveying consists of vertical electric sounding (VES) and electric profiling (EP). Combination of VES and EP is preferred for landfill surveying due to heterogeneous character of a waste pile in horizontal and vertical direction (Mondelli et al, 2007).

2D resistivity imaging has been developed quite recently and it is currently almost as quick as 1D surveying (Ahmed & Sulaiman, 2001; Soupios et al, 2007). Two-dimensional imaging assumes low variation of the third dimension. 3D modelling is not yet routinely carried because it involves larger amount of equipment and more data processing. For larger data sets this method is still under consideration (Soupios et al, 2007).

2D imaging involves inversion of apparent resistivity into true resistivity (Ahmed & Sulaiman, 2001). Subsurface is divided into small rectangles and software adjusts values in the cells, minimizing difference between calculated and the apparent resistivity. The quality of fit is called route mean square (RMS) error, expressed in percents (Soupios et al, 2007).

Induced polarization (IP) detects decay of applied voltage as a function of time (Telford, 1990). Combination of IP and resistivity can help to distinguish fine particles from coarse grained materials if information about their nature is known and saturation levels do not complicate measurements (Leroux, 2007). Most coarse-grained materials have higher resistivity than finer if not saturated with salt water. In example, combination of polarization and resistivity measurements facilitates distinction of clay from sand containing salt water. Both demonstrate similar, low resistivity. However, clays in contrary to sand show high chargeability (Abu-Zeid et al, 2004; Martinho & Almeida, 2006).

Ground penetrating radar (GPR) method is based on propagation of electromagnetic waves in the ground, with frequency between 1 MHz and 1000 MHz (Pujari et al, 2007). GPR is the most suitable geophysical method under ideal conditions. Old landfills are more demanding targets. Loose fill poorly propagates energy, clayey horizons limit emission of radar signal (Meju, 2000). Electromagnetic methods are also oversensitive to metallic objects, very common on landfills. Such obstacles often discard electromagnetic methods from landfill surveying (Leroux et al, 2007).

The map received from geophysical survey serves as a guide in a primary phase. Recorded anomalies can be subsequently investigated with invasive methods such as monitoring wells, standard penetration tests or cone penetration tests (Leroux et al, 2007; Mondelli et al, 2007). Such a combination saves money, time and eliminates ambiguity of geophysical data (Pujari et al, 2007; Hermozilha et al, 2010). Integration of two or more geophysical methods is usually done to improve data interpretation (Djadia et al, 2010). Electric and electromagnetic methods are the most popular geophysical techniques (Meju, 2000). Geotechnical data provides reliable information but only from point sources and in one dimension. This is insufficient for surveying of a heterogeneous waste pile.

Following issues can be investigated using geophysical methods: bedrock depth, subsurface discontinuities (fractures, cavities), changes in soil texture, structure of a waste pile (boundaries, content), depth of groundwater level, paths of groundwater flow, contamination flow in soil and groundwater (Mota et al, 2004; Al-Tarazi et al, 2006; Mondelli et al, 2007).

1.3.2 Case Study 1 — Harlov, Sweden

The study area was landfill in Harlov, Southern Sweden. Part of the site has been sealed with a cover. The landfill has been in operation from 1950s till 2002. Small river Helge flew next to the Harlov landfill. The waste was disposed on a natural ground which consisted of peat, till and clay. Such a base material had good insulating properties but due to a river proximity large fraction of the landfill was permanently saturated with water. The site has been divided into older, eastern part which was fully sealed and western part which was covered with various materials without precise recording of components.

Determination of coverage structure and thickness became necessary to fulfill permeability limit as stricter environmental law has been established. Resistivity and chargeability measurements were taken to investigate sealing properties and plan efficient reclamation work. The survey has been divided into two stages and was accompanied with auger drillings and topographic measurements.

Auger drillings reached the waste pile at 0.5-2 m depth. Various cover materials, such as gravel, sand, bricks, sludge and lime were identified as coverage components. The waste pile was so heterogeneous that 31 drillings were insufficient to provide a representative map.

Geoelectrical data was processed in Res2Dinv software. Magnitude of values was realistic and pseudo-sections had smooth appearance so quality of raw data was good.

In the first phase of geoelectrical measurements, taken at the eastern part, two layers with different properties were identified. The upper layer with high resistivity and low chargeability was attributed to covering soil material, probably medium to coarse-grained. The lower layer with high both conductivity and chargeability was assigned to a waste pile. Zone with intermediate chargeability and resistivity was also attributed to a waste pile but of different composition. Part of the cover with a low resistivity and very weak chargeability was classified as clay. The bottom of landfill could not be identified neither from 2D images nor from pseudo-sections combined into a 3D view. The depth of resistivity surveying was insufficient or contrast between the waste pile and soil saturated with leachate was too weak. Permeable zones with coarse filling or low thickness were identified. Outcomes from the first phase were taken into account to improve cover construction.

Geoelectrical survey taken in the second phase, at the western part, denoted different vertical stratification of landfill than in the first phase. The uppermost layer, attributed to clay cover, was conductive and not chargeable. The second layer had higher resistivity and mixed chargeability caused by strong heterogeneity. The zone below clay cover could be attributed to coarser covering material mixed with waste. High chargeability was typical for waste. The lowest zone had high both conductivity and chargeability which were typical for a waste pile. The uppermost clay cover could be easily identified along all profiles. Thickness of clay at the slopes was insufficient and required improvement. As in the first phase of the survey, landfill bottom could not be identified.

Combination of induced polarization and resistivity imaging provided useful information about waste pile and coverage properties. The lining and waste pile were resolved. Fine clay cover was distinguished from coarser sealing material. The uncertainties were caused by limited penetration depth and insufficient reference data. More covering material was added to existing lining but only at selected locations and at suggested amount, saving time and money. Geophysical survey could be used in future to monitor coverage permeability and indicate zones which require reparation (Leroux et al, 2007).

1.3.3 Case Study 2 — Illhavo, NW Portugal

The study area has served as municipal landfill for over 30 years and was closed in 1999. The waste was disposed on porous and permeable gravel and sands. Thickness of the waste pile was estimated as approximately 8 m. After closure the landfill was covered with liner and 10-20 cm thick sand layer.

The aim of this study was investigation of landfill properties such as structure, thickness, boundaries and sealing effectiveness. Furthermore, migration of contamination plume was evaluated. The survey consisted of 2D resistivity measurements and 3D ground penetrating radar (GPR). GPS coordinates were added for locating purposes. Measurements, taken at the expected location of contamination plume, were compared with studies done few years earlier. The data was also verified with boreholes drilled before landfill closure.

GPR survey was taken to investigate time evolution of leachate contamination and structure of the waste pile in 3D. Two series were made, containing 139 and 14 profiles. The data was processed in ReflexW software.

Quick GPR survey was taken to compare contamination spread with data taken from 1999. It was noted that the plume was expanding to the north so the landfill was still leaking and polluting local aquifers. The GPR graphic profiles correlated well with general geology of the site.

From longer, 3D GPR survey it was possible to identify coverage discontinuity zones, determine cover thickness and distinguish layer of waste saturated with fluid from other type of waste.

Resistivity measurements were made with dipole-dipole electrode array which had good penetration depth at robust lateral sensitivity. Coarse imaging, with large electrode spacing, was done to determine waste pile thickness, landfill cover and detect eventual leachate pathways through landfill bottom. Finer imaging provided information about waste pile structure, landfill heterogeneity and denoted diffusion pathways. The data was processed in Res2Dinv

software. The root mean square (RMS) error at 6 iterations was below 20.4 %.

Resistivity pseudo-sections defined cover layer as highly resistive and indicated large resistivity variation inside the waste pile caused by strong heterogeneity. Resistivity increase at the level of 8-10 m below surface was attributed to landfill bottom. The cover was characterized as discontinuous in some places. Fracturing of base material was noted as well. Coverage permeability would lead to rainfall infiltration and later leachate migration through cracks in bedrock.

Combination of GPR and resistivity data provided information about landfill structure. Coverage, lateral discontinuity and collapse zones were identified. Such information was useful in coping with rainfall infiltration and later leachate migration. Zones with high leachate content were identified due to conductivity variations and attenuation strength. Both methods denoted landfill bottom with an aid of geological information. According to geophysical measurements, landfill thickness was estimated as 7-10 m which was in agreement with 8 m value taken from the borehole logs. Geophysical methods indicated that the base material was not protected and contained channels for leachate migration. The nature of fluids inside the waste pile was not studied and it could be done later with seismic methods or multi-frequency GPR survey (Hermozilha et al, 2010).

1.3.4 Case Study 3 — Rio Claro, SE Brazil

The study area was situated approximately 170 km from Sao Paulo. The base material over the landfill consisted of two formations: upper Rio Claro and lower Coumbatai. Rio Claro consisted of consolidated sand with clay lenses. Coumbatai, present at the depth of 13 m, contained mainly clay and silt with compact shale and the bottom.

Geophysical measurements were taken at the landfill and surroundings to provide information about contaminant extension, landfill bottom, groundwater table and stratigraphy outside the landfill. The survey consisted of eight ground penetrating radar (GPR) profiles and six vertical electric soundings (VES).

GPR measurements were taken with 50 MHz and 100 MHz antennas. Six profiles were taken inside and two outside the landfill. GPR data was processed in GRADIX software. Interpretation of GPR profiles was based on available geological information and borehole data.

The GPR outcome denoted contaminant migration from landfill to neighbouring zones through pore spaces, caused by elevation difference. Groundwater contamination was attributed to zones where emitted signal was attenuated. Continuous reflection was classified as groundwater table. The lower reflection of emitted signal was attributed to interface between two base material formations: upper Rio Claro and lower Coumbatai. Contamination was denoted at profile taken 20 m from landfill border. No contamination was recorded from the GPR profile taken 100 m from landfill border.

Four VES measurements were made within the site while two soundings took place outside landfill borders. Electrodes were arranged in Schlumberger array, collected data was inverted in Res1X1P software. VES measurements within the landfill indicated a very conductive horizon attributed to contamination layer. The landfill bottom was between 11 m and 15 m. No contamination was noted outside the landfill. The groundwater table and contact zone between Rio Claro and Coumbatai formations were denoted.

GPR survey detected contaminant migration from the waste pile at the short distance away from the landfill. No contamination was recorded 100 m from site. Attenuation of emitted energy was classified as zones where leachate reached groundwater. VES measurements at the site denoted layer saturated with leachate and landfill bottom. Resistivity soundings outside the landfill resolved groundwater table and contact zone between two base material formations. The results of GPR and VES surveys were in a good correlation with local geology and borehole data (Porsani et al, 2004).

1.3.5 Case Study 4 — Chania, Greece

The Greek case study was located in Akrotiri Peninsula, 12 km from Chania city, on the Creete Island. The municipal landfill was built in Kouroupitos gorge which had a maximum depth of 40 m. The area used to be an uncontrolled landfill, opened in 1966. Karst depressions were frequent phenomena in the study area. Limestones covered with layer of weathered clay formed local geological characteristic. The area lacked any historical information or documents related to the landfill base.

The research concerned three issues: prospect of resistivity imaging to detect near-surface cavities in a limestone-kartsic environment; evaluation of hydrogeological, geological and geotechnical feasibility of suggested areas for landfilling; investigation and detailed description of present landfill to suggest efficient leachate barrier. Surveying was divided into 4 subareas and consisted of 7 resistivity profiles accompanied with 8 ambient noise measurements. Three profiles were verified with four boreholes.

Dipole-dipole array with 2-5 m electrode spacing was selected for geolelectrical measurements. Penetration depth was 30 m. Apparent resistivity data was processed in Res2Dinv and 2DINVSCR software. The root mean square (RMS) error varied from 3 % to 25 % which was a large spread, probably due to heterogeneous character of the waste pile and high contrast with underlain bedrock.

One profile was taken in area 1 to verify presence of voids and investigate their spatial distribution. High resistivity anomaly was attributed to karstic void while high conductivity anomaly was assigned to the waste pile.

One profile, passing through two boreholes, was taken in area 2 to locate eventual leakages. The area was located downhill to the site so was vulnerable for plume migration. Two anomalies were recorded. Anomaly of high resistivity corresponded to karstic cave. This was a useful information because tanks for leachate collection were planned to be set above detected cave. Construction could crash due to weight of tanks. Anomaly of high conductivity was regarded as leachate. Resistivity pseudo-section was in a good correlation with borehole data and local geology.

Three resistivity profiles were taken in area 3. Recorded conductivity anomaly corresponded to waste deposited in gorge. Pseudo 3D model was processed to estimate volume of collected waste. Strong contrast between waste pile and underlain bedrock enabled quantification of waste to be removed.

Two profiles were taken at area 4 which was considered as future landfill. Processed pseudo-sections displayed almost homogeneous subsurface, consisting of limestone and marly limestone.

The study area was comprehensively mapped, resistivity images were in a good agreement with borehole logs. The number of excavations was reduced to zones where anomalies were recorded, saving time and money. The 3D model of deposited waste was useful to finalize many actions such as remediation process. Ambient noise measurements overlapped with resistivity images, improving interpretation of resistivity anomalies. Applied methods could be successfully used to detect karstic voids (Soupios et al, 2007).

1.3.6 Case Study 5 — Haifa, Israel

The study area, Har HaAshpaa landfill, was located in the coastline part of Haifa city, Northern Israel. The landfill has been in use since 1944 when waste was uncontrollably disposed by British Army. Since the military documents disappeared site topography became unknown.

The aim of this study was to define a border between water-saturated clay and overlaid leachate-saturated waste, identify landfill bottom and assess leachate content. This was a challenge because electrical resistivity of water-saturated clay and leachate were very similar. The landfill was close to Mediterranean Sea so clay could be saturated with salt water which had high ion content as leachate had. Electrical resistivity imaging (ERI) technique was applied.

The survey consisted of ten profiles with length 150-420 m and electrode spacing 5-6 m. Collected data was inverted into true resistivity pseudo-sections with AGI Earth Imager 2D software. The root mean square (RMS) error ranged between 2.5 % and 5 % so measurements quality was high.

95 % of collected data had resistivity below 450 Ωm. The upper layer of landfill had resistivity between 5 Ωm and 30 Ωm (Fig. 2) which was typical for municipal waste. The resistivity at lower depths, between 0.9 Ωm and 5 Ωm (Fig. 2), corresponded to leachate and clay saturated with salt water. Precise border between leachate and clay could not be found from visual interpretation of pseudo-sections.

Statistical analysis of the whole data set denoted that alteration of standard deviation could be divided into 3 groups: upper at 25 m to 31 m depth, intermediate at −2 m to 25 m and lower at −2 m to −21 m depth (Fig. 3). Two parameters: standard deviation rate (SDR) and confidence level rate (CLR) were introduced to quantify standard deviation and confidence level changes. The maximum values of SDR and CLR were recorded at the depth of −2.5 m. SDR and CLR extremes corresponded to maximum difference of properties between the waste pile and underlying soil.

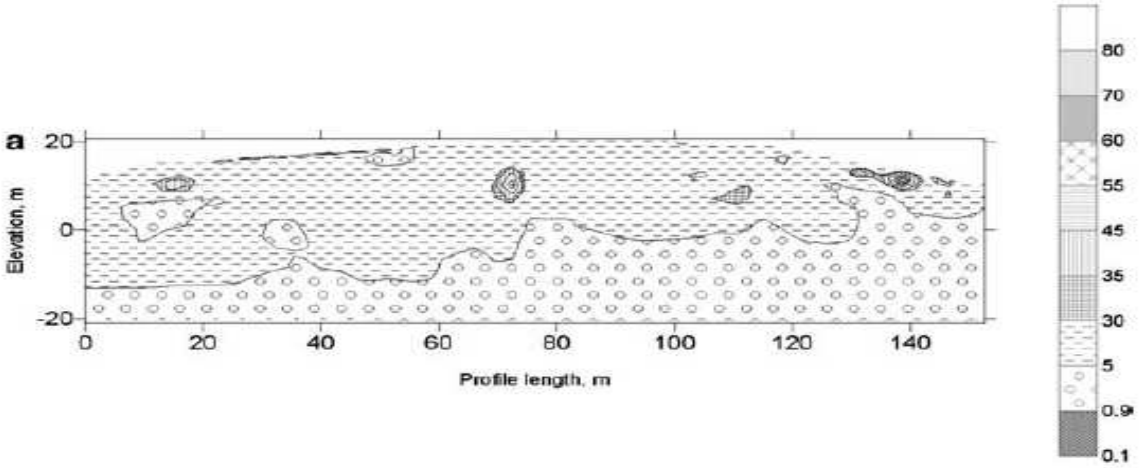

Fig. 2 An example of processed resistivity pseudo-section, given in Ωm (Frid et al, 2008).

The boundary between layers of saturated leachate-waste and saturated water-clay was assumed to be at the depth between −2 m and −3 m. This statistical argument was subsequently confirmed by two boreholes.

The research denoted that electrical resistivity imaging could be applied to display subsurface stratification and detect landfill boundaries. Statistical analysis provided information which could not be visually interpreted from geoelectrical imaging (Frid et al, 2008).

1.3.7 Case Study 6 — Nagpur, India

The study area was located in the vicinity of municipal landfill in Nagpur, India. The landfill was opened in 1972. Local bedrock was made of granitic gneiss covered with clay topsoil.

The aim was to indicate leachate pathways, assess groundwater contamination and identify subsurface properties which could be verified with geological information. Survey consisted of one resistivity profile (L1) and two radar profiles (P1, P2), located downstream direction from the landfill (Fig. 4).

Resistivity measurements involved one 126 m long profile with three different electrode arrays. Dipole-dipole configuration had better horizontal resolution while Schlumberger and Wenner arrays were more sensitive for vertical variations. Apparent resistivity was processed into true resistivity in EarthImager2D. The root mean square (RMS) error ranged between 5 % and 6 %, at less than 5 iterations, denoting good quality of collected data.

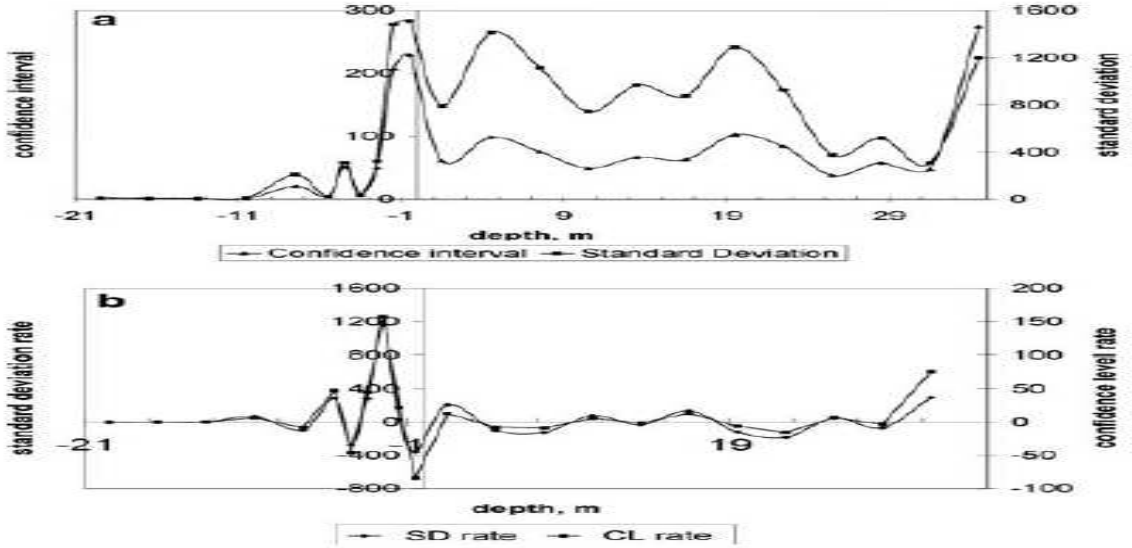

Fig. 3 a) Changes of standard deviation and confidence interval versus depth of the waste body (top); b) Changes of standard deviation (SD) rate and confidence level (CL) rate versus depth of the waste body (bottom) (Frid et al, 2008).

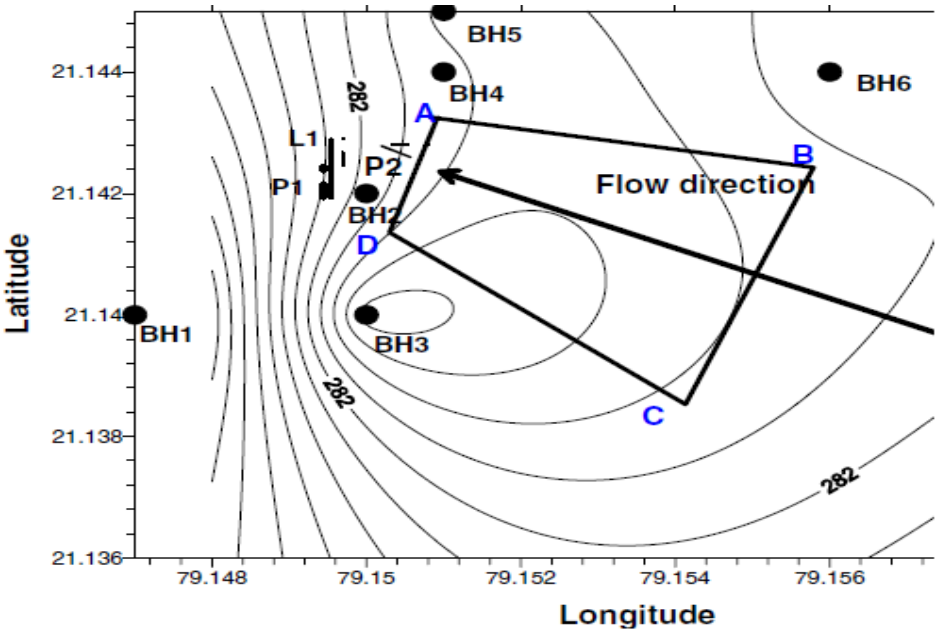

Fig. 4 Location of the study area and geophysical profiles (Pujari et al, 2007)

Two ground penetrating radar (GPR) profiles were taken, one of them was boundary with landfill edge. 200 MHz antenna was selected to receive high resolution. Ragargrams were processed in RADAN 6 software. Local peak and Hilbert transform modules were applied to map significant reflection of emitted energy. Strong reflection was characterized by bright spots in Hilbert transform or white and black lines in local peaks. Such anomalies were typical for zones with elevated conductivity.

Resistivity pseudo-sections displayed vertical stratification of subsurface (Fig. 5). Three layers could be distinguished. Highly conductive surface in the top 4-7 m, attributed to clay topsoil. The second layer, with intermediate conductivity, regarded as fractured rock and leachate released from the waste pile through granite cracks. Third, highly resistive layer was assigned to bedrock.

The radargrams displayed the same vertical stratification as resistivity images (Fig. 6 and 7). Strong reflection of radargram boundary with landfill edge corresponded to contamination plume or heterogeneous character of the waste pile. Fractures identified in the deeper layer

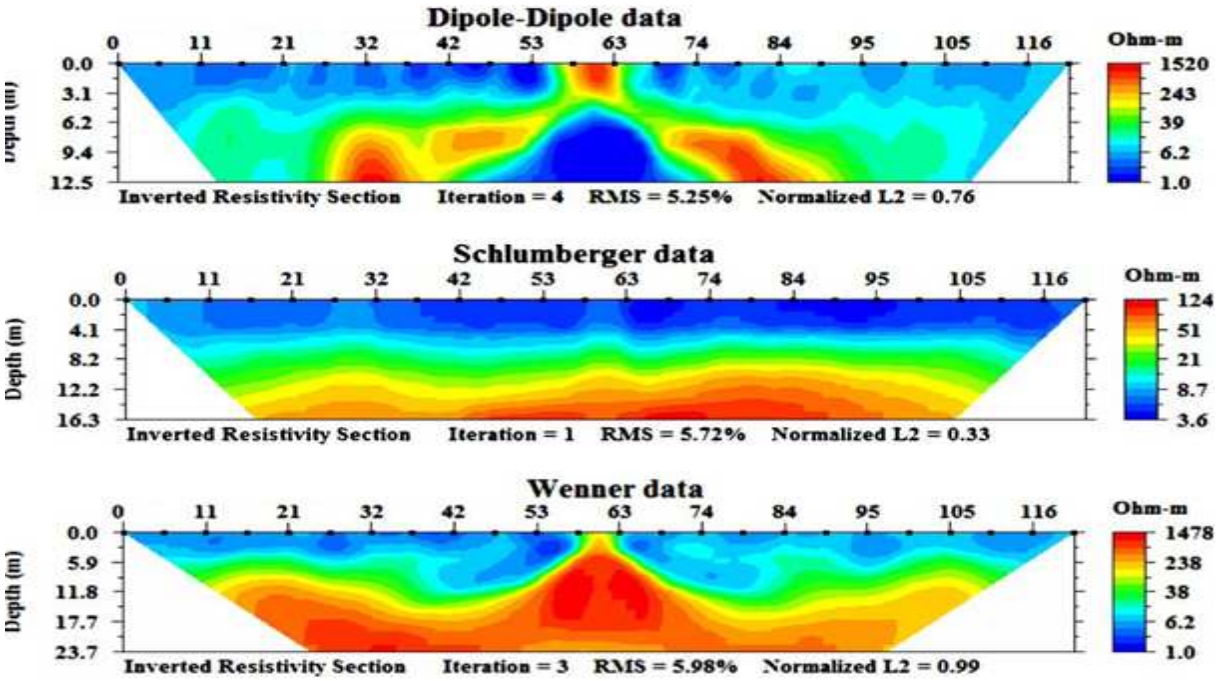

Fig. 5 Pseudo-sections from three different electrode arrays at profile L1 (Pujari et al, 2007).

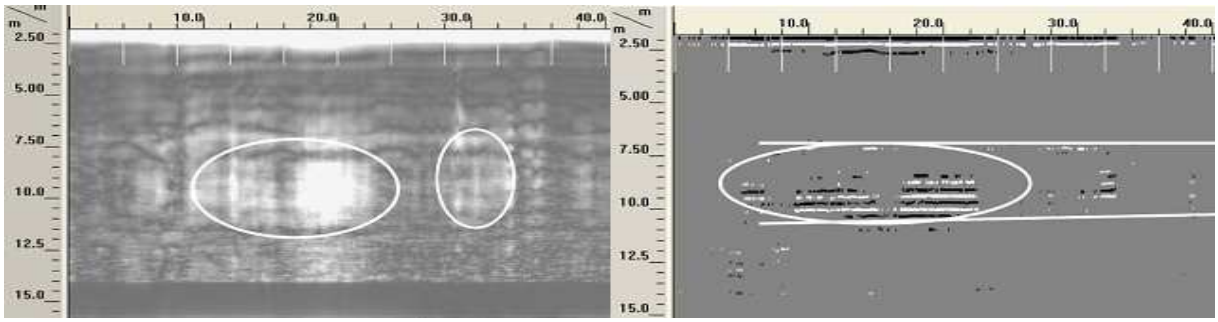

Fig. 6 Radargrams of profile P1 after application of Hilbert transform (left) and extraction with local peaks (right) (Pujari et al, 2007).

supported argument taken from resistivity measurements that the leachate was present below topsoil.

Plume migration into downstream part of the landfill was additionally confirmed by analysis of groundwater samples. Conductivity of samples taken from the downstream zone was much higher than in the upstream zone.

Combination of two geophysical methods enabled identification of rock fractures acting as migration pathways for contamination plume. Both methods led to corroborating outcomes, supported by groundwater analysis. The research recommended landfill upgrading with liner and leachate collection system to improve quality of groundwater resources (Pujari et al, 2007).

1.3.8 Case Study 7 — Edmonton, Canada

The Arum site was recommended as a waste management centre for Edmonton Three hydrological investigations, using boreholes and pumping wells have been previously taken at the site. The bedrock consisted of sandstones, shales, coal seams and two channel aquifers (east and south). The aquifers were separated by a sheet of ice thrust bedrock.

Electric resistivity imaging (ERI) combined with borehole logs was made to denote terrace sands and sand channels, investigate top of the thrust bedrock and identify sand channels beneath the thrust bedrock.

Wenner array was selected because it was robust for noise and had high vertical sensitivity. Three resistivity profiles with 5 m electrode spacing were taken to penetrate subsurface down to 40 m. Collected data was inverted in Res2Dinv, topography was added. The root mean square (RMS) error ranged between 1.7 % and 3.4 %. Processed pseudo-sections were compared with simplified borehole logs.

The first profile (Fig. 8) was taken to investigate if south channel of sand and gravel could be resolved. The second (Fig. 9) and third (Fig. 10) profiles were taken to display top of the thrust bedrock and verify if geology beneath the thrust bedrock could be imagined.

Three layers could be distinguished from the first profile (Fig. 8). The top, thin layer of moderate resistivity corresponded to unconsolidated clay and till. The middle, thick layer of high resistivity was assigned to sand and gravel channel. The lowest, low to moderate resistivity layer was attributed to bentonite rich bedrock.

High resistivity spot was present in the Western end of second profile (Fig. 9). The anomaly corresponded to terrace sand and gravel directly overlaying bedrock. A low resistivity anomaly, from 80 m to the eastern end, was attributed to thrust bedrock.. Moderate resistivity anomaly present above and below thrust bedrock corresponded to clay and till. The very bottom

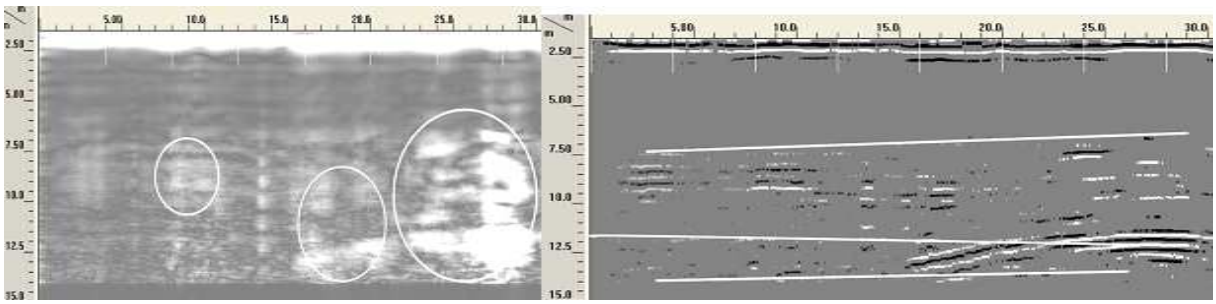

Fig. 7 Radargrams of profile P2 after application of Hilbert transform (left) and extraction with local peaks (right) (Pujari et al, 2007).

layer of low resistivity was assigned to the bedrock.

High resistivity anomaly at the western part of the third profile (Fig. 10) corresponded to terrace sand and gravel directly covering bedrock. The zone of low resistivity, present at the eastern top of the cross-section, was attributed to irregular blocks of thrust bedrock. Two anomalies of moderate resistivity, above and below thrust bedrock, corresponded to clay and till. The bottom layer of low resistivity was assigned to bedrock.

For each profile sand and gravel were regarded as zones of highest resistivity, bedrock and thrust bedrock corresponded to the lowest resistivity, clay and till were assigned to moderate values. Low resistivity of the bedrock was related to high content of bentonite. Resistivity profiles were in a good correlation with borehole logs.

ERI survey enabled extension of conclusions from previously performed site investigation. Resistivity method demonstrated ability to identify south channel and to resolve top of the thrust bedrock. The east channel, covered with thrust bedrock, was not detected. It was possible to resolve bedrock surface placed below thrust bedrock. The bedrock top ranged from 10 m to 40 m below surface. Combination of ERI with borehole logs significantly reduced cost of measurements (Meads et al, 2003).

1.3.9 Case Study 8 — Kuala Lumpur, Malaysia

The study area was a Seri Petaling landfill, situated near Kuala Lumpur. The facility has been in operation from 1979 till 1991. The elevation difference between a landfill top and surrounding area was up to 28.74 m which was responsible for high groundwater head differential. The bedrock consisted of sandstones, shales and mudstones.

Resistivity profile was taken to investigate extent of water and soil pollution within and around the landfill. Geoelectrical measurements were accompanied with analysis of water samples. The profile consisted of 50 electrodes with 5 m spacing. Collected data was processed into the true resistivity in Res2Dinv.

Three zones of low resistivity were attributed to decomposed waste saturated with leachate (Fig. 11). The zones had horizontal array. Soil and sand resistivity was reduced to moderate values due to leachate content. High resistivity at the bottom of pseudo-section was assigned to bedrock, approximately at 38 m depth. The thin layer of high resistivity at the top corresponded to weathered matter, dry sand and hard rock.

According to groundwater analysis from upstream and downstream, the leachate migrated downwards and reached the water table, mixed with groundwater and followed the flow further downstream. Leachate migration was accelerated by the high steepness of the landfill.

This case study showed that resistivity imaging combined with point and reliable data, such as water sampling, could be an efficient method to investigate leachate formation and migration (Ahmed & Sulaiman, 2001).

1.3.10 Recapitulation of studied literature

Geophysical surveying provides continuous, large-scale data, reduces time and cost of measurements done with invasive methods such as the boreholes. Data interpretation problems are solved by combining different geophysical methods and use of reference data such as geological information, auger drillings or analysis of water samples. Measurements taken in case studies were in a good correlation with borehole logs and local geology. Statistical analysis can provide outcomes which cannot be noticed from visual interpretation of pseudo-sections. Resistivity imaging was the most popular method used in case studies. Geophysical surveying is usually applied in investigation of landfill structure, subsurface properties, coverage condition and leachate migration.

1.3.11 Research motivation

The coverage constructed at Tveta landfill has a prototype structure with unique composition. Lysimeters records are the only source of reference data (Tham & Andreas, 2008). Non-invasive surveying is preferred to verify insulating properties of the coverage because drilling can damage landfill sealing and provides only point source of information.

According to studied literature, geophysical surveying has not been done on a coverage with parameters similar to construction at Tveta. Landfill capping has been investigated by Leroux et al (2007) and Hermozilha et al (2010) but coverages in both case studies had different composition, thickness and profile steepness. Studied literature provided an idea what non-invasive methods can be used at Tveta slope. Geoelectrical methods or ground penetrating radar were the most common in presented case studies.

In Leroux et al (2007), landfill coverage has been investigated with resistivity method, producing

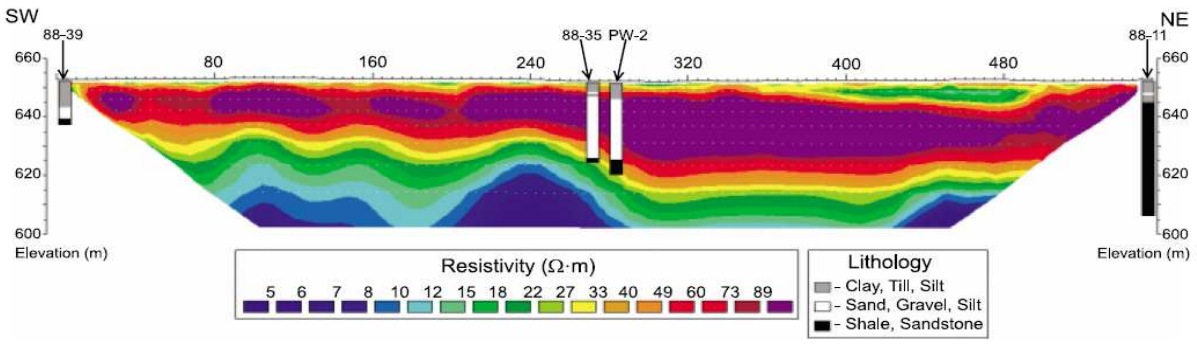

Fig. 8 Resistivity pseudo-section of profile 1 (Meads et al, 2003).

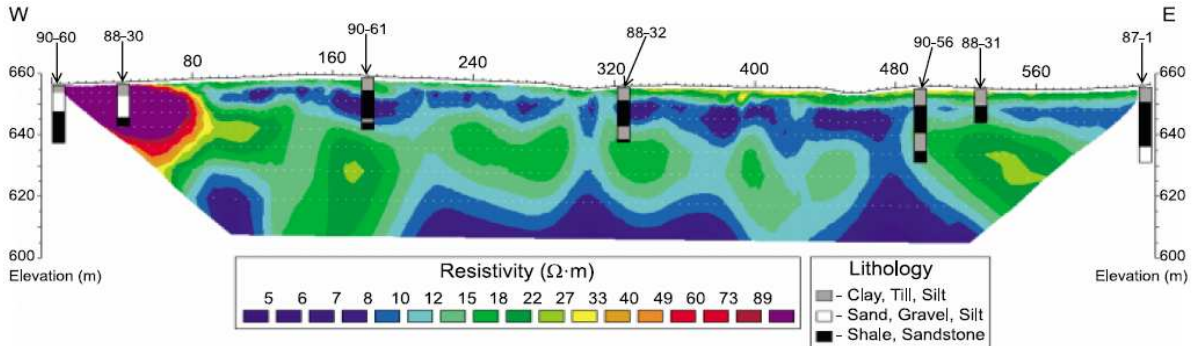

Fig. 9 Resistivity pseudo-section of profile 2 (Meads et al, 2003).

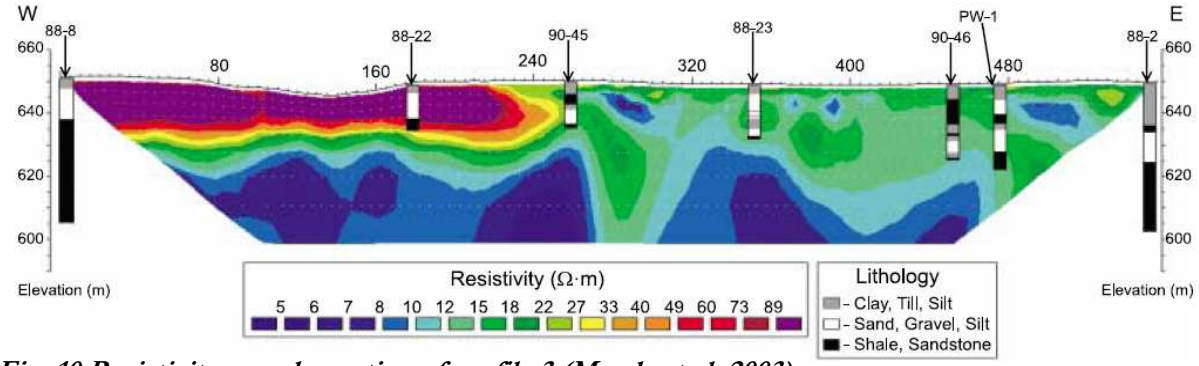

Fig. 10 Resistivity pseudo-section of profile 3 (Meads et al, 2003).

results in 2D pseudo-sections and in a 3D view. However, interpolation has not been applied in the 3D view. Three-dimensional model has been also produced by Hermozilha et al (2010) but it concerned GPR survey, not resistivity. 3D model of resistivity distribution with interpolated data, isosurfaces and masking of low resistivity regions is a purpose of DC resistivity surveying at Tveta.

According to presented case studies, landfill investigation was usually made with one or two geophysical methods. Coverage at Tveta will be surveyed with three, most commonly used techniques in the studied literature: DC resistivity, IP and GPR. This research is an opportunity to compare data quality of applied methods and assess which one of them is the most suitable for investigation of sealed landfills.

Summing up, novel aspects included in this research are: a non-invasive survey at Tveta in itself, processing resistivity distribution at thr coverage in 3D and investigation of the landfill cover with three geophysical techniques.

1.4 Problem Identification

Water permeability through the tested coverage has been monitored from March 2004 till November 2007. Recorded average annual infiltration rate varied between 0.8 dm^3/m^2 and 21.9 dm^3/m^2 which was well below the limit 50 dm^3/m^2 per year for non-hazardous waste (Tham & Andreas, 2008).

However, water infiltration recorded by lysimeters in 2008 has significantly increased, especially in the area 3 (Table 1). This could be caused by deformation of the lining material. Leachate could pass further through the waste

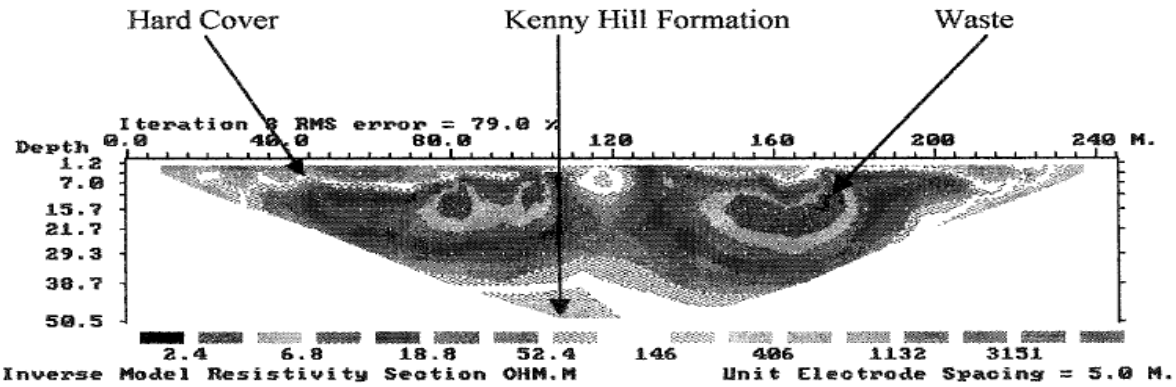

Fig. 11 Resistivity pseudo-section (Ahmed & Sulaiman, 2001).

pile deposited below coverage and later reach the groundwater as a highly contaminated substance polluting local water resources.

1.5 Aim

The purpose of this study was to verify insulating properties of the lining material and detect eventual zones with elevated infiltration rate. The thesis would support assessment if the tested materials were suitable for landfill coverage. The investigation could also recommend improvements of the coverage structure if measurements confirmed leakiness of the lining material. If this research provided insufficient outcomes what additional studies would need to be done?

2. METHODOLOGY

This section explains suitability of geophysical surveying as a measuring technique applied in this thesis. Selected methods are briefly described, following key principle of operation and measurements schedule. Each technique has a theoretical background, listed advantages and limitations, description of field measurements and data processing.

2.1 Selection of geophysical methods

Geophysical surveying seemed be the most suitable technique for the site investigation due to a non-invasive character of measurements and sensitive structure of landfill cover. Methodology was consulted with the thesis advisor, Bosse Olofsson, who is well experienced in geophysical measurements. Scientific literature, available measuring equipment and properties of the landfill cover were taken into account. Three geophysical methods were selected for subsurface investigation:

Direct current (DC) resistivity — the most important method of the research. Electric current was applied to measure soil resistivity.

Induced Polarization (IP) — operation was similar to DC resistivity. The applied current was cut off and the magnitude of the remaining charge provided information about subsurface chargeability.

Ground Penetrating Radar (GPR) — used as a reference method for geoelectrical measurements. Infiltrated water was assumed to be characterized by increased attenuation of the transmitted radiation.

These methods utilized coverage layering and contrast in ion content, were quick and easy to operate, did not affect coverage structure and provided 2D/3D visualizations.

2.2 Principle of operation — key assumption

It has been assumed that water containing dissolved ions had a higher electric conductivity than the surrounding environment. Detected regions with lower resistivity were therefore regarded as zones with an elevated infiltration rate.

2.3 Measurements schedule

Surveying of the landfill coverage took place in spring to avoid snowy conditions at the site. Methodology consisted of field studies and data processing. Field studies involved geophysical surveying and collection of coordinates with GPS. Data were subsequently processed in the specialized software. Field surveying and data processing steps were presented in a simple diagram (Fig. 12).

2.4 Theoretical background

Key elements, operation and surveying process of selected geophysical techniques were presented with reference to scientific literature.

Table 1 Lysimeter readings from 2008 [L/m²] (Telge AB own sources).

Area	Lysimeter	1	2	3	4	5	6	7	8	9	10	Sum
1	Jun 08	23	19	1.5	1	3.5	9	34	7	43	24	165
	Oct 08	1.5	1	2	5.8	0	0	5	2	0	7	24.3
												189.3
		1	2	3	4	5	6	7	8	9	10	
2	Jun 08	16	4	0	2.5	0.5	0	0	0	0	0	23
	Oct 08	3	10	0	8	0	0	0	0	0	0	21
												44
		1	2	3	4	5	6	7	8	9	10	
3	Jun 08	89	0	69	106	0	1	54	9	23	113	**464**
	Oct 08	47	2	55	0	0	59	41	66	273	10	**553**
												1017
		1	2	3	4	5	6	7	8	9	10	
4	Jun 08	8	0	3	0	0.7	0	0	5.5	5	2.5	24.7
	Oct 08	14.5	0	4.5	0	6	0	0.5	10	17.5	8	61
												85.7
		1	2	3	4	5	6	7	8	9	10	
6	Jun 08	2.5	2.5	0	0	14	0.3	0	0	9	4	32.3
	Oct 08	0	3	0	0	1	0.5	0	0	18.5	0	23
												55.3
		1	2	3	4	5	6	7	8	9	10	
7	Jun 08	0	2	0	1	0	0	2.5	4.5	2	0	12
	Oct 08	0	0	0	2	0	0	1.5	11	2	0	16.5
												28.5

2.4.1 Direct Current (DC) resistivity

Electric properties of soil can be investigated either electrically or electromagnetically.

Electrical methods determine direct current (DC) flow in the ground. DC resistivity is a technique which measures vertical and horizontal variations in electrical conductivity of subsurface (Robinson & Coruh, 1988; Chapel, 1992; Henry, 1997; Parasnis, 1997). Maximum penetration depth is practically 1 km (Kearey et al, 2002). To avoid contact resistances, which are dependant on soil humidity, two pairs of electrodes are used in resistivity measurements (Milsom, 2003).

Key Elements

Equipment used in DC resistivity measurements consists of electrodes (acting as potential and reference electrodes), cables, crocodiles, battery and current/voltage meters.

Operation

Artificially generated electric current is introduced under the ground surface from two current electrodes. Potential distribution, which gives information about soil resistivity, is

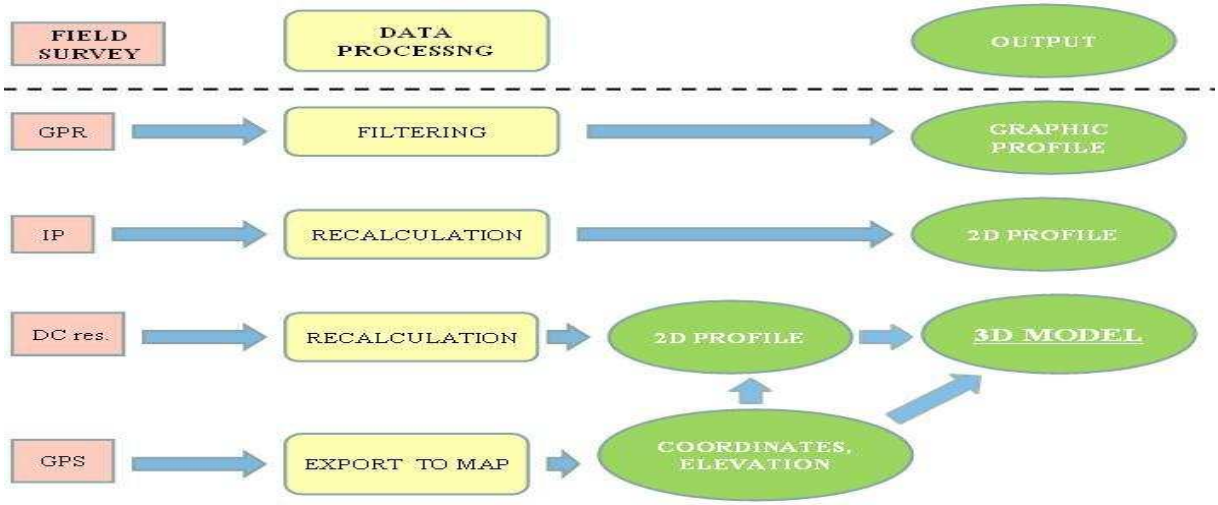

Fig. 12 Schematic diagram of field surveying and data processing steps.

detected by two inner electrodes (Fig. 13). The resistivity method is based on Ohm's Law (Parasnis, 1997):

$$I = -dV/R$$

Where: I is current [A], $-dV$ is voltage [V], R is resistance [Ω].

Resistivity ρ of studied material is defined as resistance in Ω between the opposite faces of a unit cube of the material. The unit of resistivity is Ωm. Resistivity of a conductive cylinder is defined as (Parasnis, 1997):

$$\rho = R * s/dL$$

Where: R is resistance [Ω], s is a cross sectional area [m²], dL is length [m].

Resistance is a characteristic of a particular path of an electric current. Resistivity is a physical property of a given material (Parasnis, 1997).

Surveying with DC does not give a value of subsurface true resistivity. It is assumed that the studied material is homogeneous, thus obtained results are called apparent resistivity. True resistivity is equal to apparent resistivity only in homogeneous materials. Resistivity measurements are also affected when electrode spacing or array is changed (Parasnis, 1997; Milsom, 2003).

Rock and minerals are insulators in a dry state. However, in natural environment they contain some water with dissolved salts, thus are conductive. Rock conductivity is proportional to pore fraction (Parasnis, 1986). Resistivity of different geological materials ranges from a fraction of Ω to thousands of Ω (Fig. 14) (ABEM Instrument AB, 2009).

Surveying

Subsurface properties can be investigated in two ways: as vertical electric sounding (VES) and electric profiling (EP). Two dimensional map of subsurface resistivity, called continuous vertical electrical sounding (CVES), is a combination of these two methods.

The aim of the sounding method is to determine vertical variation in soil conductivity. It is efficient only for subsurface with no lateral variations. The most efficient is surveying of sediment layers. Two electrodes are held in the same place while the second pair is moved step by step along the profile.

Conductivity variations along the profile are determined using electrical mapping. Distance between electrodes is fixed and the whole array is moved along the profile. When one profile is finished, next parallel traverse is surveyed (Parasnis, 1997).

2.4.2 Induced Polarization (IP)

Phenomenon of induced polarization (IP) was discovered at the beginning of 20th century by Schlumberger (Parasnis, 1986). IP has been utilized for geophysical purposes since approximately 1950 (Angoran & Fitterman, 1974). Induced polarization is a measurement of potential difference which remains a couple of seconds after an artificial current in resistivity array is switched-off. The charge is accumulated on small conductive particles present in insulating matrix, such as ore grains present in rocks (Mussett et al, 2000). This is why the first goal of IP was detection of metallic minerals (Angoran & Fitterman, 1974). Measurement of the impedance function can be determined in time and frequency domain (Angoran & Fitterman, 1974; Parasnis, 1986).

Key Elements

Induced polarization can be measured with the same equipment as DC resistivity.

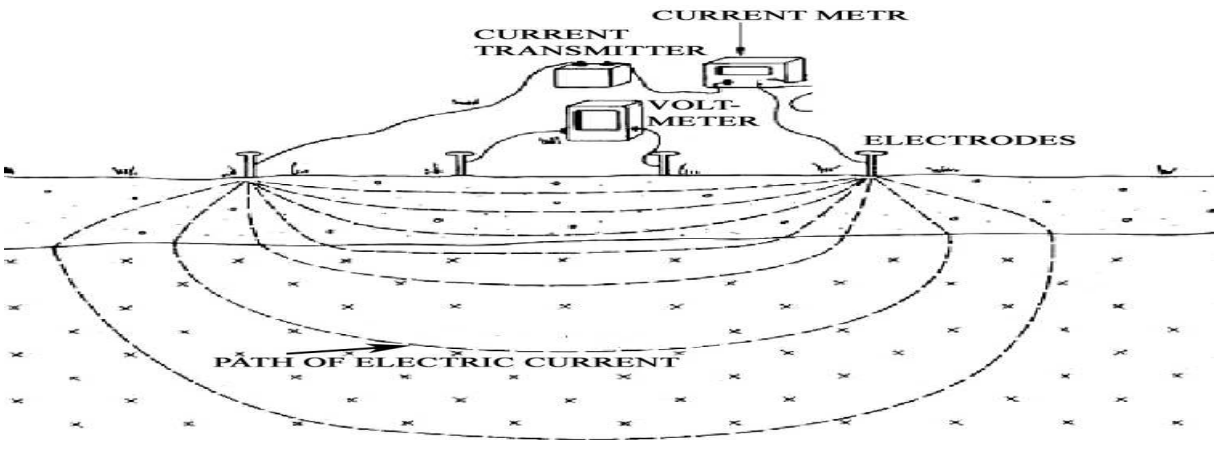

Fig. 13 Example of DC resistivity measurement (modified after Robinson & Coruh, 1988).

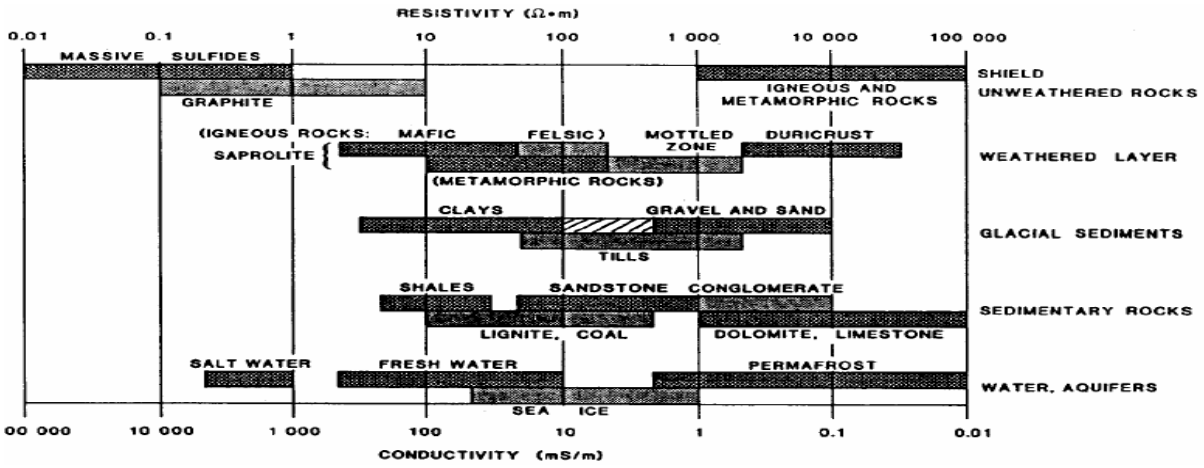

Fig. 14 Typical ranges of resistivity of geological materials (ABEM Instrument AB, 2009).

Operation

IP is determined by switching-off battery and measuring potential drop of conductive particles in soil. Two microscopic mechanisms, which cannot be distinguished, that contribute to IP magnitude are electrode and membrane polarization (Parasnis, 1986; Sjogren, 2004).

Electrode Polarization

When a pore channel in rock is blocked by insulating grain, no current flow is present. If the grain is conductive, for example in an ore, ions are blocked but electrons can pass through it. Anions on one side become neutral and the same happens to cations on the other side of a grain. The process of electron exchange is slow, so charges are accumulated on both sides of grain-water interface (Fig. 15). When the artificial current is switched off, ions are dispersed back into equilibrium state. Small current is produced which is recorded by potential electrodes during a few seconds. If the rock does not contain any conductive grains voltage drops to zero at once. Such accumulation of charges on grain-electrolyte interface is called electrode polarization. Detection of ores in rock matrix is much more difficult with resistivity method (Mussett et al, 2000).

Magnitude of polarization is proportional to the contact surface-area. This mechanism is stronger than membrane polarization but less common because metallic conductors are not as abundant as clay (Milsom, 2003).

Membrane Polarization

This mechanism is a source of noise in ore surveying. Membrane polarization is produced when clay particles are attached to pore-channel walls. Clay surface is negatively charged so cations dissolved in water are attracted when current is applied (Fig. 15) (Mussett et al, 2000). Electrical double layer is formed. The charges are accumulated on the clay-electrolyte interface. When the current is switched off, ions are dispersed back and small current is produced. This concentration of ions is called membrane polarization. It is a weak IP mechanism due to limited ion mobility (Sumner, 1976). Membrane polarization is applied in groundwater searching (Majumdar, 1973).

Surveying - Time domain IP

The elements measured in this method are polarizability and chargeability.

Polarizability (P) is a remaining potential difference ΔV, which is measured time t after the current V_0 is switched off. Parameter T expresses duration of applied current V_0. The

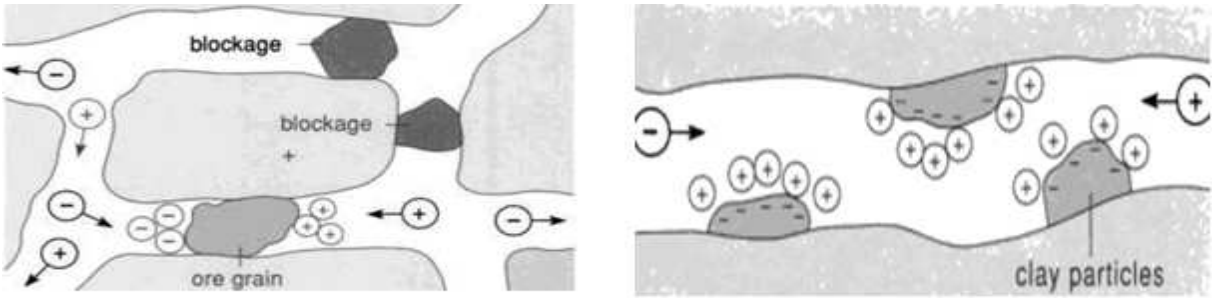

Fig. 15 Electrode (left) and membrane (right) polarization (Mussett et al, 2000).

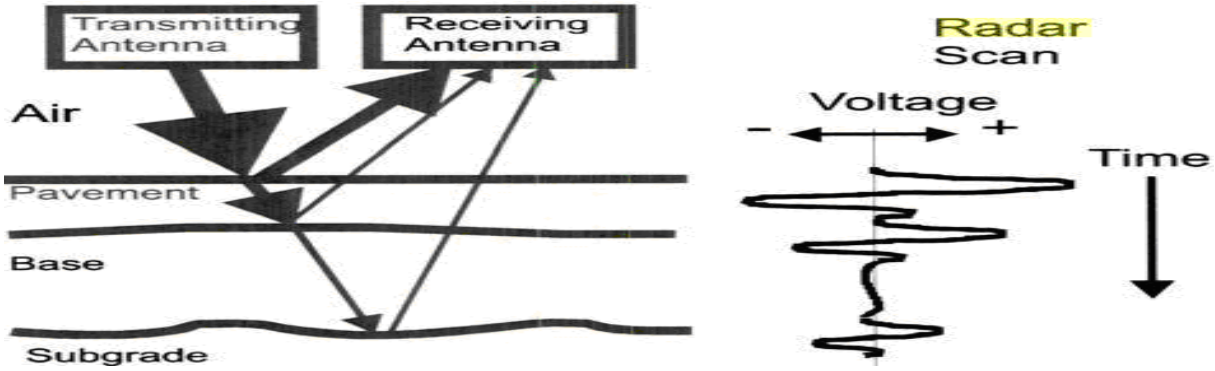

Fig. 16 Transmission and reflection from the interfaces in a pavement section (Morey, 1988).

unit of polarizability is often expressed in mV/V. *T* is in a range of 1-20 seconds, parameter *t* is a fraction of *T*.

$$P_t^T = \Delta V_t / V_0^T$$

This measure is called apparent polarizability due to inhomogeneous character of the ground.

Chargeability (*M*) is expressed as an area under decay curve during period bounded by t_1 and t_2. The unit is milisecond.

$$M_{t_1,t_2}^T = (1/V)\int_{t_1}^{t_2} \Delta V_{IP}\, dt$$

Where: ΔV_{IP} is decaying voltage during t_1 to t_2, V is a voltage level before cut-off, T is the period when voltage V was applied, t_1 and t_2 are two time values after the cut-off (Parasnis, 1986).

2.4.3 Ground Penetrating Radar (GPR)

GPR development is related to the use of echo sounds which were applied to determine thickness of ice-core. It was noticed that, except the permafrost layer, underlain unfrozen ground could also be investigated. GPR is an electromagnetic sounding method which uses radio waves of higher frequencies than very low frequency (VLF) technique (Milsom, 2003). It has many applications. Purposes related to this master thesis are: classification of soil stratigraphy and detection of conductive zones such as ionized water or leachate (Daniels, 2004).

Key Elements

GPR consists of transmitter, receiver, central recording unit (CRU) and antenna. Coils in the first two elements are made from the optical fibres. Most of antennas are simple dipoles (Milsom, 2003).

Operation

Radar operation is based on emission of short beams of electromagnetic energy. If the signal encounters interface with two layers of different electromagnetic properties part of the signal is reflected back to receiver and part is still travelling down through the material unless the next interface is met. Reflection is proportional to difference in electromagnetic properties (Fig. 16) (Morey, 1998; Milsom, 2003). Reflected signals are presented on computer recording unit (CRU) as a waveform of voltage changes as a function of time. The stored signals can be displayed as a graphical profile (Fig. 17) (Morey, 1998).

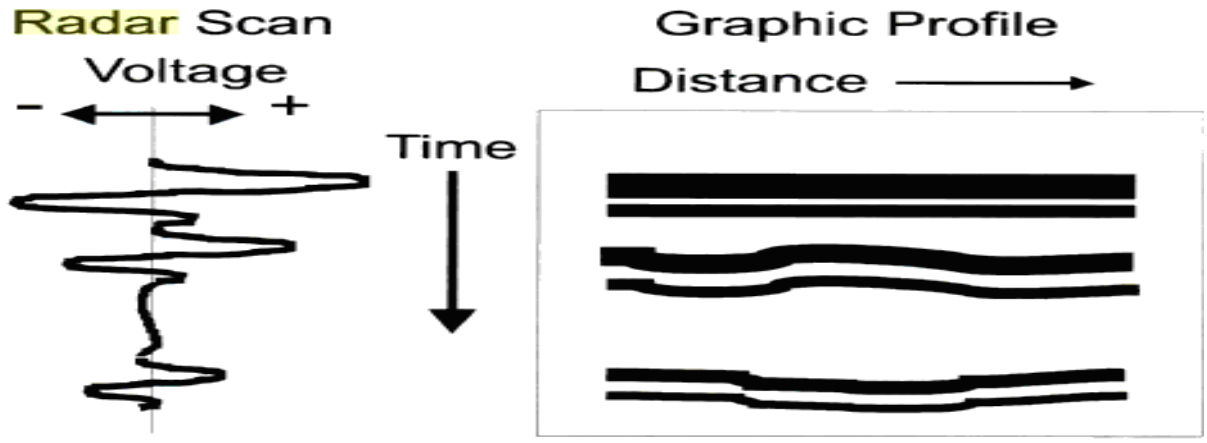

Fig. 17 Graphic profile that results from pavement section in Fig. 16 (Morey, 1988).

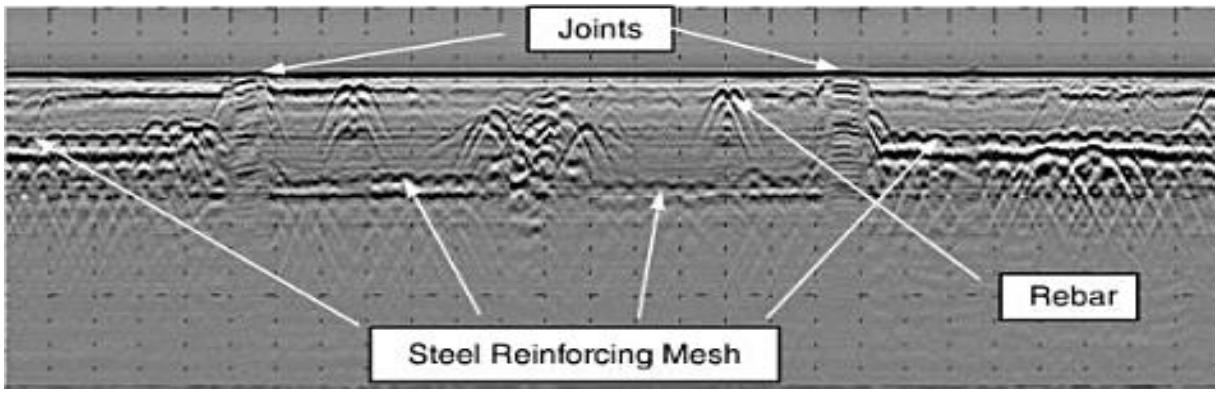

Fig. 18 Typical GPR image of concrete floor showing rears, joins, mesh. "U" shaped waves are formed due to strong reflection (Britsow & Jol, 2003).

The rate of reflected wave is dependant on surface roughness, size and reflection coefficient. The range of emitted frequency varies between +50 % and −50 % from the central value. At least 1 % of the emitted energy should be reflected in order to get competent data. Variation in water content is the most important factor for distinction of non-metallic bodies. Image resolution is proportional to frequency set in GPR. Depth penetration is high at low frequencies so the compromise between resolution and penetration is necessary. Depth of penetration is also dependant of material permittivity ε, known as dielectric constant (Table 2). Permittivity is proportional to the penetration depth. Another parameter which influences penetration depth is electrical conductivity σ. Attenuation of emitted wave is high at layers with low resistivity (Milsom, 2003).

When emitted radiation encounters interface of high contrast curved waves are formed on the graphic profile (Fig. 18) (Britsow & Jol, 2003). Radiation is attenuated when the beam penetrates conductive subsurface (Fig. 19) (Morey, 1988).

Surveying

GPR survey can be performed with two techniques. Constant antenna spacing method was selected for this research because it is quicker and more convenient to use than multifold common midpoint technique. During the measurements objects, which can produce noise, should be kept away from the radar. Interferences can be caused for instance by mobile phones, metallic objects, radio transmitters (Milsom, 2003).

2.5 Advantages of selected methods

The main advantages of selected geophysical methods were:

- No influence on coverage structure. Equipment was non-invasive.
- Spatial information about the subsurface was provided compared to core drilling.
- Methods were time-efficient and economically feasible. Data was collected during few days.
- Equipment was easy to operate. Training of an inexperienced person took less than one hour.

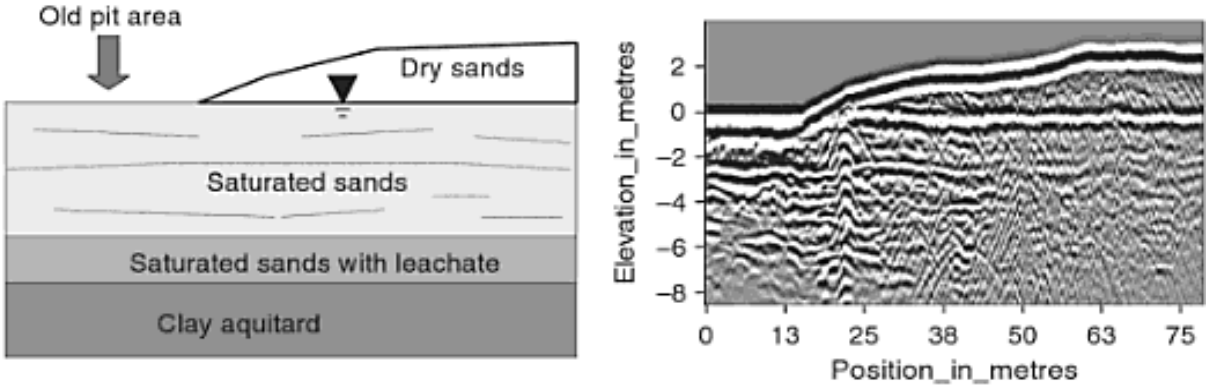

Fig. 19 Typical image of a conductive subsurface. Radiation is dispersed and no "U" shaped waves are formed due to weak resistivity contrast (Morey, 1988).

- Geophysical methods have been widely applied to similar environmental problems, especially in detection of leachate from waste deposits to groundwater.
- The methods were complementary i.e. measurements from DC resistivity could be verified with GPR data.
- Collected data was visualized in 2D profiles and in a 3D model.
- Coordinates taken from GPS were added to graphic display of the results.

2.6 Limitations of selected methods

Selected methods had also some drawbacks. The following factors had influence on the final results:

- GPR penetration depth was inversely proportional to the frequency and hence to the resolution quality, which required a compromise between depth of subsurface study and quality of graphic profiles. GPR radiation was attenuated in humid soils. If water content in the subsurface was too high, quality of data could be insufficient for analysis.
- Due to time and economic limitations only 8 DC resistivity profiles were taken from the study area. Collected data represented only the resistivity around the lines and not the whole area.
- The subsurface structure was not homogeneous. Measured resistivity values along the profiles were not true resistivity but apparent resistivity values. The data was subsequently converted into true resistivity with inversed modelling techniques.
- True resistivity values, calculated from apparent resistivity values, had limited accuracy. The size of error was dependant on the number of iterations and quality of the collected data.
- Maps and GPS data had limited accuracy. The error of GPS coordinates was up to 25 m. Strength of satellite signal was dependant of sky transparency.
- Penetration depth and density of collected data were better for the 160 m long profiles than for the shorter profiles. Only 3 out of 7 profiles were 160 m long due to a fence built in the upper part of study area.
- Ion concentration in infiltrated water could be too weak to be detected by IP. The infiltrated precipitation was not as contaminated as water percolated through the waste pile.
- Results of geophysical surveys required correct interpretation. The outcome could be ambiguous. Experience and scientific knowledge were necessary for a correct evaluation of data.

2.7 Field Surveying

Measurements involved two geoelectrical methods (DC resistivity and IP) performed on the same electrode array and radar surveying at different frequencies of antenna. Coordinates of the taken profiles were subsequently taken with GPS.

2.7.1 DC Resistivity

Geoelectrical measurements were taken between 6th and 8th of April 2009. The weather conditions were similar during all surveys, with no rainfall and temperature approximately +15 °C. Eight DC resistivity profiles were taken (Fig. 20).

Seven profiles were taken along slopes, parallel to the run-off flow direction. The remaining 8th profile, with dense electrode spacing, was

Table 2. Typical values of radar parameters for some common materials (Milsom, 2003).

Material	ε	σ, mS/m	V, m/ns	α, dB/m
Air	1	0	0.3	0
Ice	3-4	0.01	0.16	0.01
Fresh water	80	0.05	0.033	0.1
Salt water	80	3000	0.01	1000
Dry sand	3-5	0.01	0.15	0.01
Wet sand	20-30	0.01-1	0.06	0.03-0.3
Shales and clays	5-20	1-1000	0.08	1-100
Silts	5-30	1-100	0.07	1-100
Limestone	4-8	0.5-2	0.12	0.4-1
Granite	4-6	0.01-1	0.13	0.01-1
Dry salt	5-6	0.01-1	0.13	0.01-1

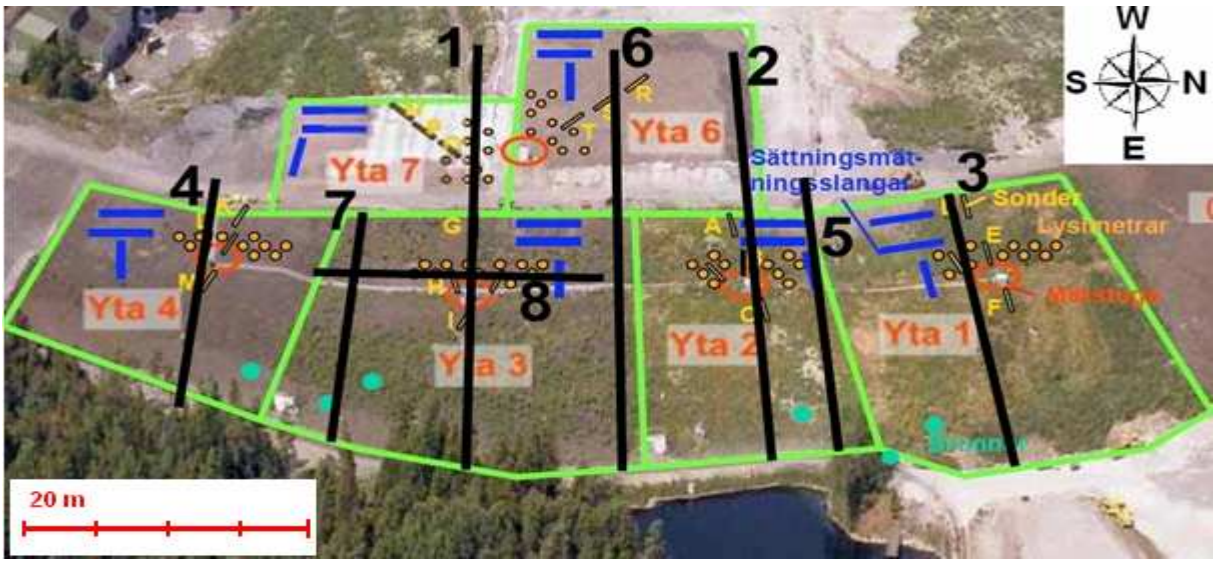

Fig. 20 Location of resistivity profiles (modified after Tham & Andreas, 2008).

located between lysimeters at the area 3. The additional survey was made at the shelf of area 3 where the lysimeters recorded the largest amount of water.

The length of the seven parallel profiles was 80 m and 160 m. Electrode spacing was 2 m and 4 m at the outer parts of the 160 m long profiles. The longer profiles provided denser measurements in the middle part. However, only three long profiles were taken because the upper part of slope was surrounded with a fence, which is not visible within the provided photo (Fig. 20). Primary profiles 1, 2, 3, 4 were taken along the lysimeters to verify their records. Complementary profiles 5, 6, 7, were taken in between. Profile 8, with 0.5 m and 1 m electrode spacing, was surveyed in order to produce denser information about the resistivity in the vicinity of well 3.

The protocols used in the resistivity survey were WENNER32SX (Fig. 21), GRAD4L8 and GRAD4S8 (Fig. 22 and 23). Data cover (Fig. 24) and processed pseudo-sections (Fig. 25) had trapezoidal shape. Parameters of geoelectrical profiles were listed (Table 3).

The measuring equipment consisted of a four-channel data acquisition system SAS4000, sets of cables with 2 m and 0.5 m electrode spacing, steel electrodes and crocodile clips. The equipment was rented from ABEM AB Company. Time-saving, four-channel gradient protocols were primarily used. One-channel Wenner protocol was also used due to technical problems with the four-channel equipment. Combination of electrodes was selected automatically. It saved time and eliminated risk of human error. The size of the electrode spacing was adjusted according to the desired density of measurements and penetration depth.

2.7.2 Induced Polarization

Initially, there were some doubts if the IP survey should provide usable results. The IP method is generally used to detect buried waste or ores due to a high contrast between the chargeability of specific objects and the surrounding environment. Ions dissolved in infiltrated water might not produce detectable strength of polarization.

Induced Polarization measurements were taken together with the DC resistivity investigation. When the first IP survey was made along profile 1, the data was exported to a laptop and processed in Res2Dinv software. The waste pile was the only detectable object in the 2D inversed model. The output from this method was assumed irrelevant regarding water infiltration through the landfill coverage. Therefore, the IP method was not further used and the investigation focused only on DC resistivity. Parameters of the IP profile were presented with resistivity profiles (Table 3).

2.7.3 Ground Penetrating Radar

GPR data was collected with two antennas: shielded 250 MHz and unshielded 100 MHz. The remaining equipment consisted of:

- MALÅ XV monitor
- ProEx Control Unit
- Distance measuring device (measuring wheel for 250 MHz antenna and hip chain for 100 MHz antenna)

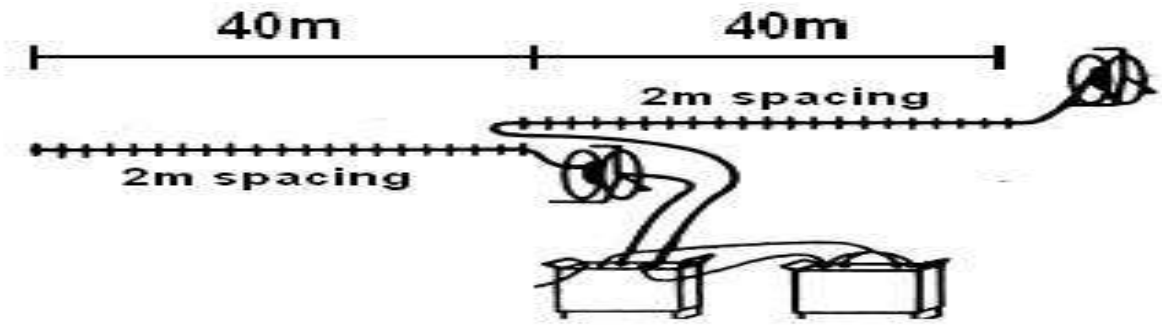

Fig. 21 Electrode array applied to profiles 3, 4, 5, 7 (ABEM Instrument AB, 2009).

- Antenna module (connects antenna with control unit)
- Optical fibre cables (communication between control unit and antenna, 50 μm diameter)
- Batteries and GPS

A survey with the 250 MHz antenna was carried out on 22nd of April 2009. The penetration depth was insufficient so additional measurements with 100 MHz antenna were made on 4th of June 2009. Antennas were rented from MALÅ Geoscience. Remaining equipment was taken from KTH. The service of MALÅ Geoscience recommended 100 MHz as the minimum frequency of antenna because at lower frequencies information about the uppermost 5 m of subsurface would not be recorded. Thus, no information about coverage structure would be collected. Weather conditions were similar during both surveys: moderate rainfall and temperature +13 °C. The height of vegetation at the waste pile slope increased from approximately 30 cm in April up to 1 m in June.

The GPR survey was primary made along the DC resistivity profiles. Additional measurements were subsequently taken at the slope because GPR surveying was less time-consuming than geoelectrical methods.

2.7.4 Coordinates collection

The position data was collected on 22nd of April 2009, before the GPR survey with 250 MHz antenna was carried out. The sky was moderately transparent. Coordinates were taken with GPS Magellan 315. The RMS accuracy of positioning was 25 m or better. Coordinates were taken along the geoelectrical profiles since they were not exactly linear from start to end points. The measurements were taken approximately every 4 m.

2.8 Data processing

The data from field surveying was exported to

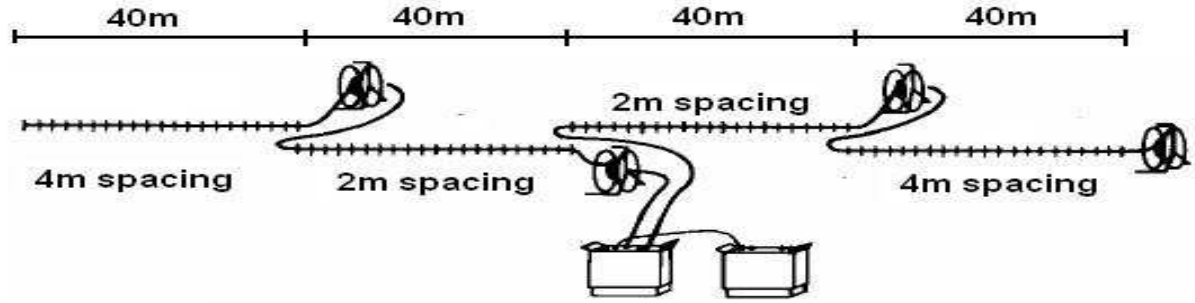

Fig. 22 Electrode array applied to profiles 1, 2, 6 (ABEM Instrument AB, 2009).

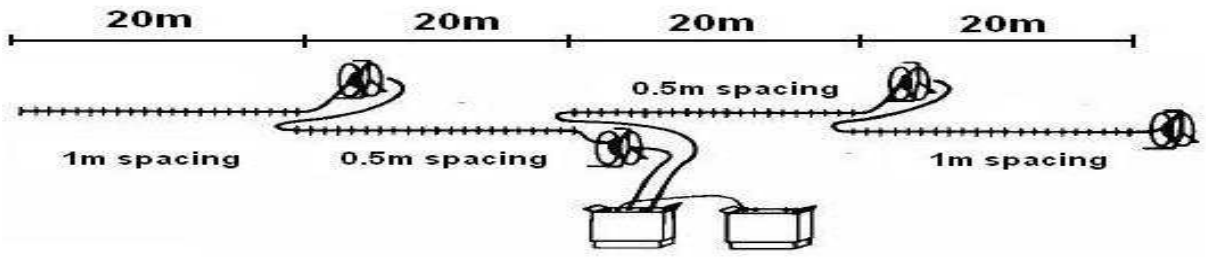

Fig. 23 Electrode array applied to profile 8 (ABEM Instrument AB, 2009).

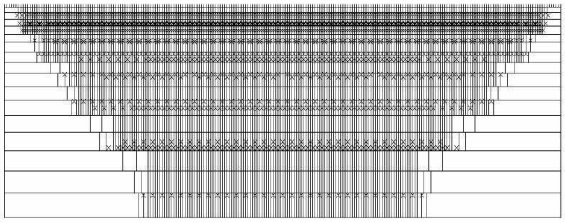

Fig. 24 Data cover for gradient protocols (ABEM Instrument AB, 2009).

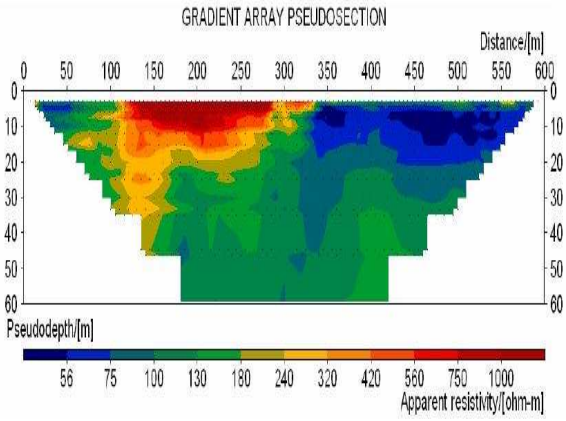

Fig. 25 Example of apparent resistivity 2D pseudo-section (ABEM Instrument AB, 2009).

computer and processed. Topography was attributed to resistivity pseudo-sections which were subsequently interpolated in order to produce a three-dimensional resistivity distribution at the study area. IP and GPR output was displayed on two-dimensional images.

2.8.1 DC resistivity

Processing of resistivity data involved three programs.

Res2Dinv (version 3.55)

Apparent resistivity data was modelled into true resistivity values using finite difference modelling techniques. The RMS error (%) expressed the size of inaccuracy between the apparent resistivity and the suggested inverted model. The RMS error was reduced after each iteration. It was not recommended to exceed five-six iterations because the recalculated data might differ too much from raw data and the model could become unstable. Resistivity measurements at Tveta were done in a good manner, thus 5 iterations per profile were sufficient. Bad points were removed before the inversions. Every profile had up to two points which significantly differed from the resistivity trend-line formed by remaining points. Smooth modelling technique was applied.

Topographical data was subsequently added to the profiles and resistivity scale was unified for all profiles. The range of resistivity was high so a logarithmic scale was applied. The two-dimensional profiles were presented in Appendix 2.

GeoElTrans (version 1.0.0)

Before preparation of the pseudo 3D model it was necessary to convert data from two-dimensional (length and elevation) into three-dimensional (longitude, latitude, altitude). This was done in the GeoElTrans software, created at KTH. Linear profiles were recalculated into X, Y coordinates. Coordinates of start and end points were taken from the GPS survey, remaining points were interpolated. The output was exported to prepare the 3D model.

Voxler (version 1.00)

The input data was processed in two modules. Firstly, resistivity values were interpolated to get a 3D box grid. Topography of the slope was not included yet, so elevation data was interpolated in the second module. Both outcomes were bound in the mathematic module in Voxler. Resistivity grid values, which were located above the elevation data (the topography along the profiles) in the second dataset, were blanked. The result was a resistivity distribution model with included slope topography. Diagram of the process is presented in Appendix 3. Resistivity values were subsequently inversed to get conductivity distribution and isosurfaces.

2.8.2 Induced Polarization

The only IP profile has been modelled in Res2Dinv (version 3.55) analogically as DC resistivity profiles. Processing involved 3 iterations. The output of the inverse model of profile 1 was presented in chapters: Results and Appendix 4.

2.8.3 Ground Penetrating Radar

The GPR files were exported to computer and analyzed in RAMAC GroundVision (version 1.4.2) software. Following filtering methods were applied to improve quality of the raw data:

- DC removal. The aim was to subtract systematic offset in the recorded amplitudes. Input data was shifted in order to get the direct wave at time equal 0.
- Automatic Gain Control. The applied gain to the signal was automatically adjusted to get similar signal strength independent on the reflection depth.

Table 3 Parameters of taken geoelectrical profiles.

Profile number	Protocole name	Profile length [m]	Electrode spacing [m]	Geoelectrical method
1	GRAD4L8 and GRAD4S8	160	2 and 4	DC
2	GRAD4L8 and GRAD4S8	160	2 and 4	DC
3	WENNER32SX	80	2	DC
4	WENNER32SX	80	2	DC
5	WENNER32SX	80	2	DC
6	GRAD4L8 and GRAD4S8	160	2 and 4	DC
7	WENNER32SX	80	2	DC
8	GRAD4L8 and GRAD4S8	80	0,5 and 1	DC
1	GRAD4L8 and GRAD4S8	160	2	IP

- Band Pass. Removal of low and high frequency noise. Frequency distribution in signal spectrum was analyzed. The range of upper and lower noise was selected and cut-off.

Examples of raw and filtered data for both antennas were presented in chapters: Results and Appendix 5.

2.8.4 Coordinates processing

Collected GPS coordinates were exported to computer. GPS-data and the topographic map, received from Telge Återvinning, had two different coordinate systems, although both were in a metric scale. Upper wells, marked by orange circles (Fig. 20) at areas 1, 2, 3 and 4 were the reference points. It was noticed that the GPS coordinate-system was translated from the map coordinate-system with constant X and Y values. GPS coordinates were reduced by 200 m on the X axis and 500 m on the Y axis in order to fit the topographic map from Telge Återvinning. (Table 4, Table 5). Profiles were marked on the map to read the elevation values (Fig. 26). Topographic data was subsequently exported to the software Res2Dinv (version 3.55).

3. RESULTS

This chapter contains description of processing steps and figures displaying resistivity distribution in 2D/3D, chargeability pseudo-section, GPR radargrams, topography model and outcome from modified resitivity data.

3.1 DC Resistivity — 2D inverse models

Eight profiles were taken in the DC resistivity measurements. Profiles 1, 2, 6 were 160 meters long. The length of remaining profiles was 80 meters each. Profiles from 1 to 7 had a west-east orientation, whereas profile 8 was south-north orientated. Collected data was processed in Res2Dinv (Fig. 27 – 34). The penetration depth ranged from 5 meters in profile 8 to 25 meters in longer profiles. The root mean square (RMS) error varied from 2.3 % to 8.9 %. The arithmetic average of RMS for the 8 profiles was approximately 4.5 %. Five iterations were taken for each profile. Analysis was focused on the uppermost 5 m of the slope subsurface.

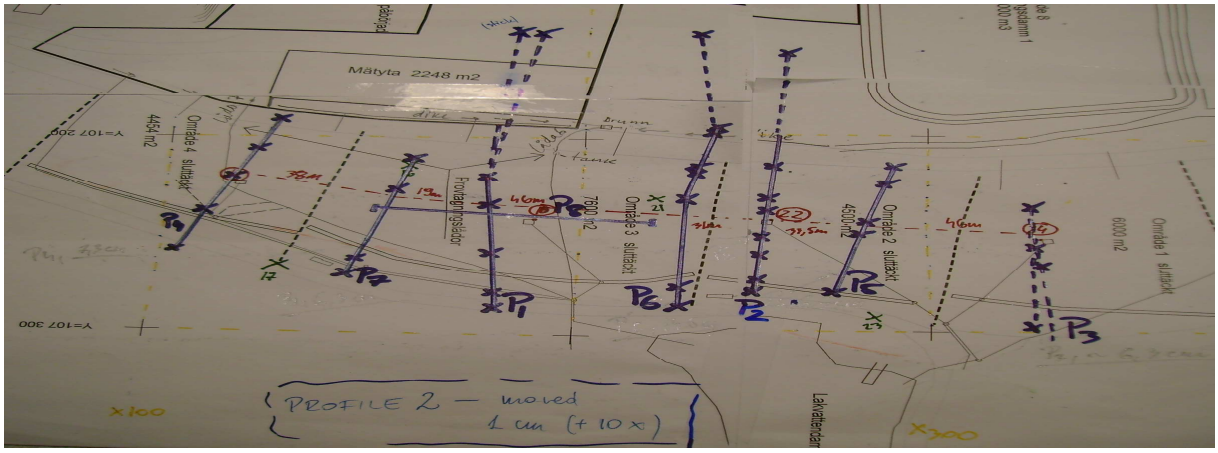

Fig. 26 Manually marked profiles on topographic map (modified after Telge AB own sources).

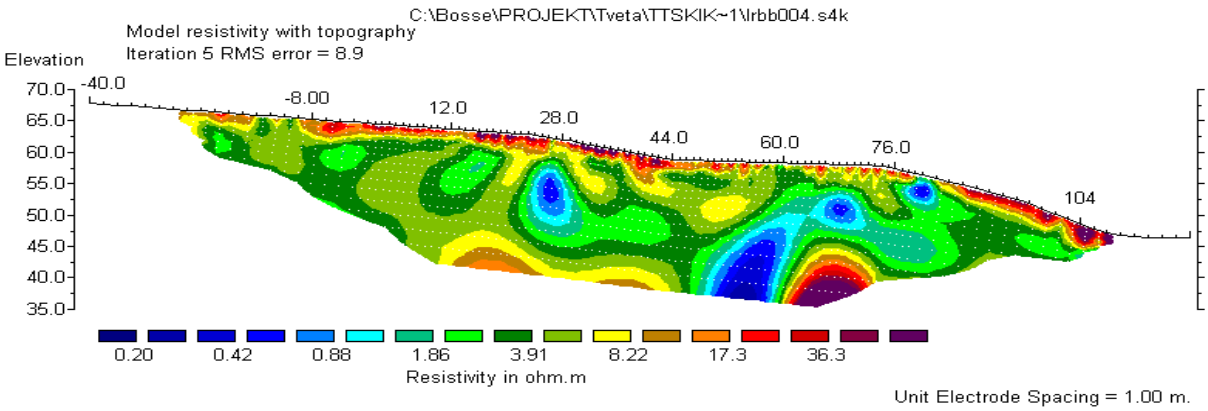

Horizontal scale is 4.52 pixels per unit spacing
Vertical exaggeration in model section display = 1.12
First electrode is located at -40.0 m.
Last electrode is located at 120.0 m.

Fig. 27 Resistivity distribution in 2D inverse modelling — profile 1.

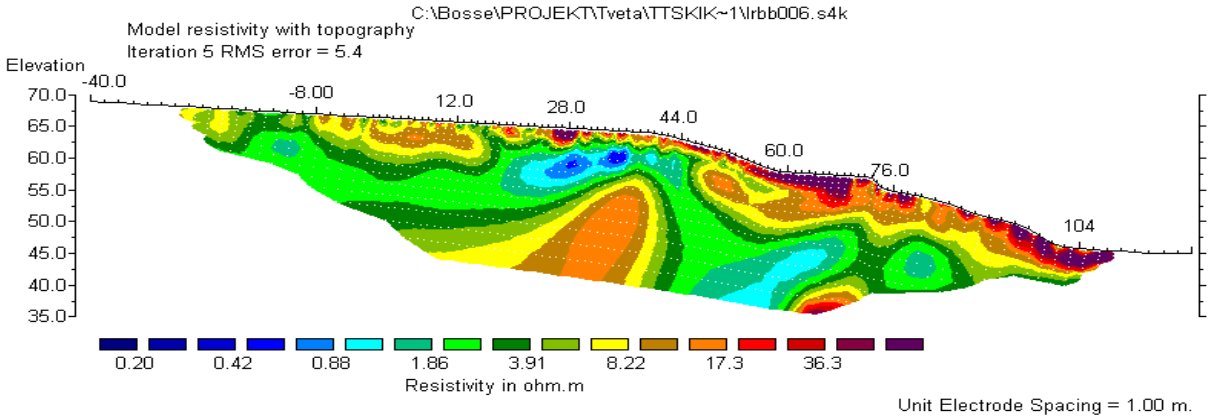

Horizontal scale is 4.60 pixels per unit spacing
Vertical exaggeration in model section display = 1.12
First electrode is located at -40.0 m.
Last electrode is located at 120.0 m.

Fig. 28 Resistivity distribution in 2D inverse modelling — profile 2.

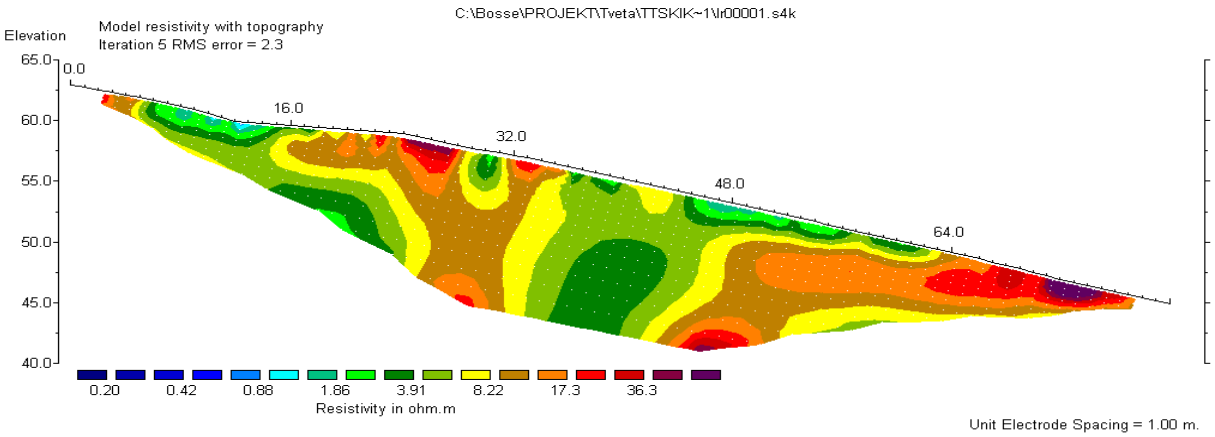

Horizontal scale is 11.79 pixels per unit spacing
Vertical exaggeration in model section display = 1.02
First electrode is located at 0.0 m.
Last electrode is located at 80.0 m.

Fig. 29 Resistivity distribution in 2D inverse modelling — profile 3.

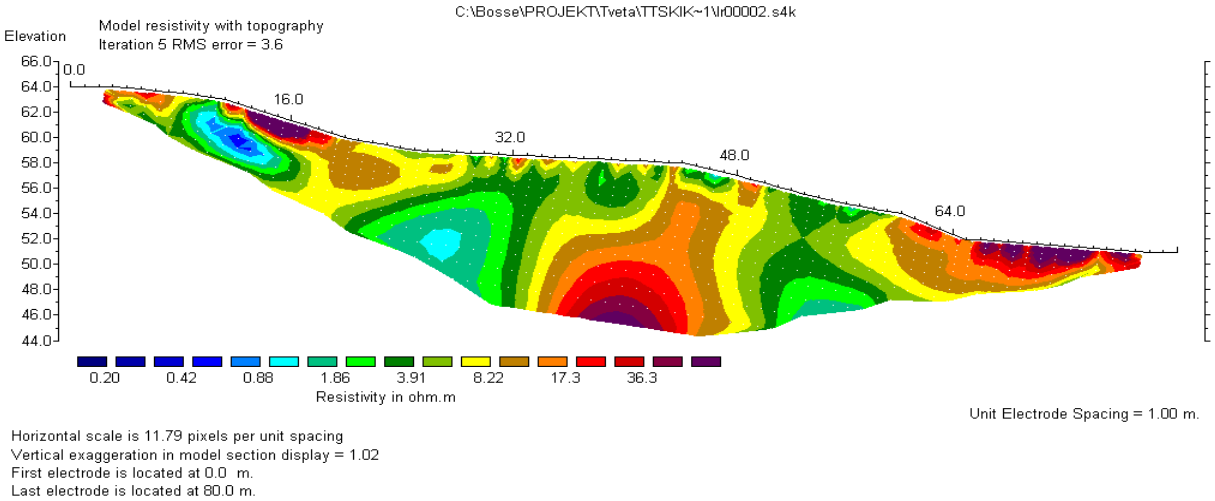

Horizontal scale is 11.79 pixels per unit spacing
Vertical exaggeration in model section display = 1.02
First electrode is located at 0.0 m.
Last electrode is located at 80.0 m.

Fig. 30 Resistivity distribution in 2D inverse modelling — profile 4.

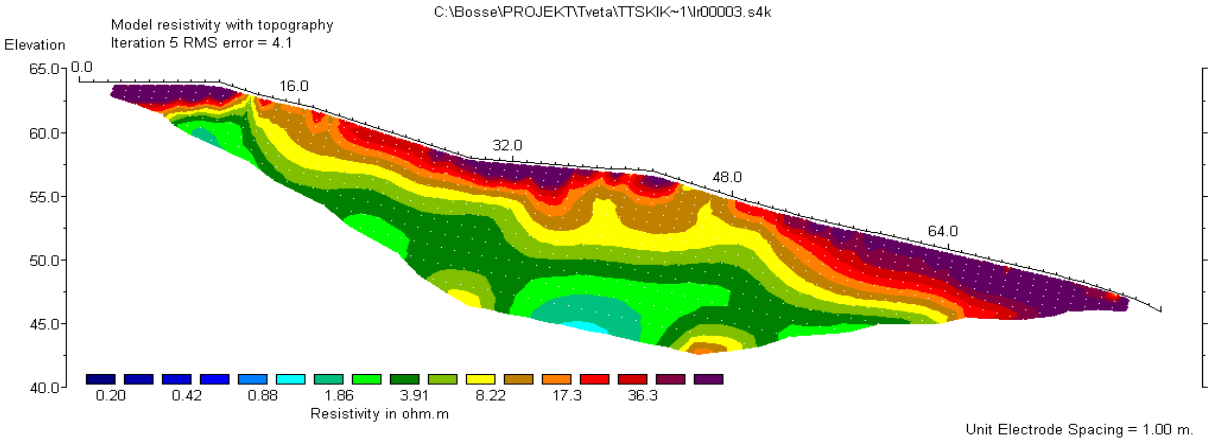

Horizontal scale is 11.79 pixels per unit spacing
Vertical exaggeration in model section display = 1.02
First electrode is located at 0.0 m.
Last electrode is located at 80.0 m.

Fig. 31 Resistivity distribution in 2D inverse modelling — profile 5.

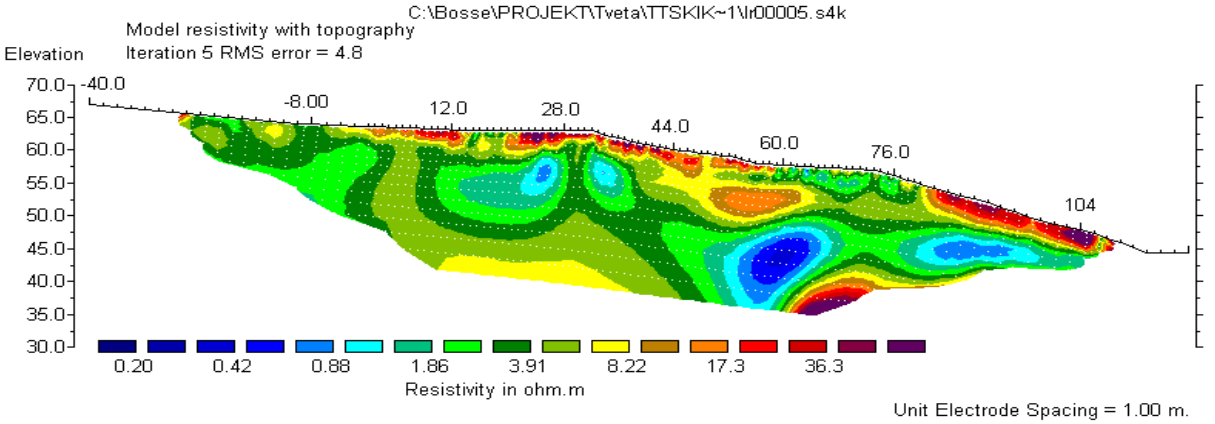

Horizontal scale is 4.53 pixels per unit spacing
Vertical exaggeration in model section display = 1.12
First electrode is located at -40.0 m.
Last electrode is located at 120.0 m.

Fig. 32 Resistivity distribution in 2D inverse modelling — profile 6.

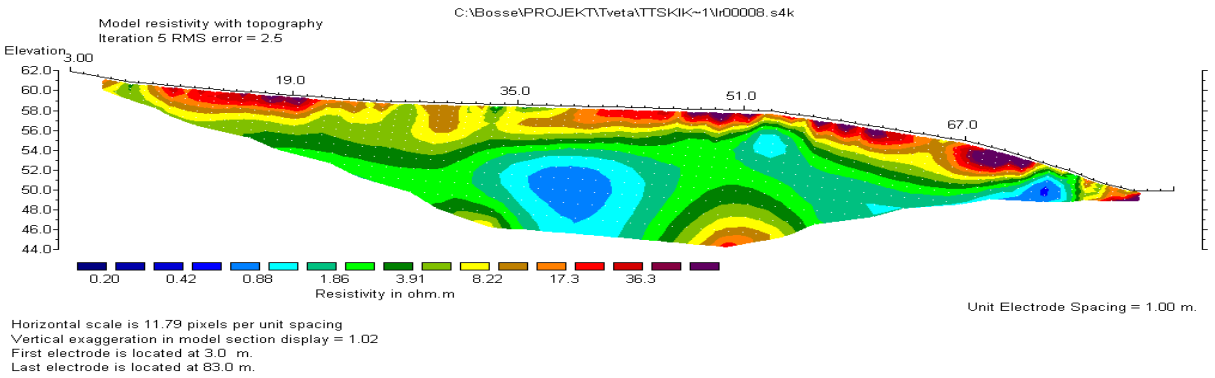

Fig. 33 Resistivity distribution in 2D inverse modelling — profile 7.

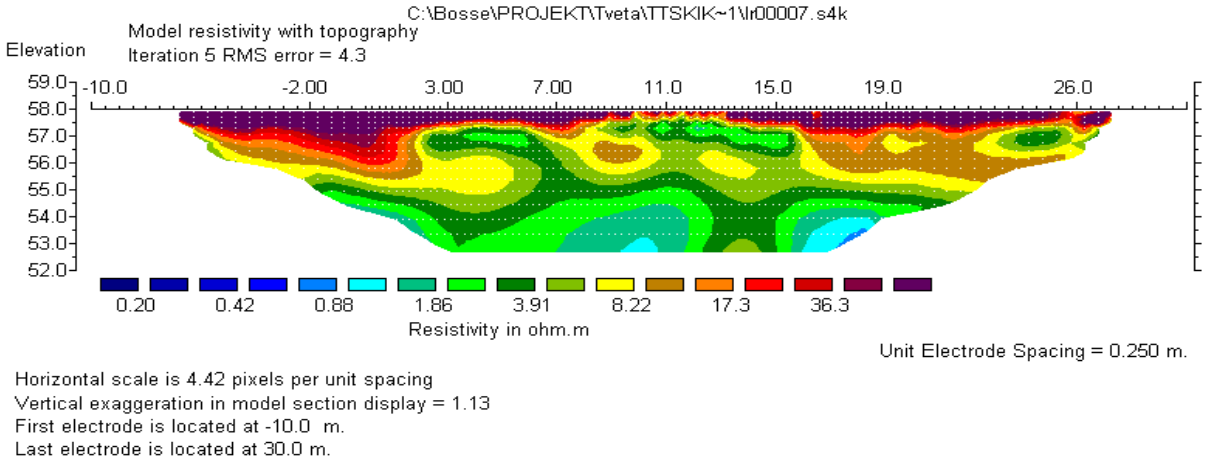

Fig. 34 Resistivity distribution in 2D inverse modelling — profile 8.

3.2 DC Resistivity — 3D model

The three-dimensional model of resistivity distribution has been created in Voxler software (Fig. 35 and 36). Resistivity values were interpolated from the 2D pseudo-sections thus the 3D model may differ from true resistivity values. The resistivity range was converted into the logarithmic scale to get smooth variations (Fig. 36).

Resistivity distribution at different depths was presented to compare insulating properties of coverage sublayers (Fig. 36 - 42). Zones with a low resistivity were marked with a blue colour, areas with high resistivity were red coloured.

3.3 Induced Polarization — 2D model

Induced polarization survey was made along profile 1. Polarization was determined in milliseconds. The data was processed in Res2Dinv, producing an inverse model of chargeability (Fig. 43). It was impossible to identify any infiltration paths from the model. Most of the chargeability contrast was due to a high ion concentration in the waste pile. Since the water infiltration along profile 1 had a low impact on the collected IP data no additional IP measurements were taken.

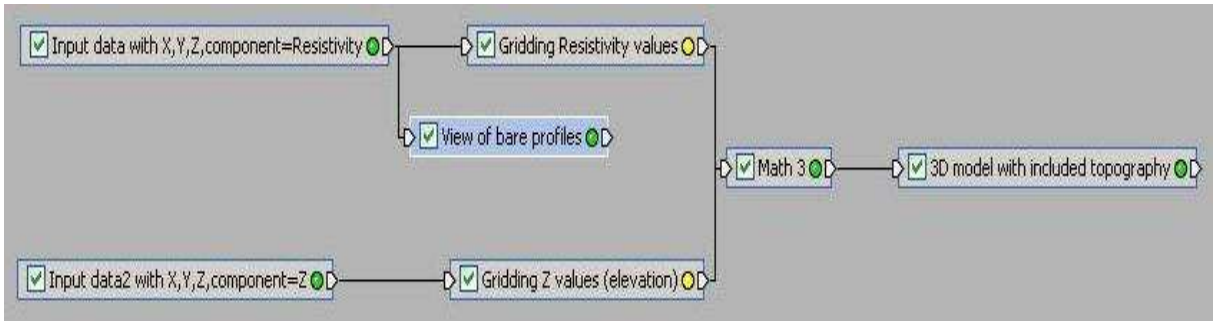

Fig. 35 Diagram displaying connection between input and output data in 3D model.

3.4 Ground penetrating radar — graphic profiles after filtering

The GPR survey was made with a shielded 250 MHz and unshielded 100 MHz antennas. The output of both surveys was filtered and graphically displayed in RAMAC GroundVision software (Fig. 44 - 51). The quality of raw data was not improved significantly. Most of the emitted radiation has been attenuated. The remaining energy has been reflected from such objects as pipes or hoses. Conductivity of coverage was too high, probably due to the high salt content of the ashes.

3.5 Presentation of 3D model with included topography

The 3D simulation of the slope has been created in Voxler (Fig. 52). Uniform colour was selected to emphasize the shape of the slope. Resistivity profiles were marked with violet colour. The projected slope had a limited accuracy. The shelf was insufficiently flat. The interface between the shelf and the small slope along profile 8 was too steep. However, the most important conditions were well represented. For example, the elevation decreases towards east and the areas 1, 2, 3, 4 were steeper than areas 6, 7.

3.6 DC resistivity — 3D model - masking of area with resistivity below 6.3 Ωm

Masking of low resistivity regions has been done in order to visualize the increase of highly conductive areas with the increasing depth. Resistivity of 6.3 Ωm was selected as a minimum value marked on the 3D model. This value was chosen because, according to resistivity models in section 3.1 "DC Resistivity – 2D inverse models" (Fig. 27 - 34), the approximate resistivity at the depth 4.5 m (coverage-waste pile interface) is in a range 4-8 Ωm. This interface was represented by a yellowish-green colour. Values lower than 6.3 Ωm were typical for the waste pile, thus were regarded as conductive. Furthermore, changes in resistivity distribution were the most visible at the value of 6.3 Ωm. Zones with resistivity below 6.3 Ωm were blanked. Masking involved interfaces of all sublayers (Fig. 53 — 59).

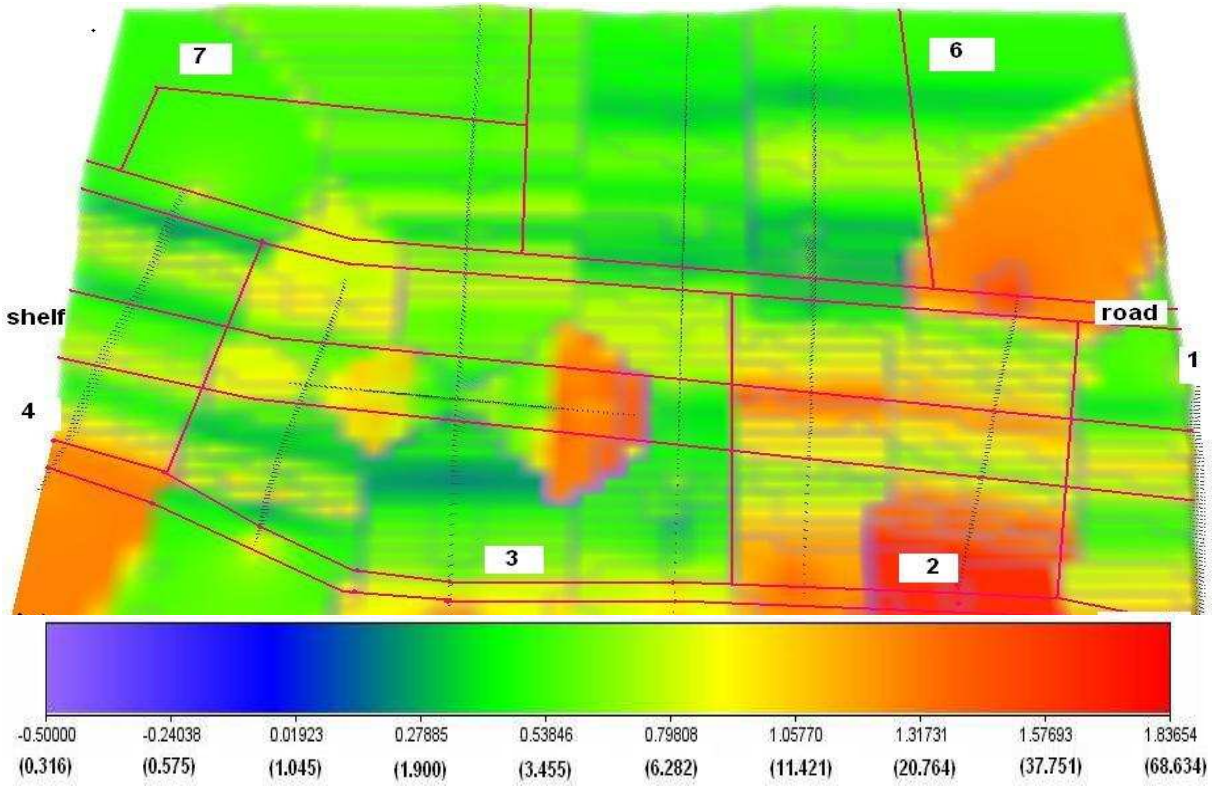

Fig. 36 3D model of resistivity distribution at surface, processed in Voxler - plane view. The pink lines indicate roads, flat shelf and borders of studied areas. Resistivity range for 3D model is given in Ωm. Logarithmic values are in the upper row. Normal values are in lower row, in brackets. Resistivity range is common to figures 36 — 42.

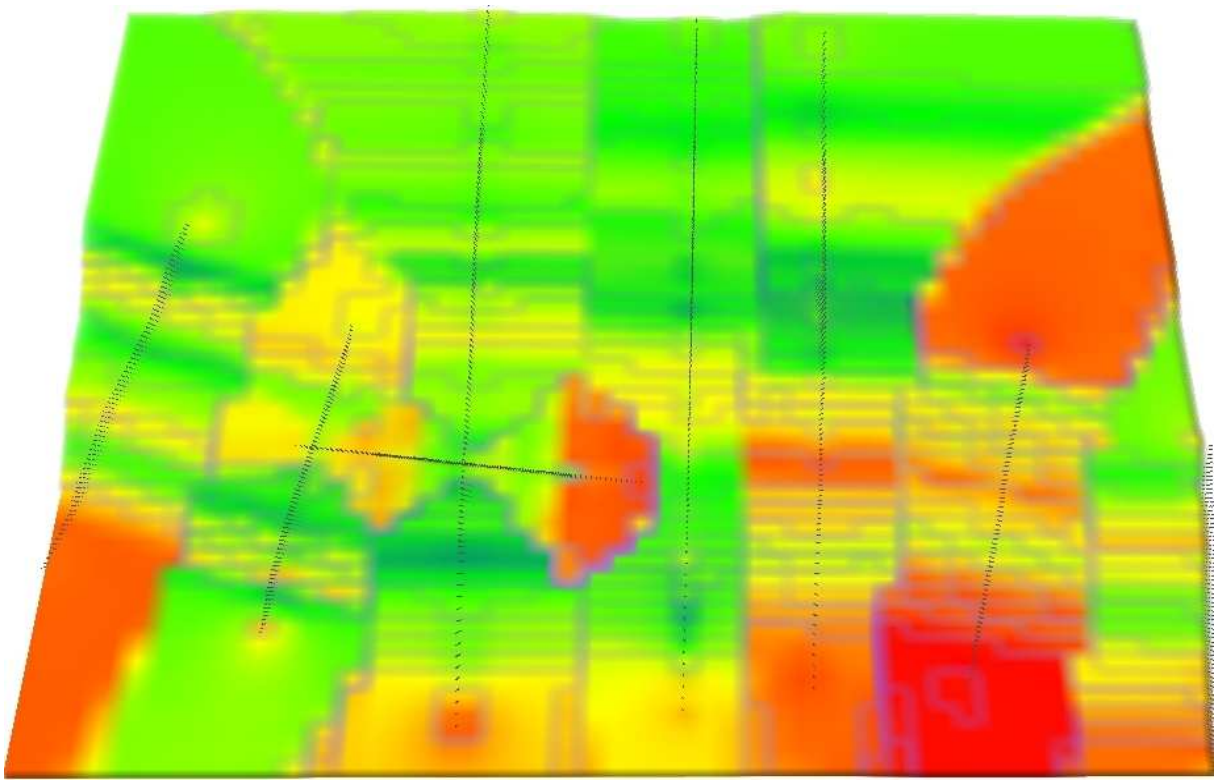

Fig. 37 3D model of resistivity distribution at the depth 30 cm (vegetation-protection interface).

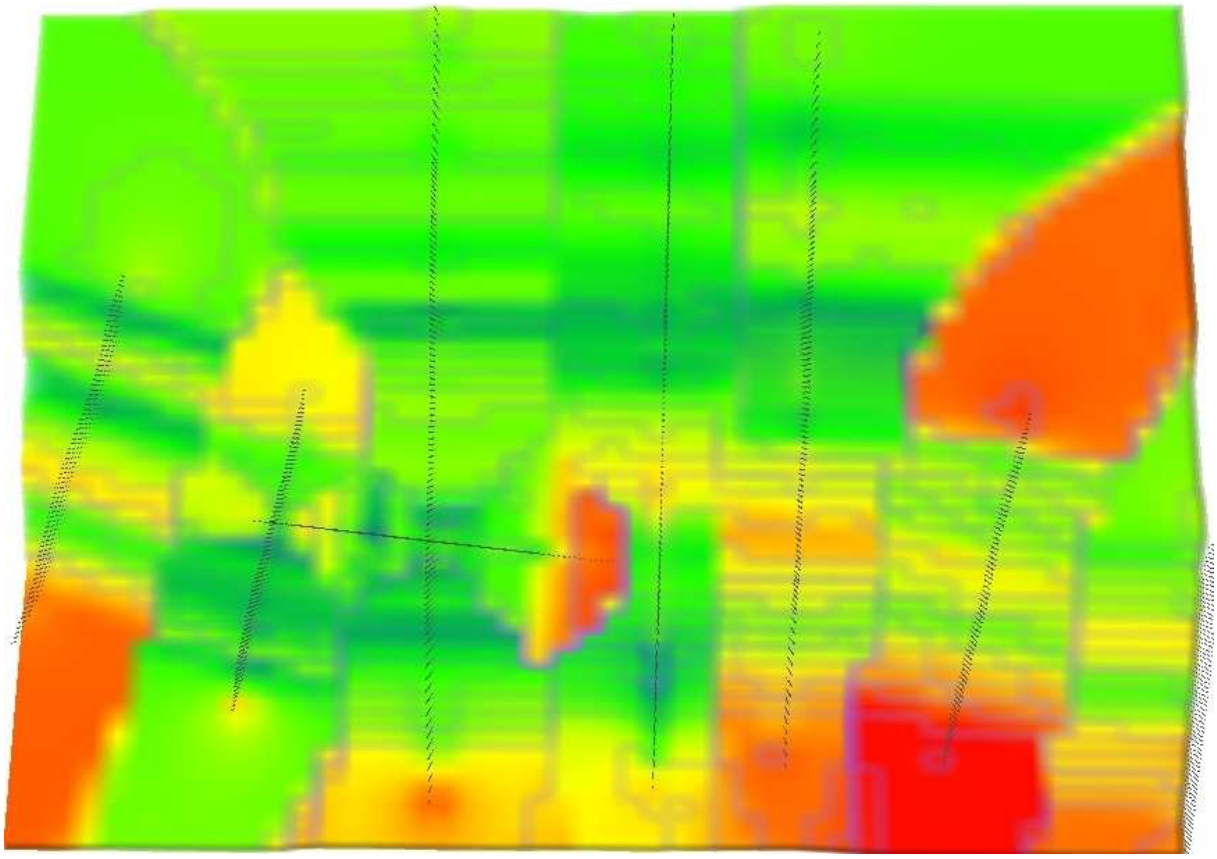

Fig. 38 3D model of resistivity distribution at the depth 180 cm (protection-drain interface).

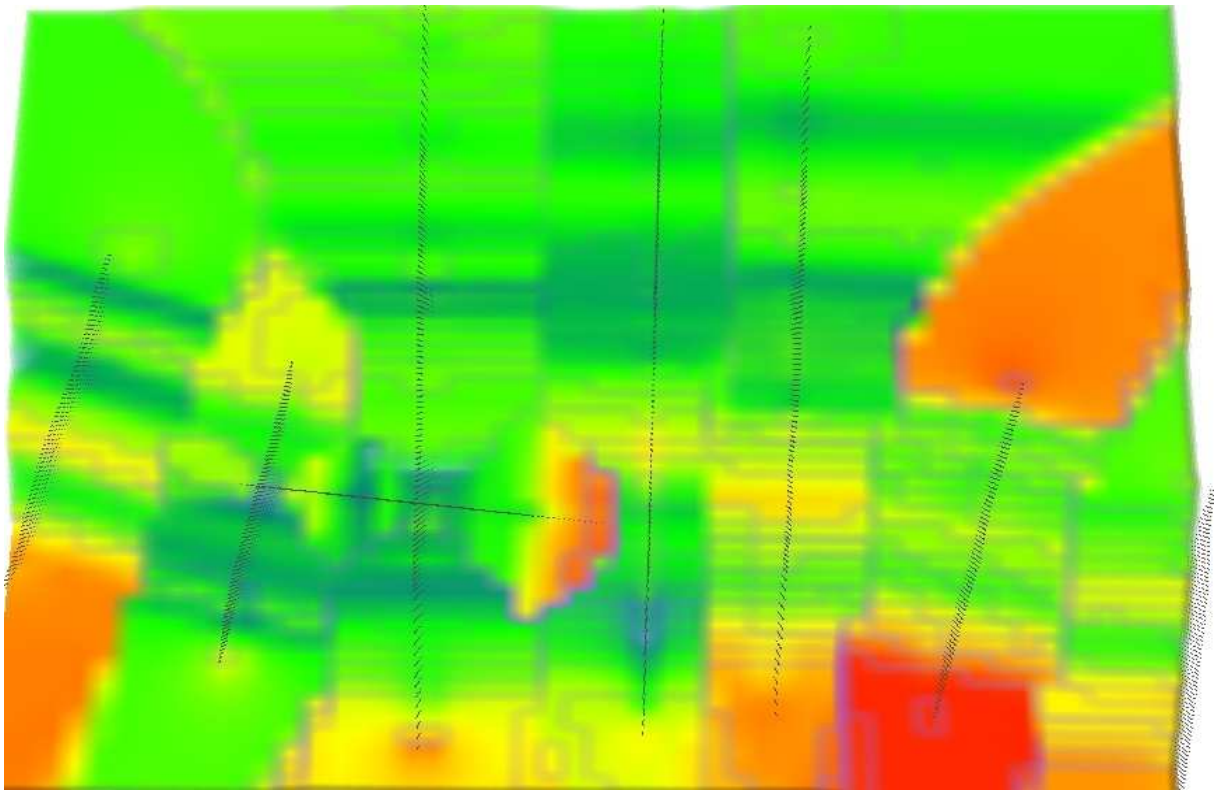

Fig. 39 3D model of resistivity distribution at the depth 210 cm (drain-impermeable interface).

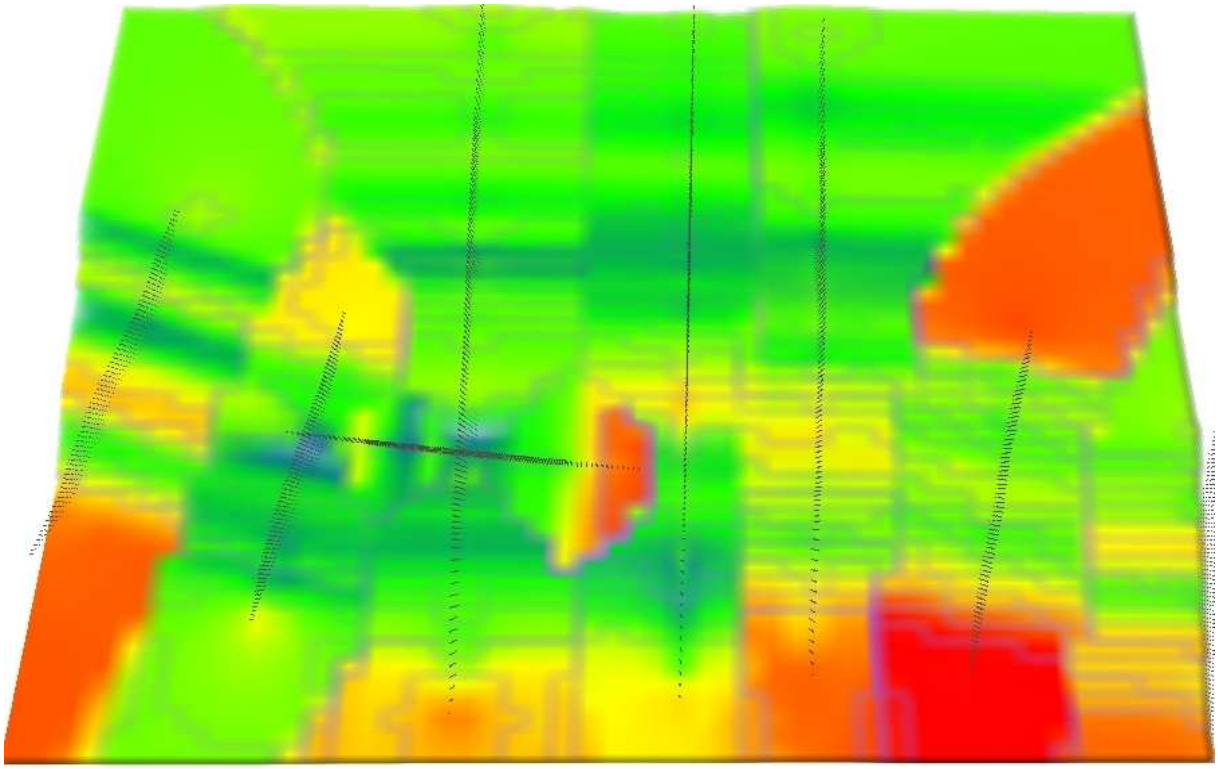

Fig. 40 3D model of resistivity distribution at the depth 310 cm (impermeable-foundation interface).

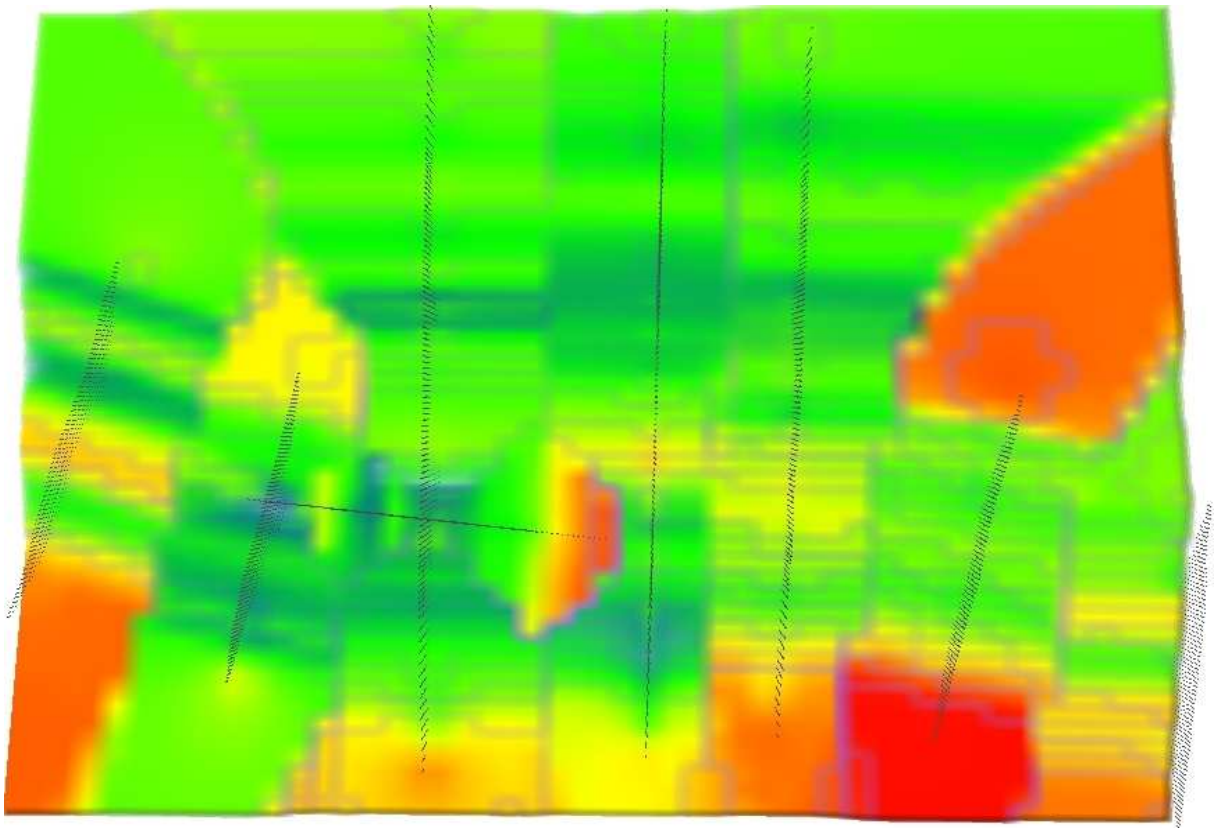

Fig. 41 3D model of resistivity distribution at the depth 340 cm (foundation-waste interface).

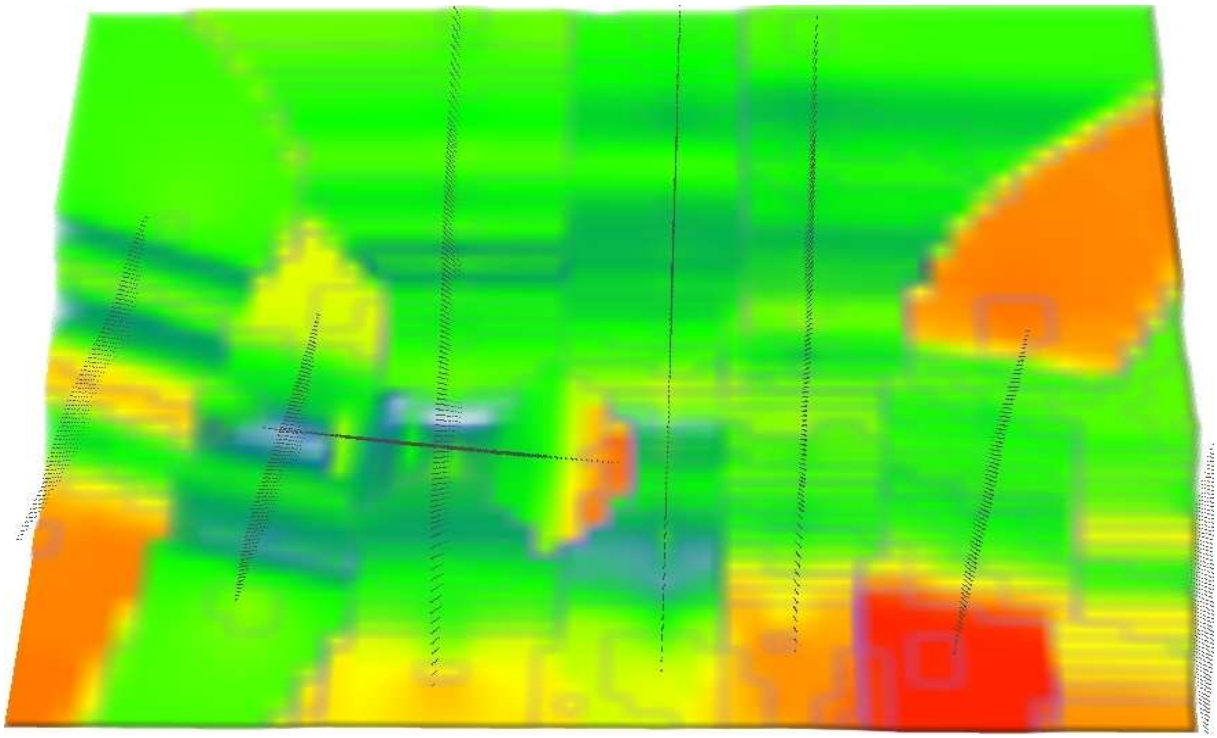

Fig. 42 3D model of resistivity distribution at the depth 450 cm (waste).

3.7 Conductivity distribution — 3D model

Model of conductivity distribution, processed in Voxler, was made in order to visualize zones with elevated conductivity. Data was processed in a similar way as for DC resistivity distribution, presented in section 3.2 "DC Resistivity — 3D model". The difference was that resistivity values were converted into conductivity values, according to equation: $\sigma = \varrho^{-1}$, where resistivity ϱ is inversely proportional to conductivity σ. The range of conductivity values was low so use of a numerical scale was sufficient. Bluish-green spots, which have been circled with red polygons, corresponded to zones with elevated conductivity (Fig. 60 — 66).

3.8 Conductivity isosurfaces — 3D model

Conductivity distribution has been divided into a few isosurfaces with different conductivity domains. Conductivity values were taken from resistivity values, in analogical way as for conductivity distribution in section 3.7 "Conductivity distribution — 3D model". Isosurfaces with conductivity higher or equal to 0.8, 1.0, 1.2, 1.5 and 2.0 Siemens per meter have been created (Fig. 67 — 73). Isosurfaces were marked with black colour.

4. Discussion

This section contains comments and interpretation of figures presented in the chapter Results.

4.1 DC resistivity — 2D modelling

The data source was the same for the 2D inverse models as for the 3D model but resistivity distribution was presented as cross-sections instead of a plane view. Precision of the topographical values was limited due to GPS inaccuracy. Longer profiles had higher penetration depth while profiles with denser electrode arrays provided preciser measurements.

The general tendency in resistivity distribution along the profiles could be defined. Conductivity increased vertically (Fig. 74). In the uppermost four meters resistivity ranged from 10-40 Ωm at surface down to 4-8 Ωm at the bottom. Comparing to natural materials, resistivity was low, similar to properties of wet clay. This layer could be identified as the landfill coverage and the low resistivity was probably because the covering was partly made of ash with a high salt content. Below a depth of four meters resistivity generally decreased down to a fraction of 1 Ωm. This was probably due to higher contamination of water percolated through the waste pile.

Zones with low resistivity have been identified at several locations along the profiles, such as the flat shelf zone (Fig. 75), where the natural density driven water flow was at minimum and at some nodes (Fig. 76), probably due to deformation of the lining caused by mass transport downwards. Low resistivity also occurred above the protection sublayer, which had lower porosity than the vegetation layer, hence water was accumulated at surface (Fig. 77). The RMS error of the inverse models after five iterations, ranged between 2.3 % and 8.9% which was regarded as fairly good quality of raw resistivity data

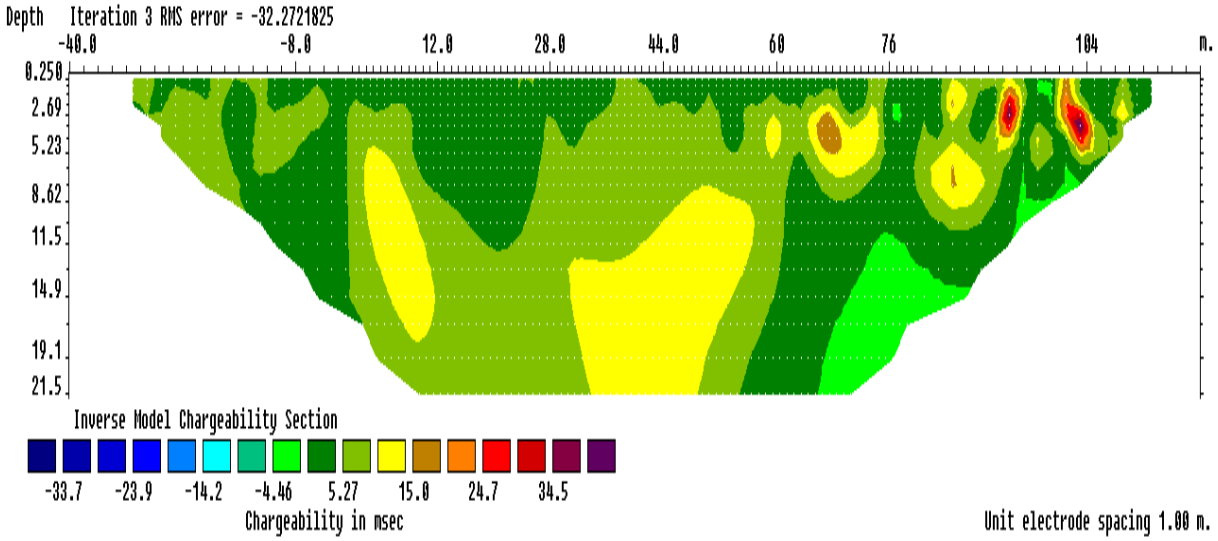

Fig. 43 Chargeability distribution in 2D inverse modelling — profile 1.

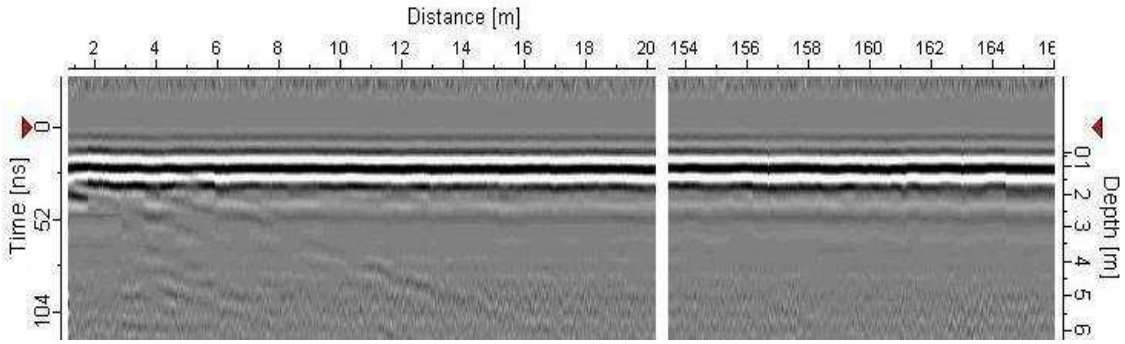

Fig. 44 GPR graphic display along profile 1 with 100 MHz antenna.

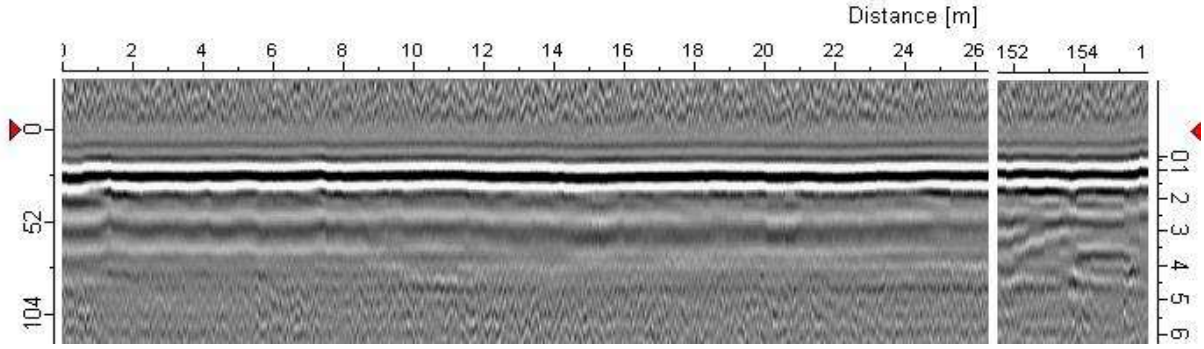

Fig. 45 GPR graphic display along profile 2 with 100 MHz antenna.

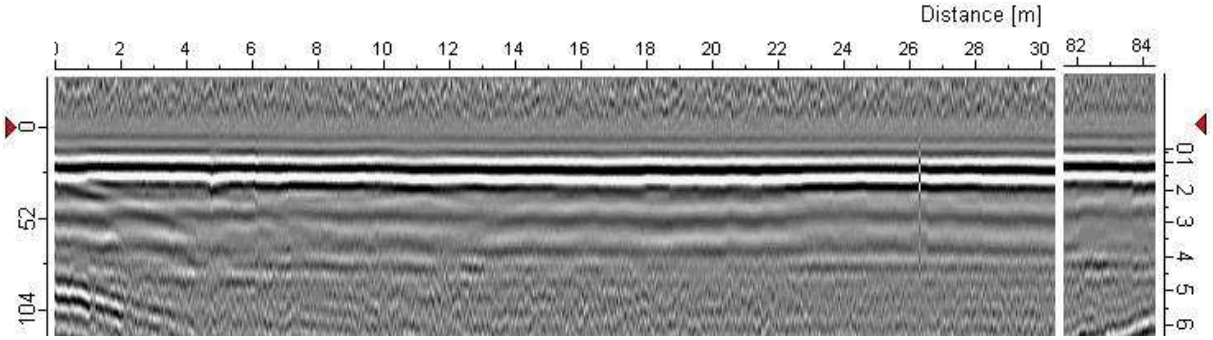

Fig. 46 GPR graphic display along profile 3 with 100 MHz antenna.

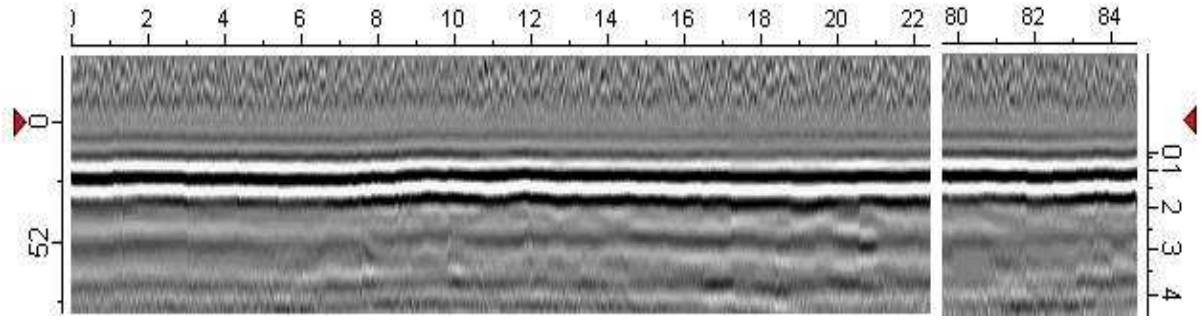

Fig. 47 GPR graphic display along profile 4 with 100 MHz antenna.

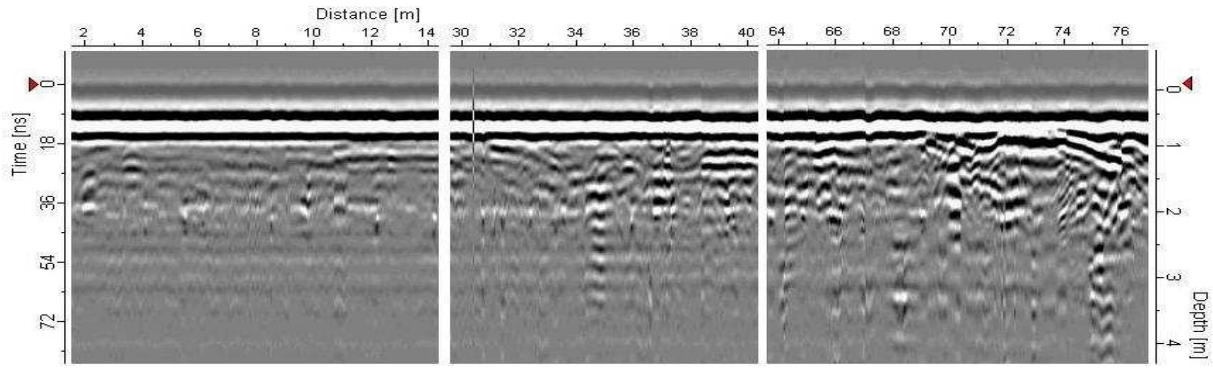

Fig. 48 GPR graphic display along profile 5 with 250 MHz antenna.

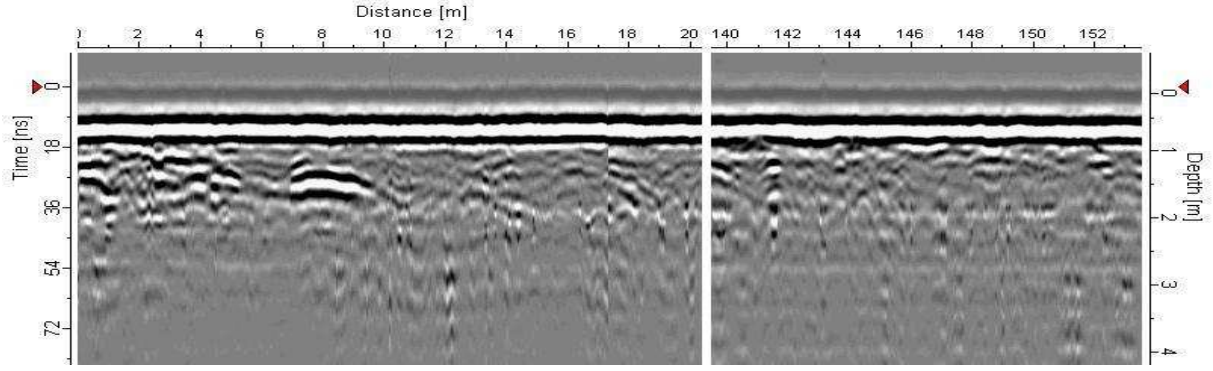

Fig. 49 GPR graphic display along profile 6 with 250 MHz antenna.

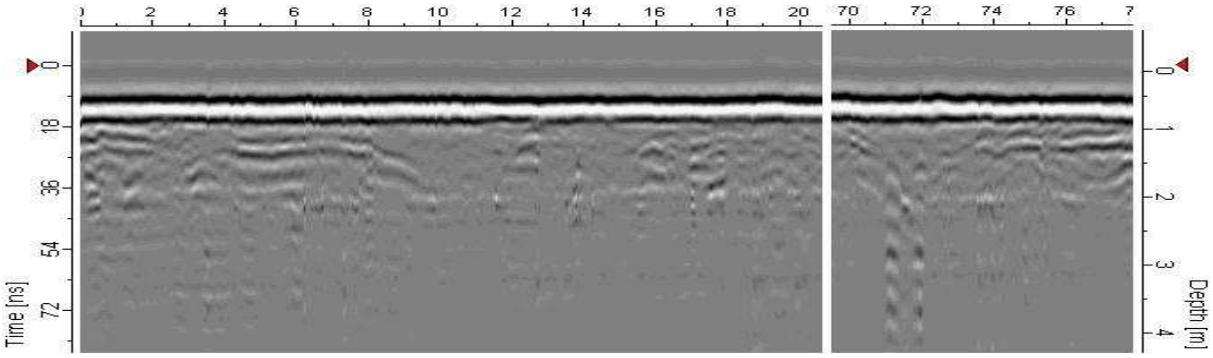

Fig. 50 GPR graphic display along profile 7 with 250 MHz antenna.

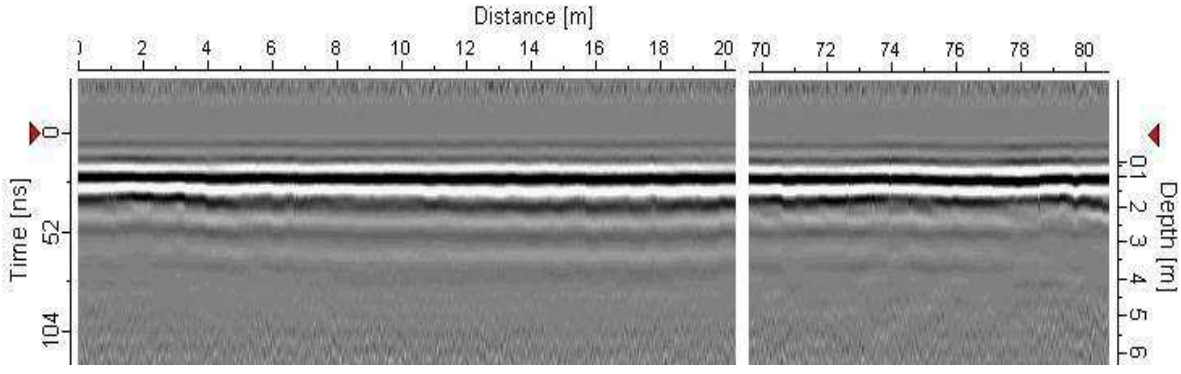

Fig. 51 GPR graphic display along profile 8 with 100 MHz antenna.

Table 4 Collected GPS data.

GPS data:				
Profile:	Start Points		End Points	
	North	East	North	East
1	6558682	1601337	6558682	1601488
2	6558754	1601345	6558749	1601481
3	6558824	1601436	6558823	1601497
4	6558625	1601391	6558603	1601459
5	6558791	1601416	6558778	1601481
6	6558727	1601340	6558724	1601485
7	6558659	1601412	6558645	1601471
8	6558650	1601436	6558716	1601443

4.2 DC resistivity — 3D model

The three-dimensional model of the resistivity distribution has been created in Voxler. Logarithmic scale was applied in the resistivity range to get smooth variations (Fig. 36). Thickness of coverage sublayers has been given in intervals (Table 6, Fig. 78). Minimal values of thickness have been selected in this project. This assumption could influence interpretation of resistivity values in 3D model since sublayers along slope did not have uniform thickness. For example resistivity distribution at 220 cm was assigned to impermeable layer. (210 cm — 310 cm). If thickness of sublayers overlaying drain layer were in total thicker more than 10 cm than minimum values (Fig. 78) then resistivity distribution at 220 cm would in fact belong to drain layer (180 cm — 210 cm).

Resistivity values in the 3D model have been interpolated from the 2D modelled sections which only covered a minor part of the area. Furthermore, the profiles did not have equal length, hence some parts of areas 1, 4 and 6 were extrapolated orders. However, the presented model was assumed to be sufficient to get a general picture of the resistivity in those areas.

Generally, vertical resistivity tendency could be characterized as:

- increased resistivity at vegetation layer, caused by circulation of water with a low salinity or less water content due to plant uptake and evaporation (Fig. 37);
- reduced resistivity at the protection layer, probably due to water retention (Fig. 38);
- further decreased resistivity at the drainage layer, caused by water collection in the drainage system (Fig. 39);
- increased resistivity at the impermeable layer, probably due to removal of drain water, low porosity and good insulating properties of the layer (Fig. 40);
- decreased resistivity at the foundation layer, caused by a higher porosity of sand grains compared to the structure of the impermeable layer (Fig. 41);

Table 5 Converted GPS data into map coordinates (subtracting constant values).

GPS data converted into map coordinates (X – 6558500, Y – 1601200)				
Profile:	X new start	Y new start	X new end	Y new end
1	182	137	182	288
2	254	145	249	281
3	324	236	323	297
4	125	191	103	259
5	291	216	278	281
6	227	140	224	285
7	159	212	145	271
8	216	243	150	236

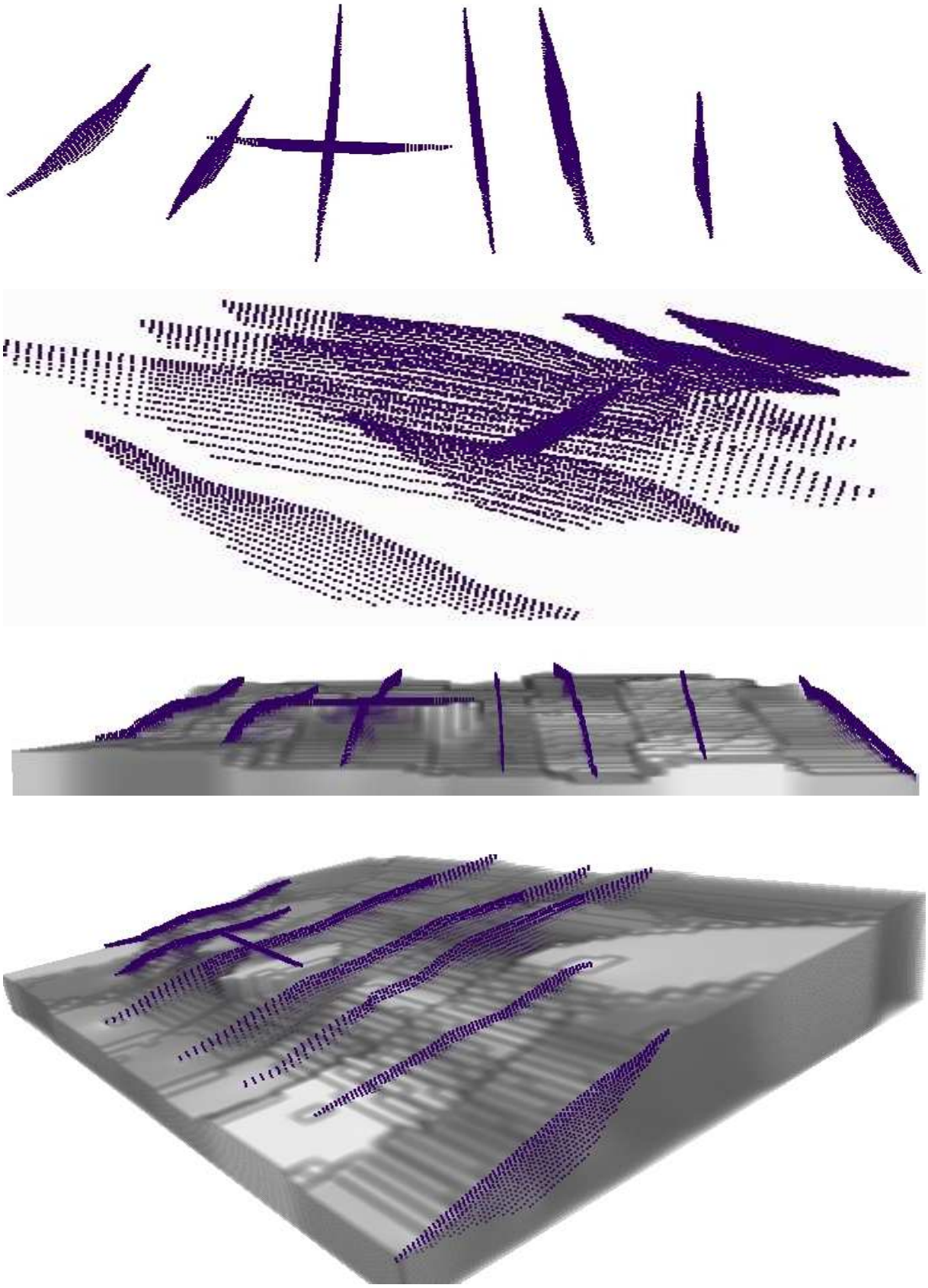

Fig. 52 Visualization of profiles and interpolated 3D model in Voxler.

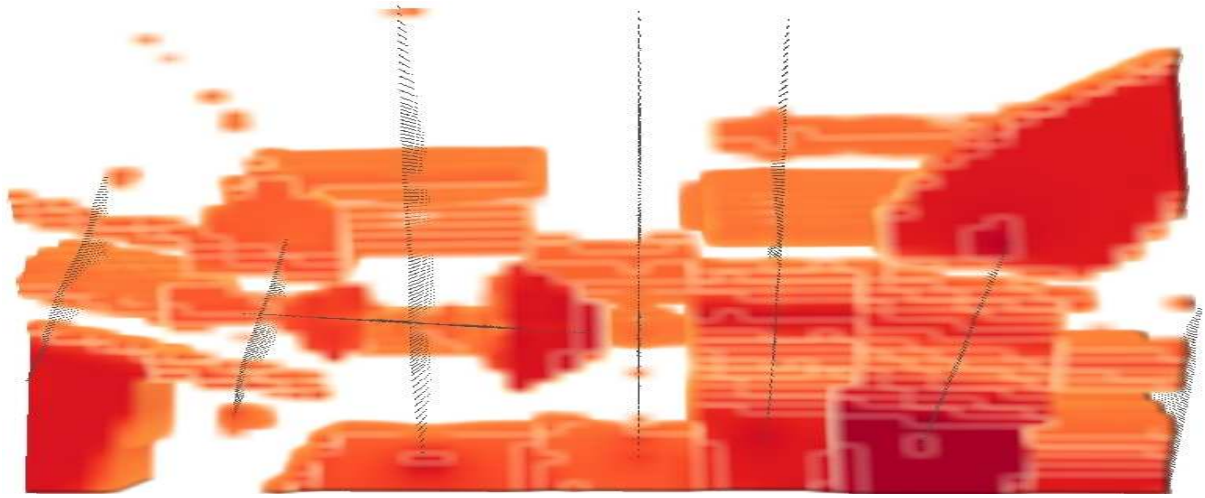

Fig. 53 Distribution of resistivity higher than 6.3 Ωm at surface.

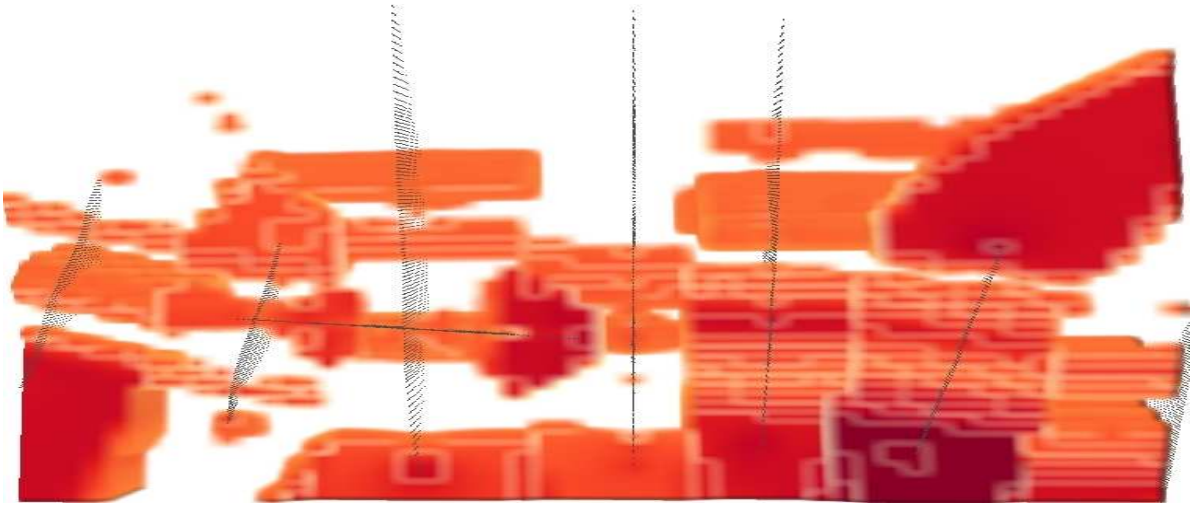

Fig. 54 Distribution of resistivity higher than 6.3 Ωm at the depth 30 cm.

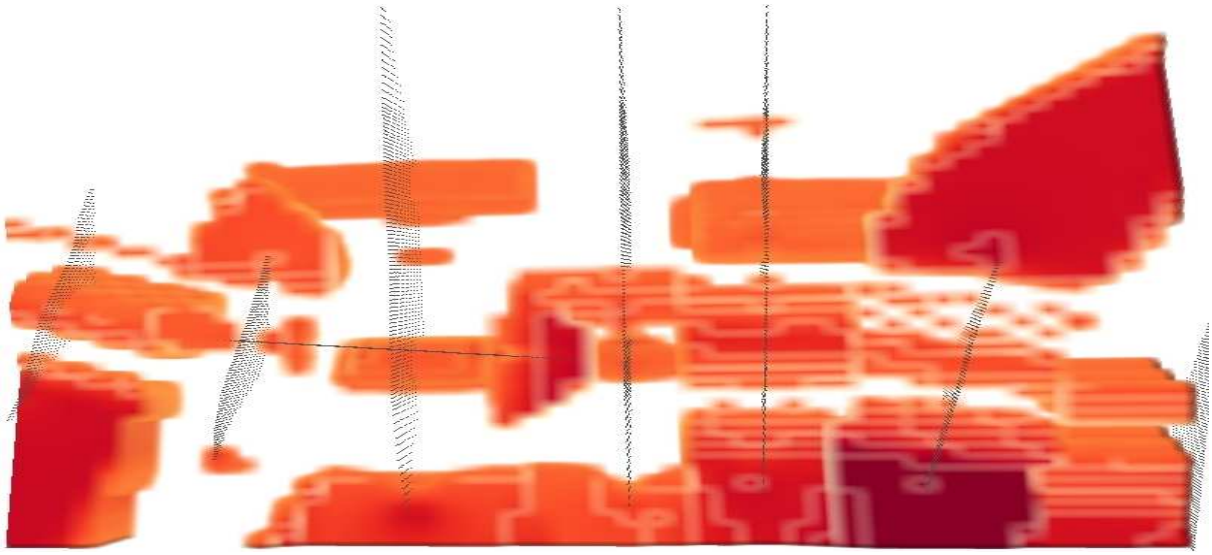

Fig. 55 Distribution of resistivity higher than 6.3 Ωm at the depth 180 cm.

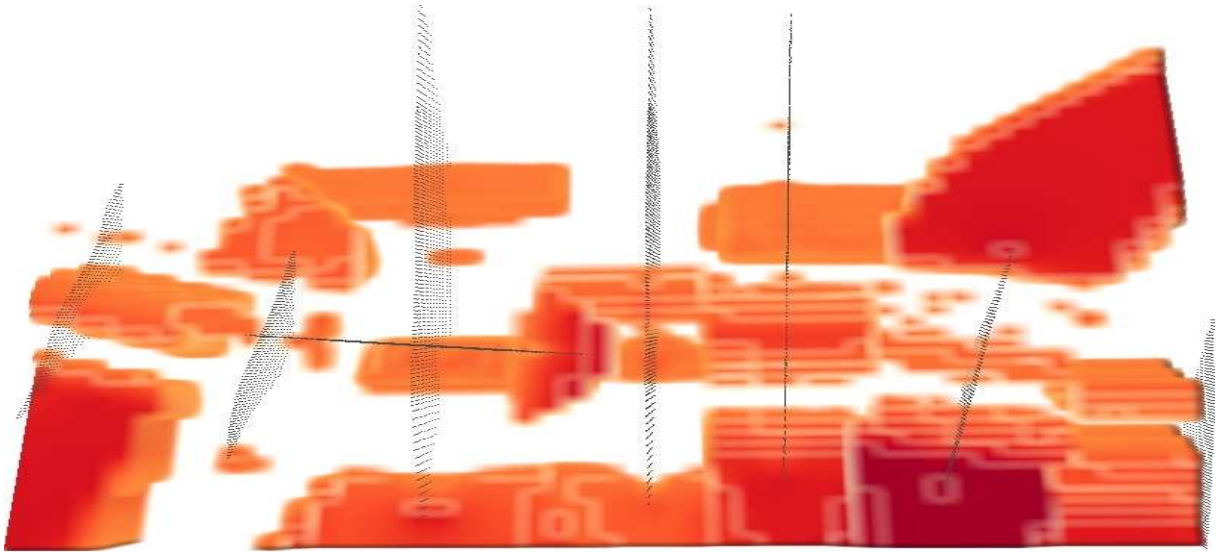

Fig. 56 Distribution of resistivity higher than 6.3 Ωm at the depth 210 cm.

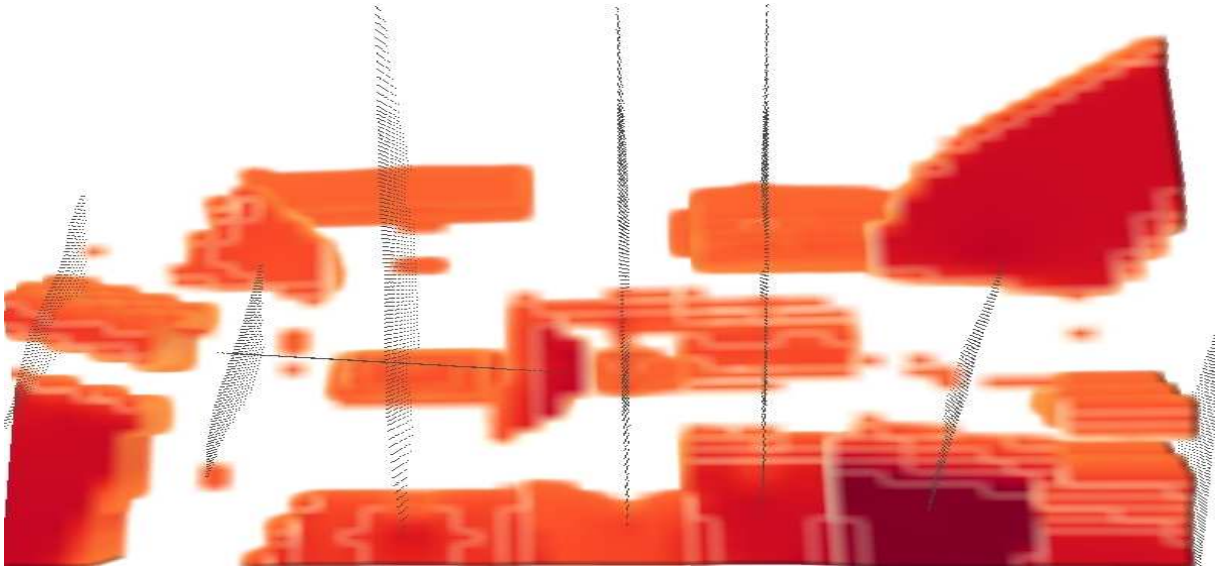

Fig. 57 Distribution of resistivity higher than 6.3 Ωm at the depth 310 cm.

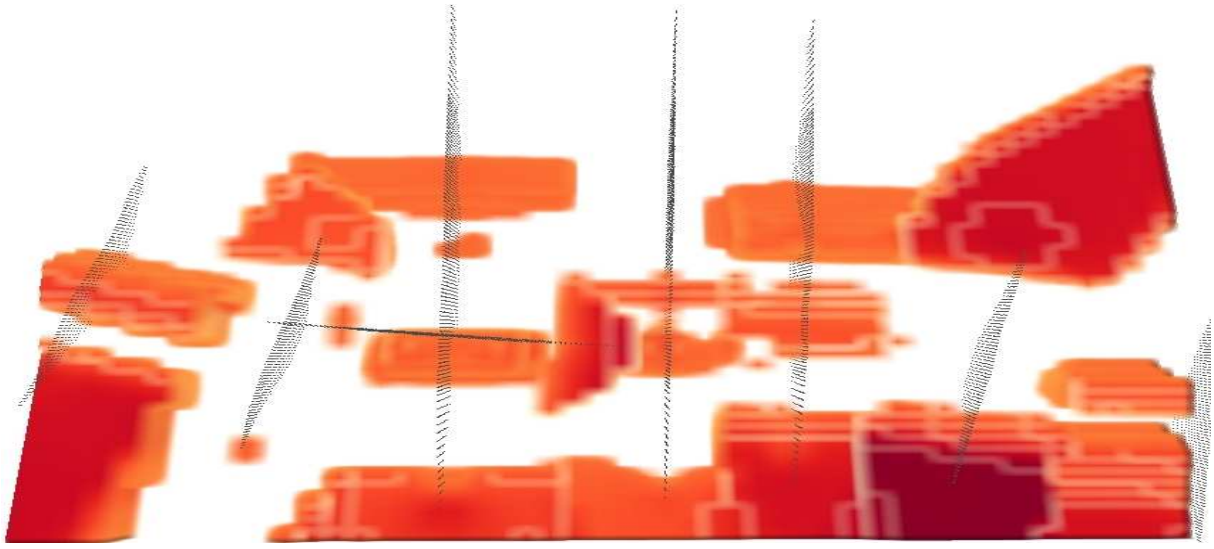

Fig. 58 Distribution of resistivity higher than 6.3 Ωm at the depth 340 cm.

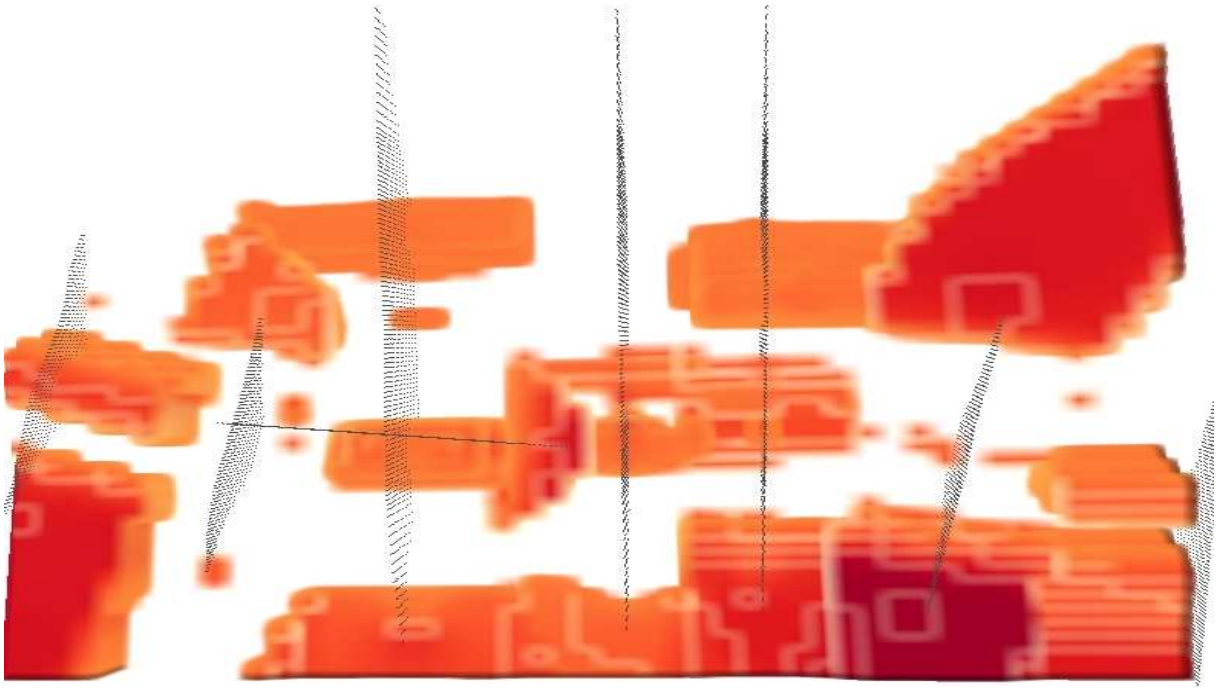

Fig. 59 Distribution of resistivity higher than 6.3 Ωm at the depth 450 cm.

Area 1 had the most stable resistivity values throughout the landfill coverage. There were no zones with decreased resistivity which could be regarded as a coverage puncture due to mass transport downwards. The 3D pseudo model covered only half of the area 1 and area 4 because interpolation could not be processed at the external parts of those areas (Fig. 36). The highest resistivity has been detected at the area 2. This was confirmed by very low values of lysimeter records (Table 1). The lowest resistivity has been recorded at the area 3 and lower part of area 6 and area 7 (Fig. 36 — 42). Elevated conductivity at the lower part of area 6 and area 7 could be due to accumulation of collected drain water in the eastern part of those areas. Elevated conductivity at the area 3 could be due to minimum run-off at the shelf or deformation of the coverage due to mass transfer, especially at the shelf-slope interface where the slope profile was not smooth enough.

The general tendency was equal for all surveyed areas. The sign of resistivity change was the same along the whole slope, though some zones reacted more significantly. This could indicate that layers had similar properties (Fig. 79). Resistivity variations were present even at the vegetation layer (Fig. 36 and 37). This could be interpreted that not composition but hydraulic conditions was a predominating factor for insulating properties of the liner. The resistivity at the bottom of the impermeable layer (Fig. 40) was lower than at the drain-impermeable layer interface (Fig. 39) but it was still higher than at the vegetation layer (Fig. 37). The most stable resistivity through the lining has been recorded at the area 1 and area 2 (Fig. 36 — 42). Perhaps these were the most suitable lining prototypes? Potential reasons for such effect could be a higher thickness of lining, better insulating properties of components (Fig. 79) or less steep profiles of the slope along area 1 and area 2.

4.3 Induced Polarization

It was possible to detect a waste pile with induced polarization surveying (Fig. 43). However, chargeability of infiltrated water was insufficient. Paths of percolated water could not be identified with IP. Both GPR and IP measurements could not be used as a reference method for DC resistivity surveying.

4.4 GPR

It was expected that the infiltration flow paths would be detected by an increased attenuation of emitted radiation. 250 MHz antenna provided insufficient penetration depth so 100 MHz antenna has been used instead. Penetration depth has increased from approximately 1.5 m to 3 m. It was possible to distinguish layers interfaces, disturbances, lysimeters, the road, especially from 250 MHz radargrams. However, the penetration depth was still insufficient. Impermeable layer, the most interesting part of subsurface for this project, was not still displayed on radargrams.

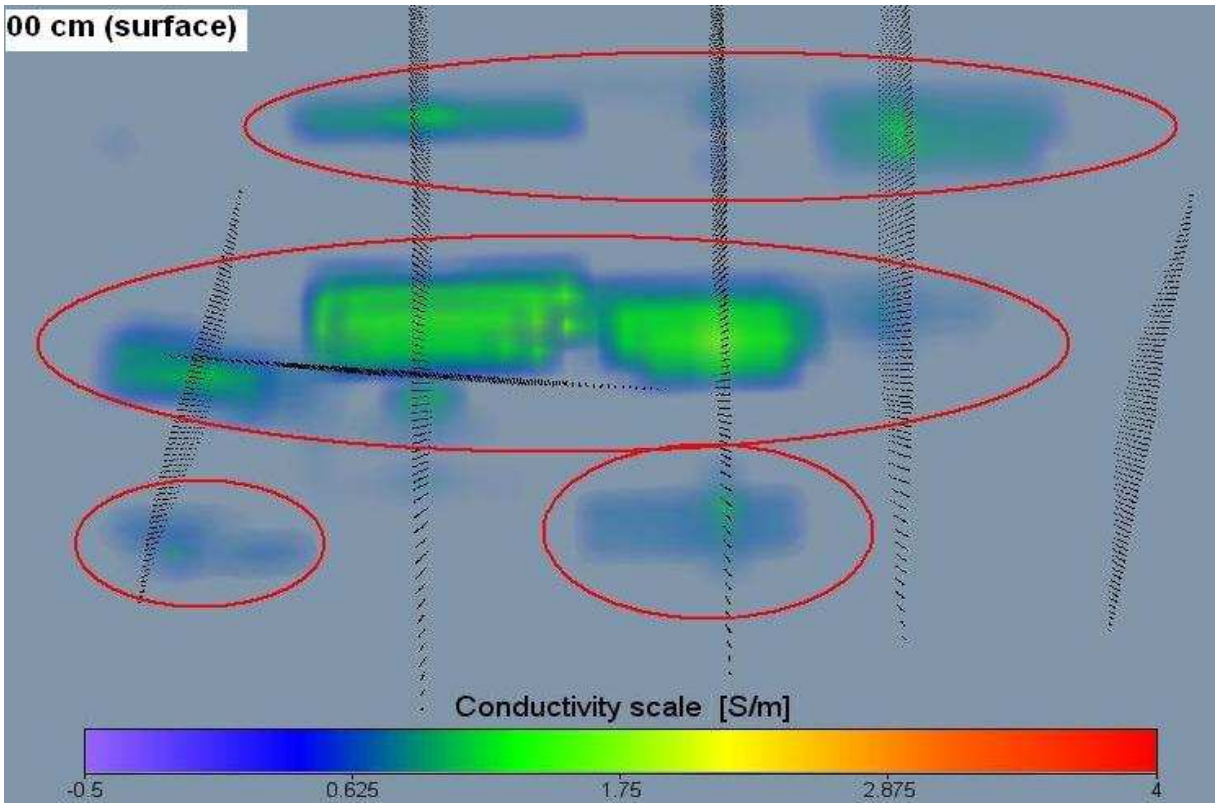

Fig. 60 Conductivity distribution at the slope surface. Regions with elevated conductivity were circled with red polygons.

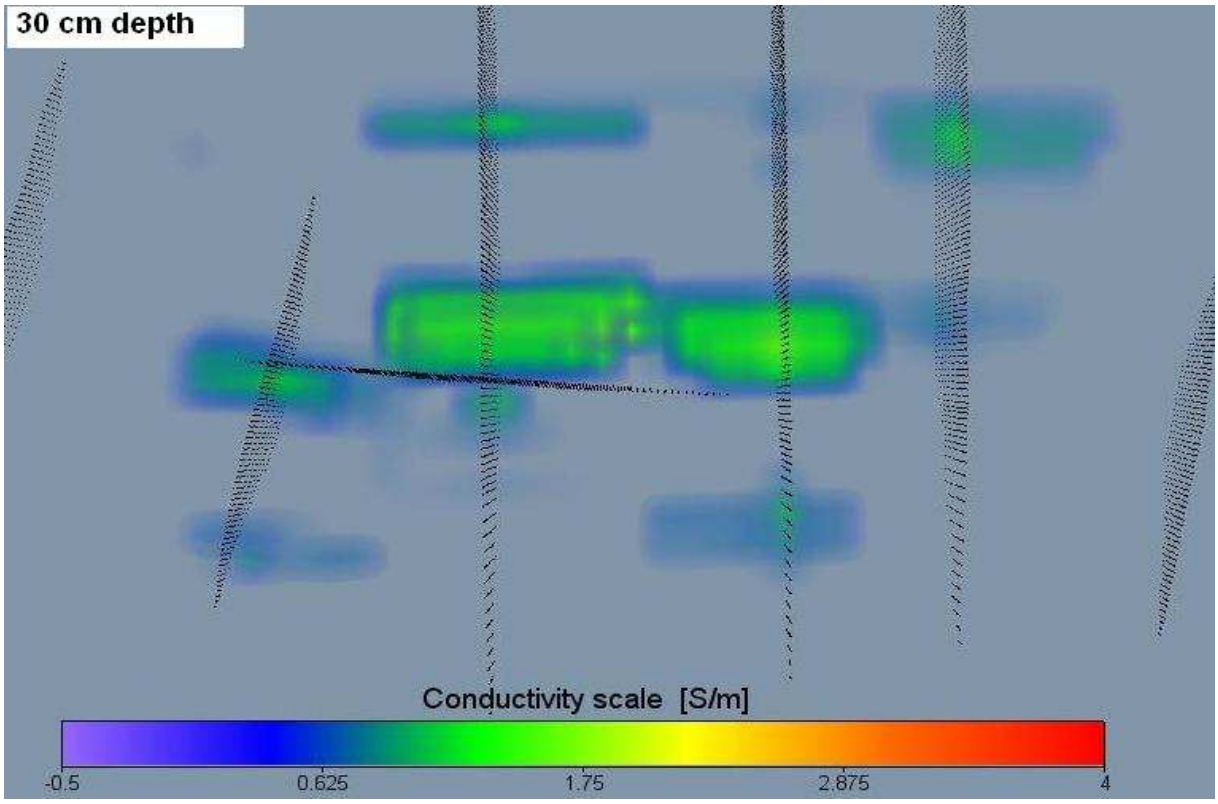

Fig. 61 Conductivity distribution at the depth 30 cm.

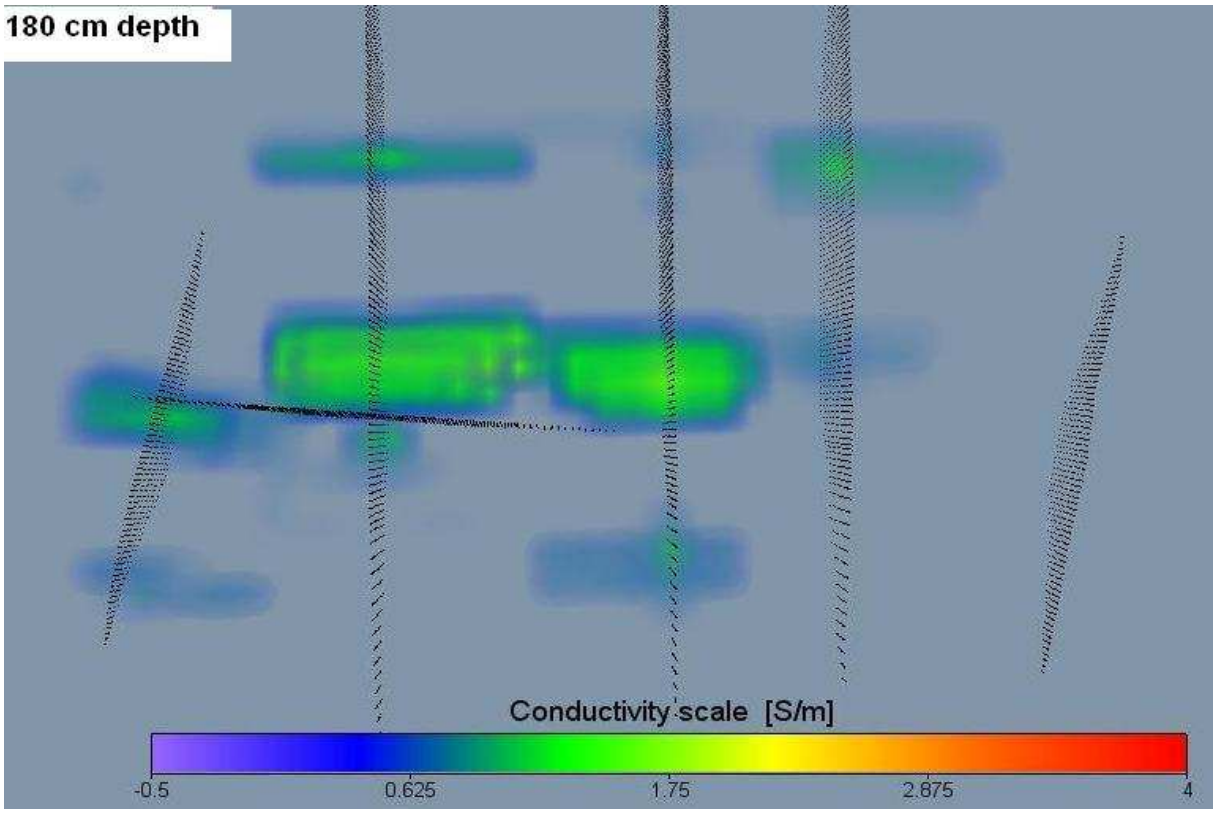

Fig. 62 Conductivity distribution at the depth 180 cm.

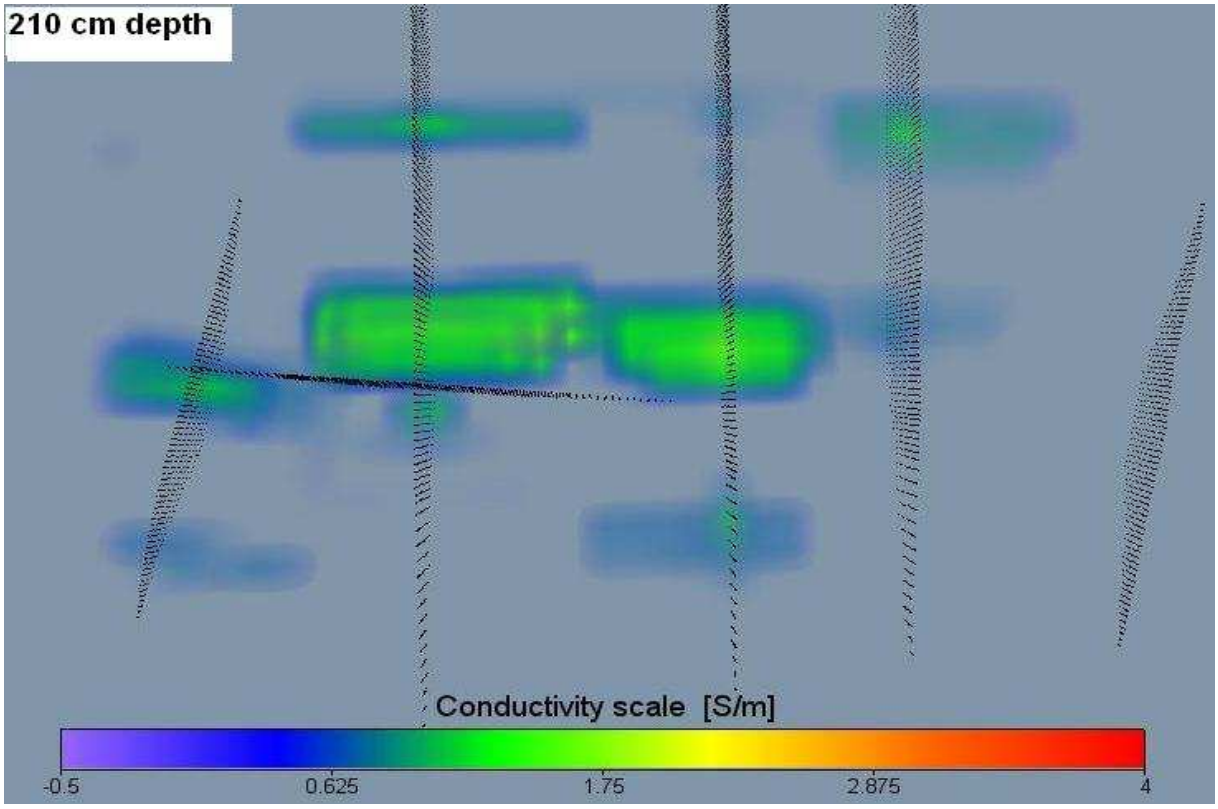

Fig. 63 Conductivity distribution at the depth 210 cm.

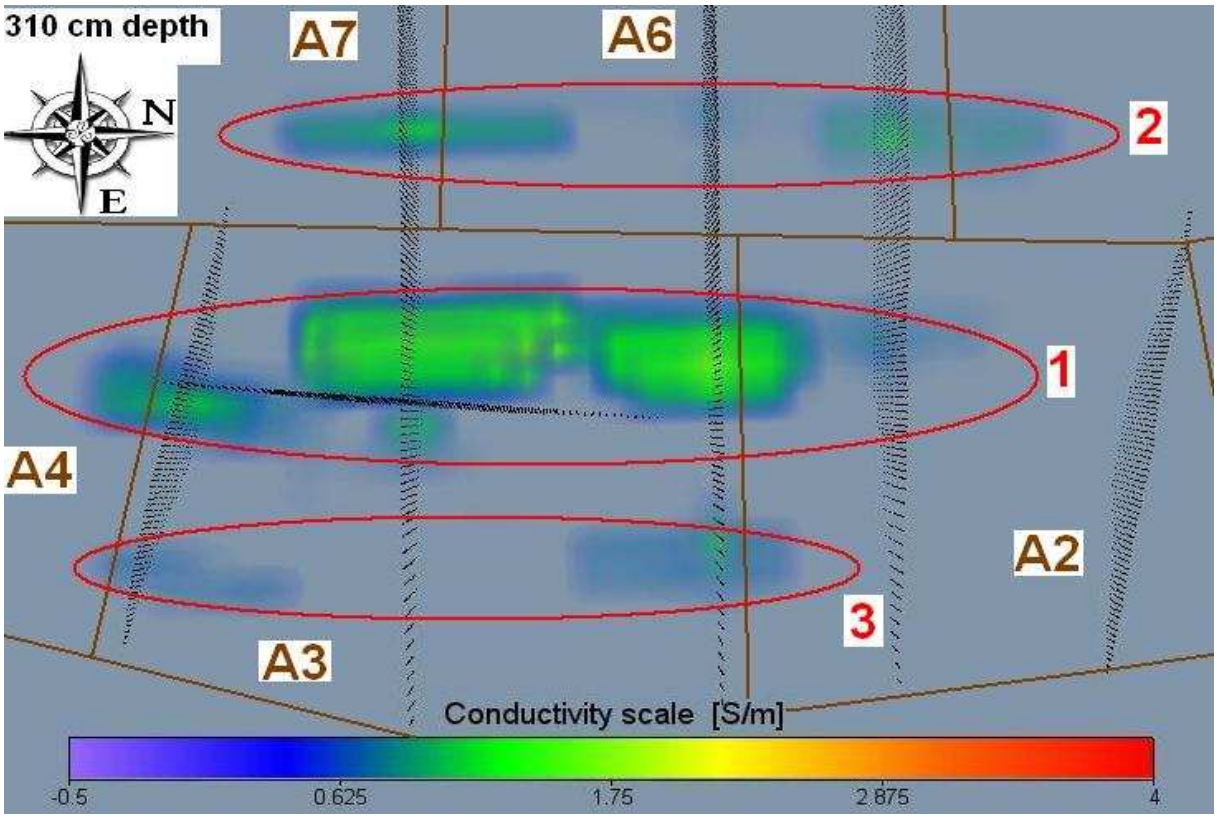

Fig. 64 3D Conductivity distribution at the depth 310 cm. The borders of areas were marked with brown lines. Regions with elevated conductivity were circled with red polygons.

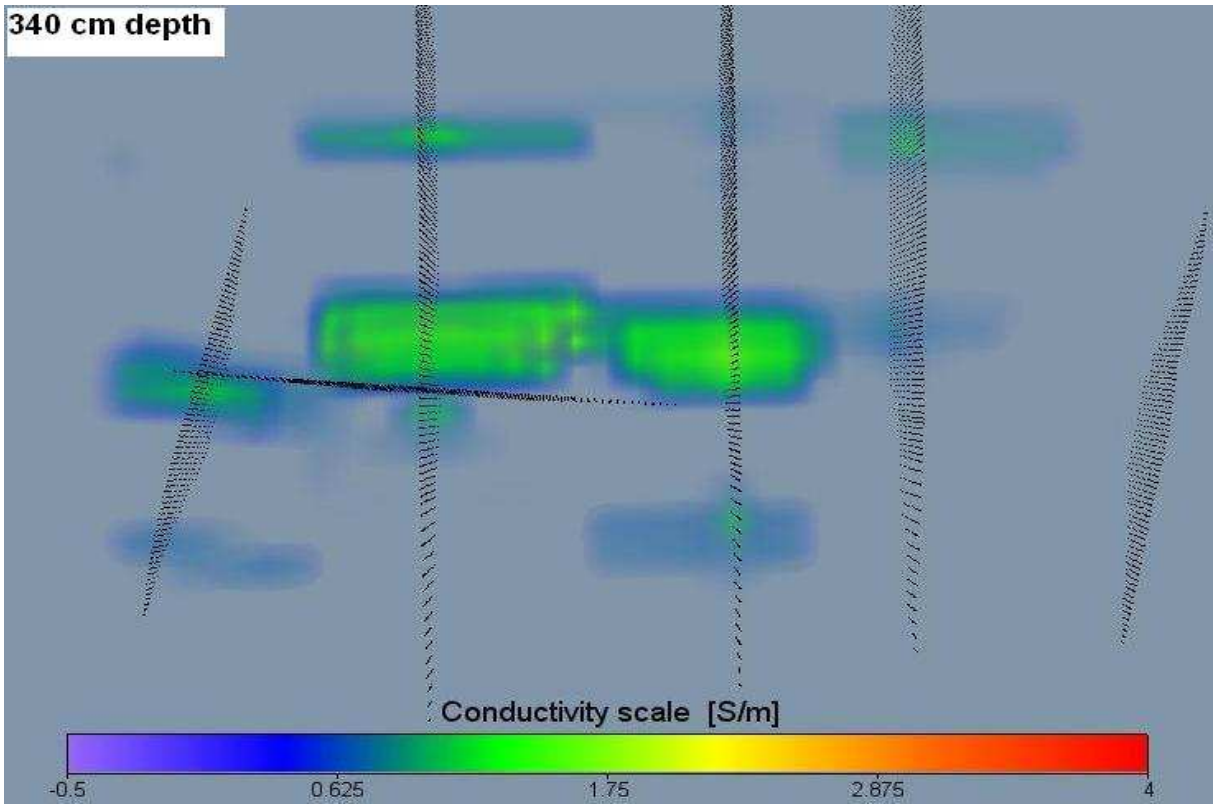

Fig. 65 Conductivity distribution at the depth 340 cm.

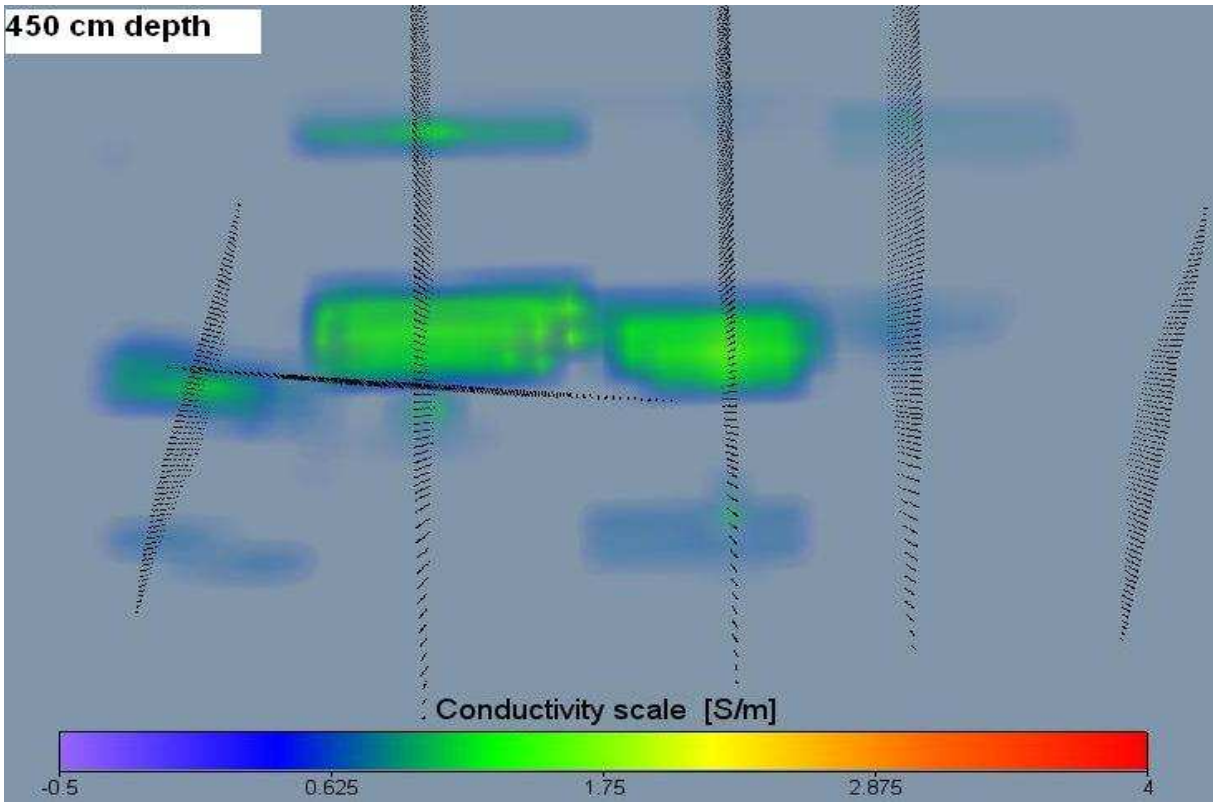

Fig. 66 Conductivity distribution at the depth 450 cm.

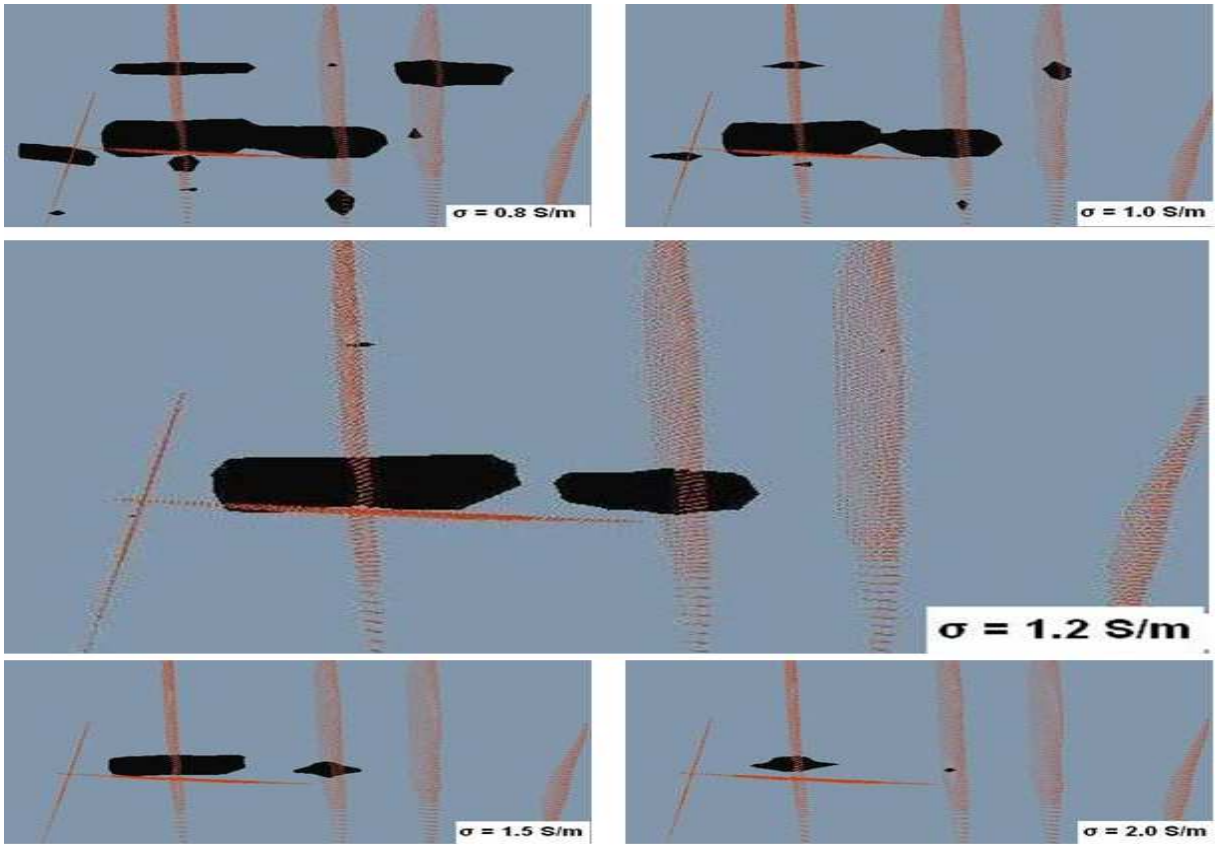

Fig. 67 Isosurfaces for 0.8, 1.0, 1.2, 1.5 and 2.0 [S/m] conductivity at the slope surface.

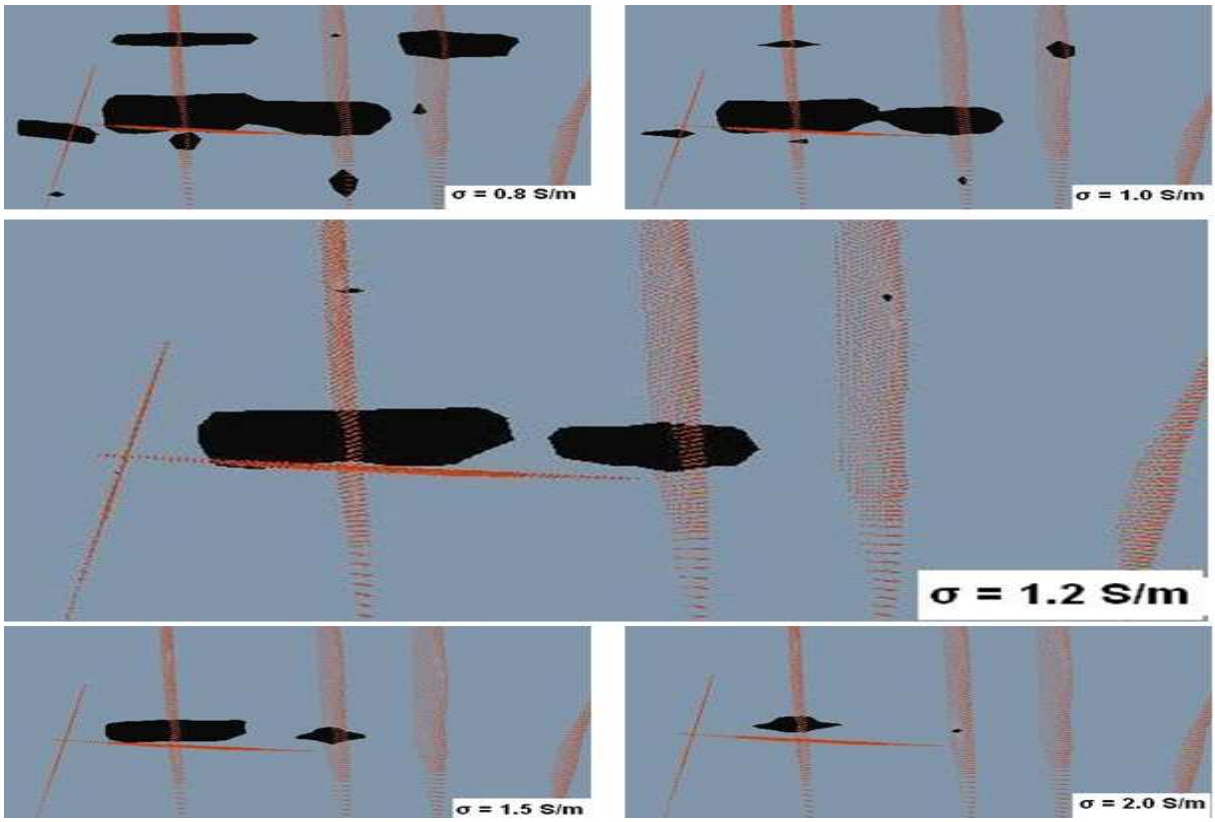

Fig. 68 Isosurfaces for 0.8, 1.0, 1.2, 1.5 and 2.0 [S/m] conductivity at the depth 30cm.

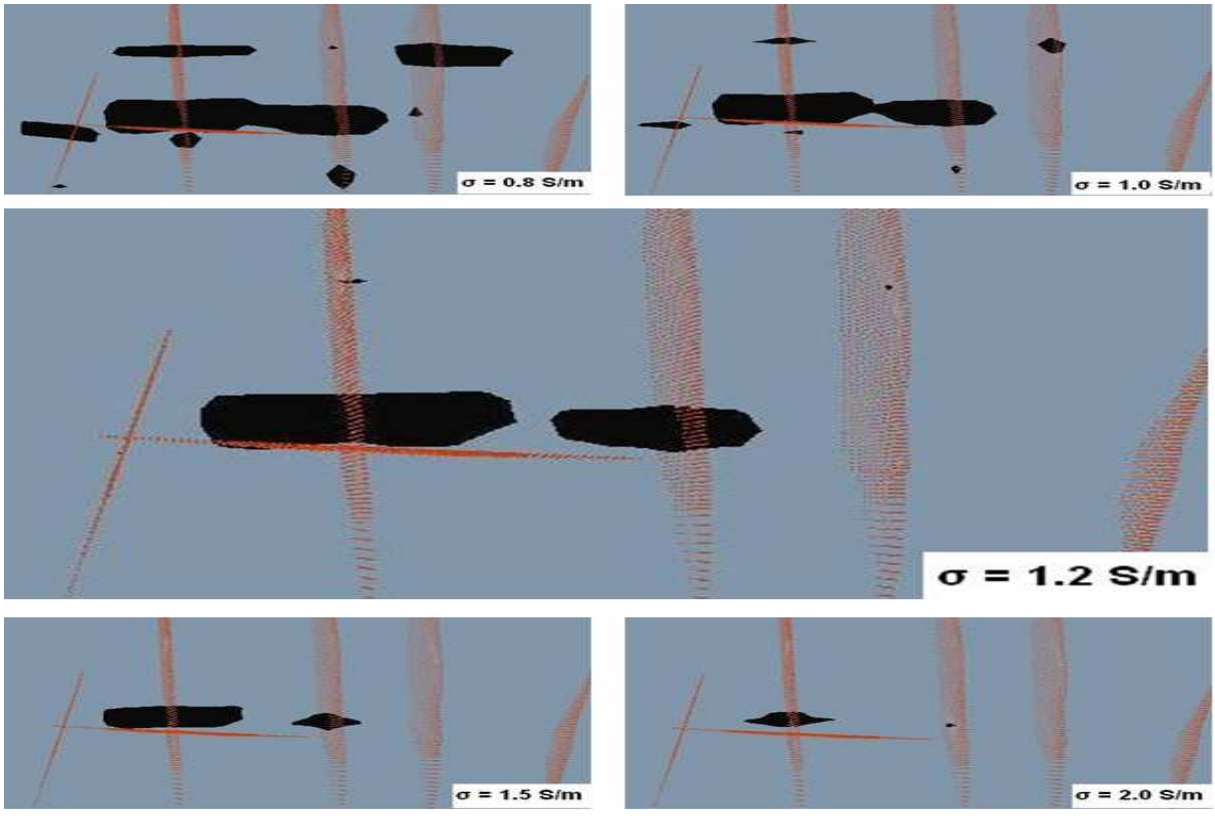

Fig. 69 Isosurfaces for 0.8, 1.0, 1.2, 1.5 and 2.0 [S/m] conductivity at the depth 180 cm.

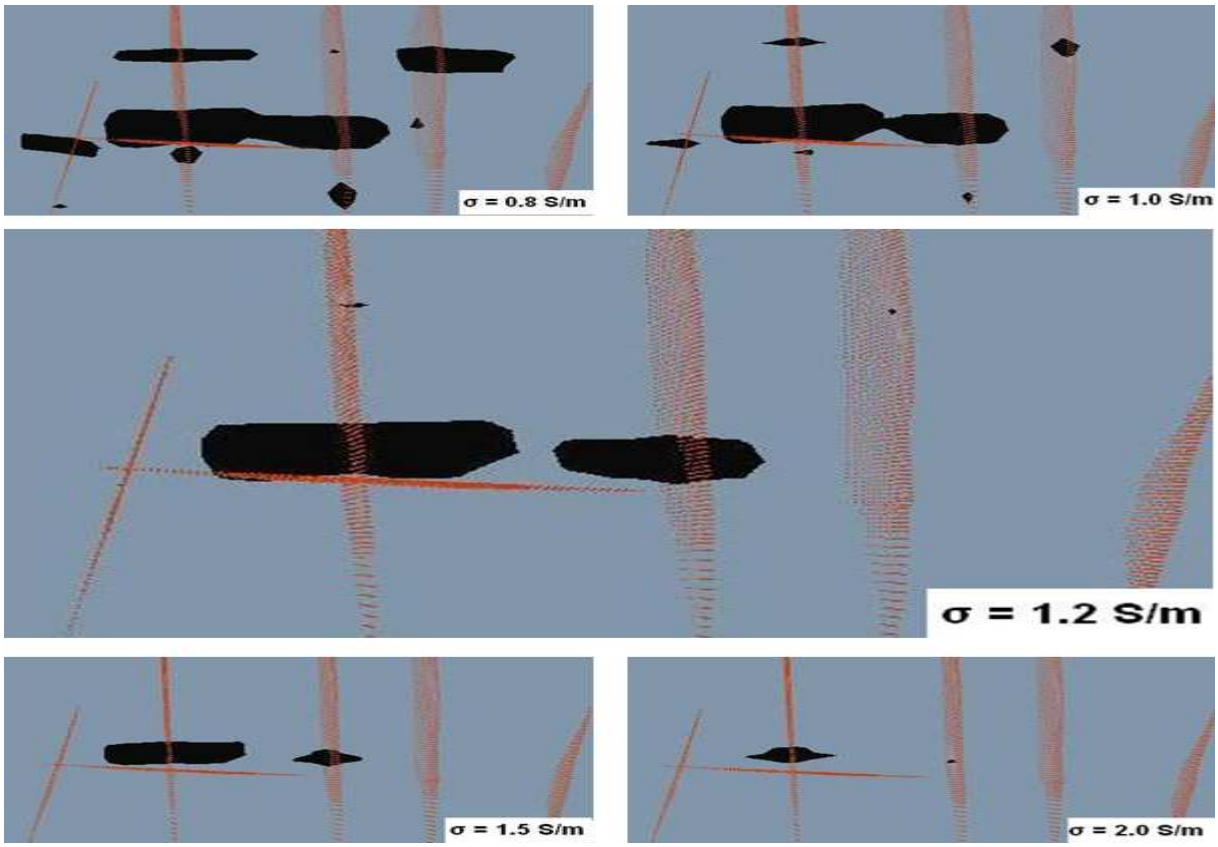

Fig. 70 Isosurfaces for 0.8, 1.0, 1.2, 1.5 and 2.0 [S/m] conductivity at the depth 210 cm.

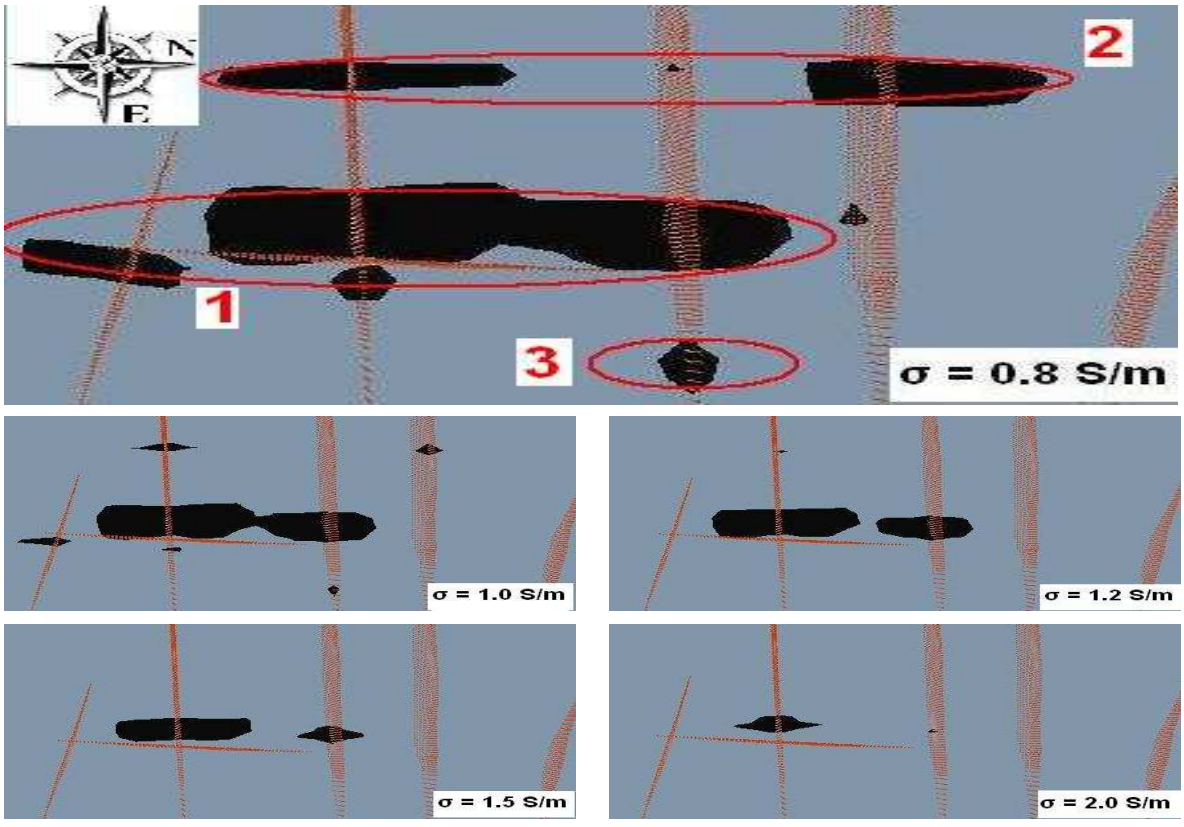

Fig. 71 Isosurfaces for 0.8, 1.0, 1.2, 1.5 and 2.0 [S/m] conductivity at the depth 310 cm.

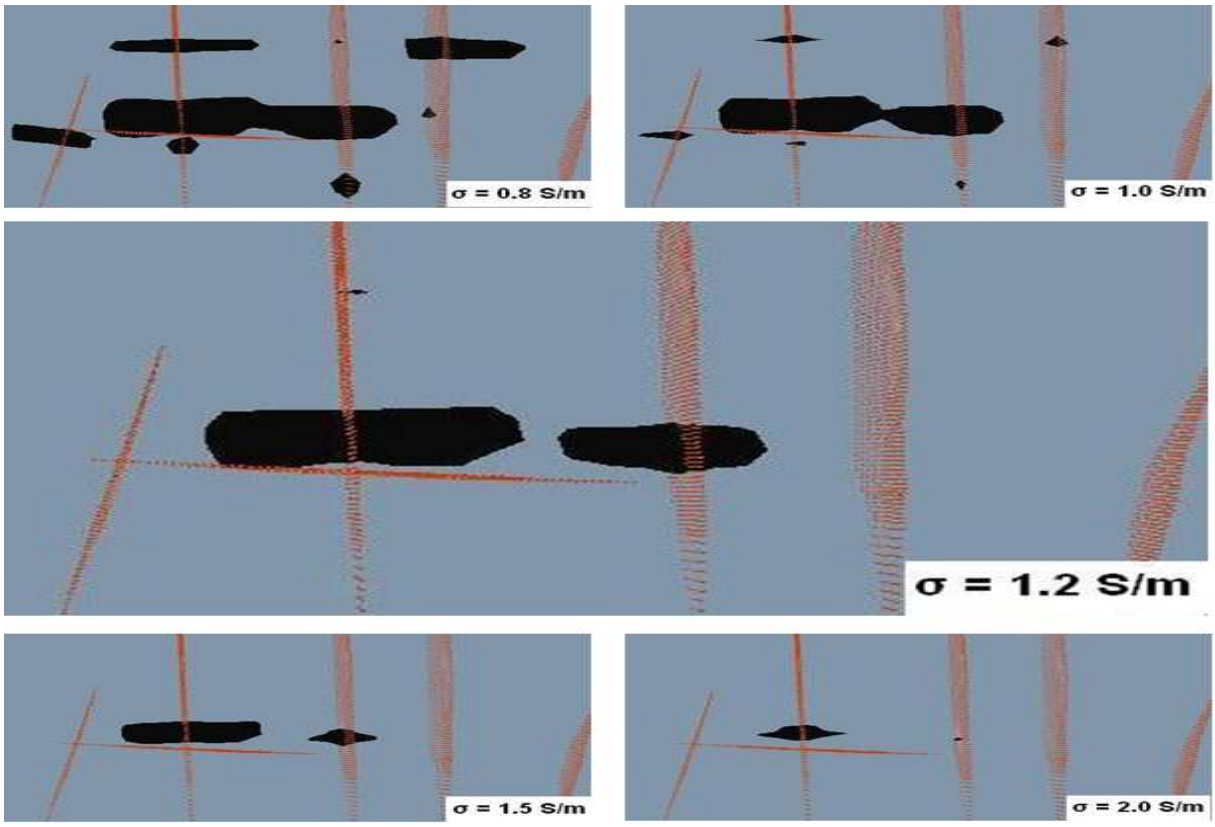

Fig. 72 Isosurfaces for 0.8, 1.0, 1.2, 1.5 and 2.0 [S/m] conductivity at the depth 340 cm.

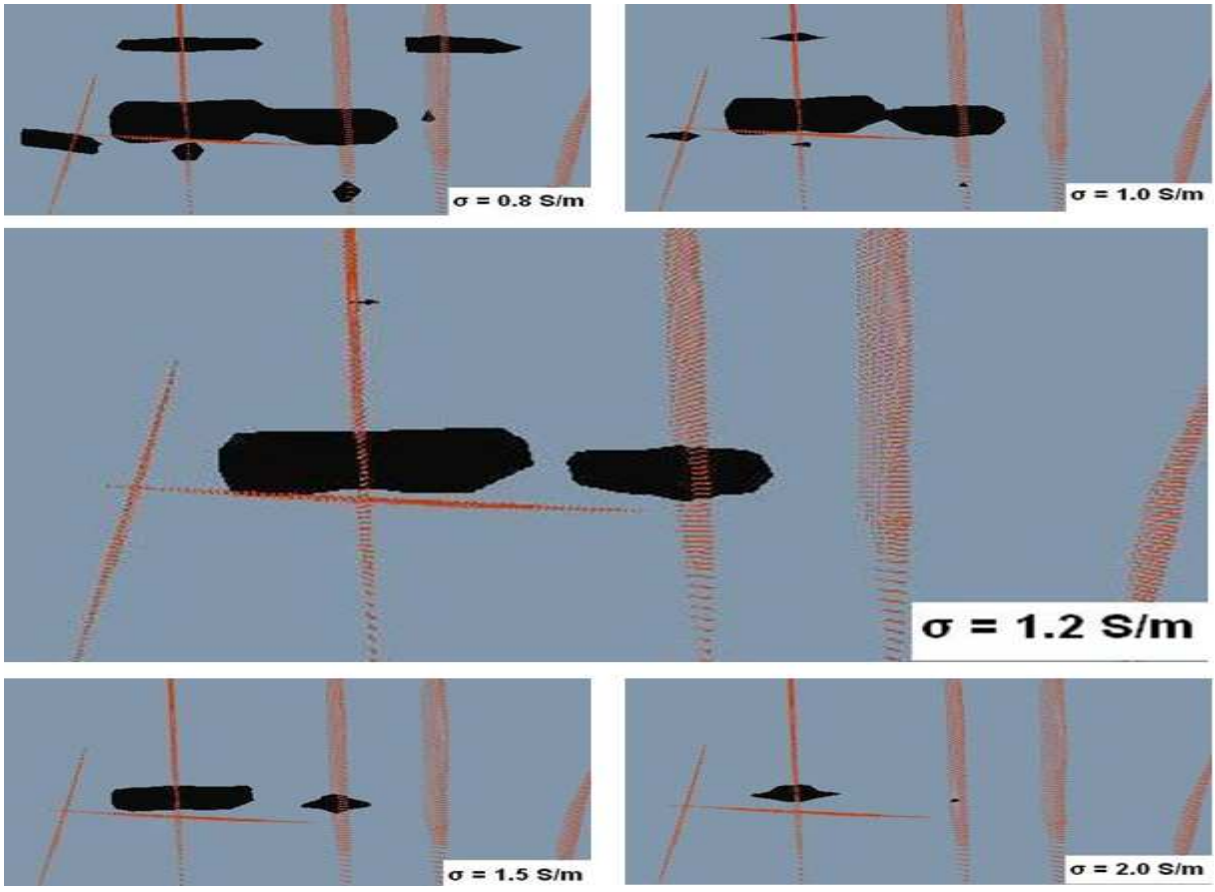

Fig. 73 Isosurfaces for 0.8, 1.0, 1.2, 1.5 and 2.0 [S/m] conductivity at the depth 450 cm.

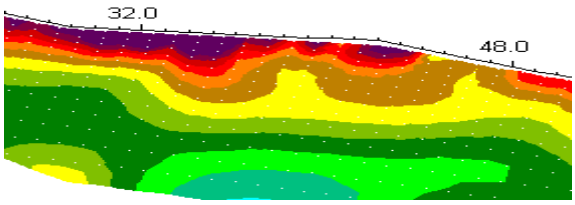

Fig. 74 Zoomed fraction of profile 5 resistivity inversed model. Example of vertical stratification of resistivity.

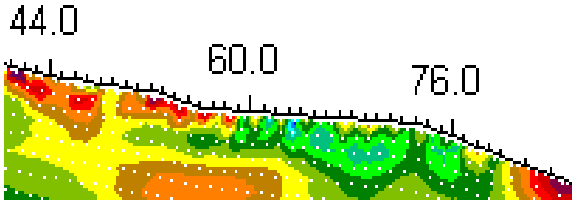

Fig. 75 Zoomed fraction of profile 6 resistivity pseudo-section. Example of increased conductivity at shelf.

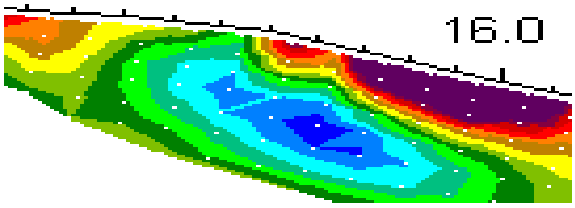

Fig. 76 Zoomed fraction of profile 4 resistivity pseudo-section. Example of increased conductivity at node.

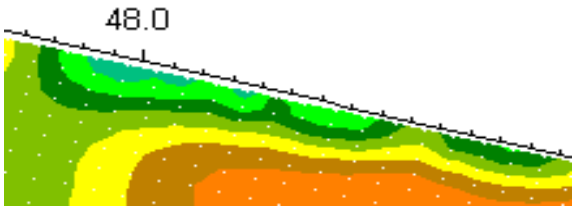

Fig. 77 Zoomed fraction of profile 3 resistivity pseudo-section. Example of increased conductivity above protection layer.

Shallow penetration and high attenuation could be interpreted that lining material had a high salinity and the contrast at interfaces between sublayers was not always strong enough to give clear reflection.

Filtering in RAMAC GroundVision did not significantly improve quality of displayed information. Example of visible structures in the radargram was between 70 m and 76 m in profile 5 surveyed with 250 MHz antenna when the radar passed a small road (Fig. 48).

No information about subsurface down to a depth of 5 m would be recorded if antennas with lower frequencies (50 MHz or 25 MHz) were used. Coverage was approximately 4.5 m thick so there was no point in making additional surveys with 50 MHz or 25 MHz antennas.

The GPR survey was supposed to provide reference data for the geoelectrical measurements. Due to the highly attenuated radar waves GPR data interpretation became more ambiguous.

4.5 Coordinates collection, processing and presentation in 3D model

GPS equipment had an accuracy 25 m or better. Such a low precision could lead to errors in the topography processing. Altitude values were less precise than longitude and latitude coordinates displayed by GPS, thus elevation data were taken manually from landfill topographic maps (Fig. 26). This method was inaccurate with a large probability of human error

The sky was moderately transparent during measurements. Such atmospheric conditions could additionally reduce the GPS precision.

The profile of eastern slope could be slightly modified due to mass transfer downwards. That could have influence on the precision of the topographic map.

Inverse distance weighting was the interpolation method applied in Voxler. Topographic values in the 3D model, same as in DC resistivity processing, have been interpolated from 2D profiles so the model only represents true values along the profiles.

The interpolated model did not ideally represent the eastern slope. However, accuracy of the slope steepness was not the main issue of concern. Topographic values were added to improve the outlook of the maps and models. The output images were more realistic than a strict box model would be.

4.6 DC resistivity — 3D model - masking of area with resistivity below 6.3 Ωm

The size of area with resistivity higher or equal to 6.3 Ωm has been gradually reduced with depth. The increase of blanked areas down trough the coverage was significant when the elevation difference between compared figures exceeded 1 m. For example between the depth 180 cm (Fig. 55) and the depth 310 cm (Fig. 57). The difference between surface (Fig. 53) and depth 30 cm (Fig. 54) or between depth 180 cm (Fig. 55) and depth 210 cm (Fig. 56) was not that relevant.

Table 6 Thickness and function of the constructed layers (Tham et al, 2006; Tham & Andreas, 2008).

Layer:	Thickness:	Name :	Function:
1	≥ 30 cm	Vegetation	Water storage, Erosion control
2	≥ 150 cm	Protection	Water storage, Protection of underlay layers from: frost, desiccation, animal and plant penetration
3	≥ 30 cm	Drainage	Collection and transportation of infiltrated water, Lateral water transport in the protective layer under unsaturated conditions Protect impermeable layer from dehydration by capillary-breaking effect (thickness>capillarity)
4	≥ 100 cm	Impermeable	Protection against gas and water transport
5	≥ 30 cm	Foundation	Smoothing, Gas collection, Capillary-breaking the water from the waste
6		Waste	

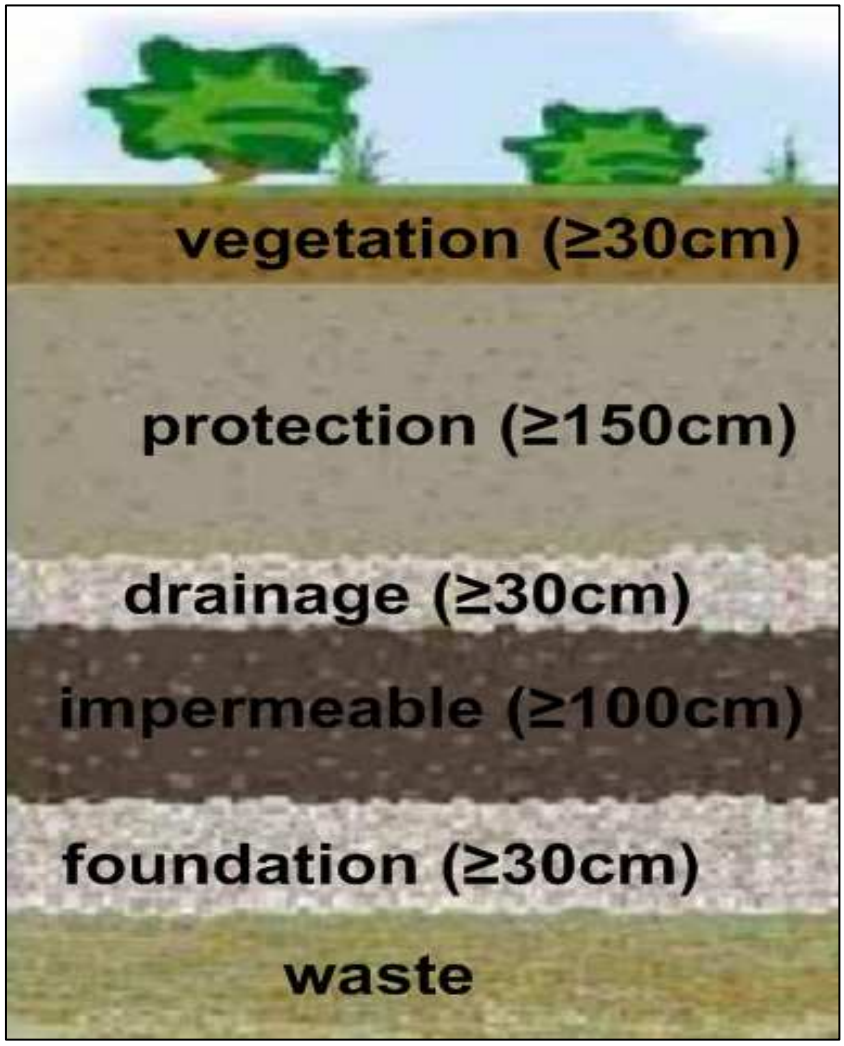

Fig. 78 Cross section of coverage layers (modified after Tham & Andreas, 2008).

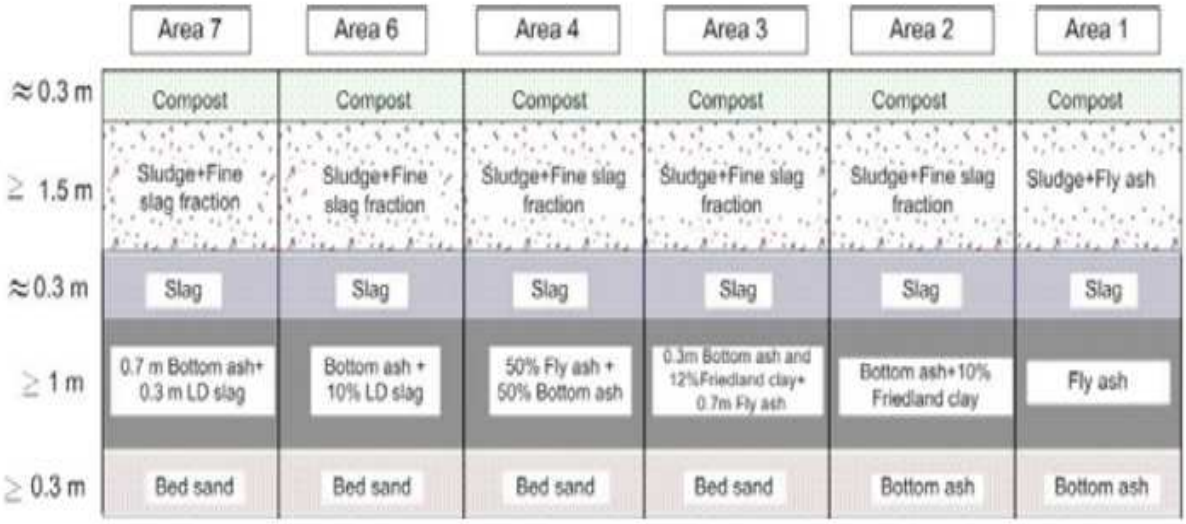

Fig. 79 Composition of layers forming cover lining (Travar et al, 2005; Tham & Andreas, 2008).

4.7 Conductivity distribution — 3D model

Conductivity distribution was displayed at the same depths as resistivity distribution. Selected depths corresponded to interfaces of lining sublayers. The size and shape of zones with elevated conductivity was almost constant throughout the coverage, vertical fluctuations could be neglected.

The highly conductive zones could be divided into three parallel regions, stretched in the north-south direction, which were circled with red polygons (Fig. 60 and 64).

Region with the highest conductivity, circled with red polygon 1 (Fig. 64), was stretched along the shelf and foot of the upper slope, parallel to profile 8. High conductivity at the region 1 was due to accumulation of run-off from upper slope and precipitation at the plain area. Water infiltration was high as a consequence of flat surface.

The second most intensive region was at the foot of area 6 and area 7, circled with the red polygon 2 (Fig 64). Elevated conductivity could be a consequence of run-off and drain water accumulation at the Eastern border of area 6 and area 7.

It is interesting that region 1 and region 2 were separated by a stripe which corresponded to the road. The slag, which had good insulating properties, was used as a base material for the constructed road. Perhaps the road acted like a barrier for the water movement downwards.

The third region, circled with the red polygon 3, was located at the shelf-lower slope interface (Fig 64). The region consisted of two spots which were located at the borders of area 3. Conductivity anomalies at the region 3 were not strong because most of the run-off was flowing along the slope. Anomalies could be due to mass transport downwards, especially in the vicinity of shelf-lower slope interface. Water could infiltrate the coverage through cracks formed by such a mass transport The conductivity spots were located at the borders between areas, perhaps because lining at the borders was not as homogeneous and consistent.

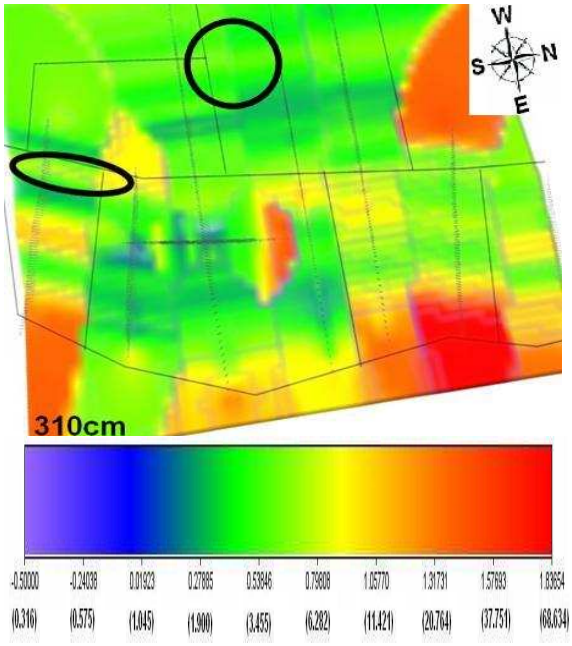

Fig. 80 3D model of resistivity distribution at 310 cm. Location of lysimeters at area 4 and area 6 is circled with black polygon.

4.8 Conductivity isosurfaces — 3D model

The coverage of black spots at isosurface with conductivity higher or equal 0.8 Siemens/m (Fig. 71) was very similar to the coverage of high conductivity zones (Fig. 64). Thus, conductivity distribution figures and conductivity isosurfaces could be interpreted in a similar way.

As for the conductivity distribution (Fig. 60 — 66), vertical fluctuations of isosurfaces were very small (Fig. 67 — 73). The thickness and heterogeneity of cover could be insufficient for relevant vertical fluctuations.

Analogically to conductivity distribution in chapter 3.7 "Conductivity distribution – 3D model" three regions could be identified from isosurface higher of equal 0.8 Siemens/m (Fig. 71), but only region 1, along profile 8, had conductivity exceeding 1.2 Siemens/m (Fig. 71). The spots were stretched in north-south direction, perpendicular to the run-off direction.

5. CONCLUSIONS

- Geoelectrical measurements, especially figures displaying conductivity distribution (Fig. 64), confirmed increased lysimeter readings from 2008 at the area 3. However, according to results from the 3D model, lysimeter values at area 6 and area 4 were surprisingly low. Perhaps the random array of lysimeters did not cover spots with increased conductivity (Fig. 80).
- Potential zones with increased infiltration, which were marked with a blue colour on the 3D resistivity model (Fig. 36) and green-yellowish colour on 3D conductivity distribution (Fig. 64), have been detected. Spots with increased infiltration were located mainly at the area 3 and also at the bottom of area 6 and 7. Conductivity exceeding 1.2 Siemens/meter was present only at the shelf of area 3 (Fig. 64). The maximum recorded conductivity was approximately 2 S/m.
- Prototypes constructed at the eastern slope had generally sufficient structure as a cover barrier, except flat shelf at the area 3.
- Suggested improvements for constructed prototypes were:

Increased thickness of the impermeable layer, which could further reduce conductivity at the bottom of this layer.

Modification of the slope profile and increased slope smoothness, especially at the slope-shelf interfaces. Such improvement could lead to reduced mass transfer downwards. The risk of lining damaging would decrease.

The coverage composition could be improved to enhance lining resistance for cracking

- PR and IP measurements could not act as reference methods for the DC resistivity survey. Additional DC measurements were recommended, especially at the blue-coloured zones at the area 3, 4 and bottom of area 6 and 7.

6. REFERENCES

ABEM Instrument AB, (2009) Instruction Manual, ABEM Terrameter SAS 4000/SAS 1000. ABEM Instrument AB, Sundyberg. 148 p.

Abu-Zeid, N., Bianchini, G., Santarato, G., Vaccaro, C., (2004) Geochemical characterisation and geophysical mapping of Landfill leachates: the Marozzo canal case study (NE Italy). Environmental Geology, 45 (4): 439-447.

Ahmed, A.M. & Sulaiman, W.N., (2001) Evaluation of Groundwater and Soil Pollution in a Landfill Area Using Electrical Resistivity Imaging Survey. Environmental Management, 28 (5): 655–663.

Al-Tarazi, E., El-Naqa, A., El-Waheidi, M., Abu Rajab, J., (2006) Electrical geophysical and hydrogeological investigations of groundwater aquifers in Ruseifa municipal landfill, Jordan. Environmental Geology, 50 (7): 1095-1103.

Angoran, Y.E., Fitterman, D.V. & Marshall, D.J., (1974) Induced Polarization: A Geophysical Method for Locating Cultural Metallic Refuse. Science Magazine, 184 (4143): 1287-1288.

Aristodemou, E. & Thomas-Betts, A., (2000) DC resistivity and induced polarisation investigations at a waste disposal site and its environments. Journal of Applied Geophysics, 44 (2-3): 275-302.

Britsow, C.S. & Jol, H.M., (2003) Ground penetrating radar in sediments. Geological Society, London. 330 p.

Carpenter, P.J., Calkin, S.F. & Kaufmann, R.S., (1991) Assessing a fractured landfill cover using electrical resistivity and seismic refraction techniques. Geophysics, 56 (11): 1896-1904.

Chapel, P.A., (1992) Handbook of Exploration Geophysics. Taylor & Francis. 411 p.

Daniels, D.J., (2004) Ground Penetrating Radar, Second edition. Institution of Engineering and Technology. 726 p.

Djadia, L., Machane, D., Chatelain, J.L., Abtout, A., Bentalem, R., Guemache, M.A., Guillier, B., Boudella, A., Oubaiche, E.H., (2010) Evidence for an underground runoff and soil permeability at the Ouled Fayet (Algiers, Algeria) subsurface landfill pilot project from geophysical investigations. Environmental Earth Sciences, 59 (5): 1149-1158.

Frid, V., Liskevich, G., Doudkinski, D., Korostishevsky, N., (2008) Evaluation of landfill disposal boundary by means of electrical resistivity imaging. Environmental Geology, 53 (7): 1503-1508.

Henry, G., (1997) Geophysics for Sedimentary Basins. Editions Technip, Paris. 445 p.

Hermozilha, H., Grangeia, C. & Senos Matias, M., (2010) An integrated 3D constant offset GPR and resistivity survey on a sealed landfill - Ilhavo, NW Portugal. Journal of Applied Geophysics, 70 (1): 58-71.

Jernberg, H. & Rosenqvist, A., (2002) Geophysical investigations at Tweta waste site. TRITA LWR Degree Project 02-11, 72 p.

Kearey, P., Brooks, M. & Hill, I., (2002) An introduction to geophysical exploration. Wiley-Blackwell. 262 p.

Leroux, V., Dahlin, T. & Svensson, M., (2007) Dense resistivity and induced polarization profiling for a landfill restoration project at Härlöv, Southern Sweden. Waste Management and Research, 25 (1): 49-60.

Ljungberg, V. & Rodriguez, A., (2006) Geophysical surveying at Tveta recycling plant: flow paths and leachate delineation. TRITA LWR Degree Project 06-15, 59 p.

Majumdar, R.K. & Rao, S. H, (1973) Some studies on induced polarization. Pure and Applied Geophysics, 109 (1): 1789-1795.

Martinho, E. & Almeida, F., (2006) 3D behavior of contamination in landfill sites using 2D resistivity/IP imaging: case studies in Portugal. Environmental Geology, 49 (7): 1071-1078.

Meads, L.N., Bentley, L.R. & Mendoza, C.A., (2003) Application of electrical resistivity imaging to the development of a geologic model for a proposed Edmonton landfill site. Canadian Geotechnical Journal, 40 (3): 551–558.

Meju, M.A., (2000) Geoelectrical investigation of old/abandoned, covered landfill sites in urban areas: model development with a genetic diagnosis approach. Journal of Applied Geophysics, 44 (2-3): 115-150.

Milsom J., (2003) Field Geophysics, Third edition. John Wiley & Sons Ltd, Chichester, England. 232 p.

Mondelli, G., Giacheti, H.L., Boscov, M.E., Elis, V.R., Hamada, J., (2007) Geoenvironmental site investigation using different techniques in a municipal solid waste disposal site in Brazil. Environmental Geology, 52 (5): 871-887.

Morey, M.R., (1998) Ground Penetrating Radar for Evaluating Subsurface Conditions for Transportation Facilities. National Academy Press, Washington D.C. 37 p.

Mota, R., Monteiro Santos, F.A., Mateus, A., Marques, F.O., Gonçalves, M.A., Figueiras, J., Amaral, H., (2004) Granite fracturing and incipient pollution beneath a recent landfill facility as detected by geoelectrical surveys. Journal of Applied Geophysics, 57 (1): 11-22.

Mussett, E.A., Aftab Khan, M. & Button, S., (2000) Looking into the earth: an introduction to geological geophysics. Cambridge University Press. 470 p.

Parasnis, D.S., (1997) Principles of Applied Geophysics, Fifth edition. Chapman and Hall Ltd. 429 p.

Parasnis, D.S., (1986) Principles of Applied Geophysics, Fourth edition. Chapman and Hall Ltd. 402 p.

Porsani, J.L., Filho, W.M., Elis, V.R., Shimeles, F., Dourado, J.C., Moura, H.P., (2004) The use of GPR and VES in delineating a contamination plume in a landfill site: a case study in SE Brazil. Journal of Applied Geophysics, 55 (3-4): 199-209.

Pujari, P.R., Pardhi, P., Muduli, P., Harkare, P., Nanoti, M.V., (2007) Assessment of Pollution Near Landfill Site in Nagpur, India by Resistivity Imaging and GPR. Environmental Monitoring and Assessment, 131 (1-3): 489-500.

Reyes-López, J.A., Ramírez-Hernández, J., Lázaro-Mancilla, O., Carreón-Diazconti, C., Garrido, M.M., (2008) Assessment of groundwater contamination by landfill leachate: a case in México. Waste Management, 28 (1): S33-S39.

Robinson, E.S. & Coruh, C., (1988) Basic Exploration Geophysics. John Wiley & Sons Ltd, New York, USA. 562 p.

Sjogren, E., (2004) Environmental Application of IP and DC resistivity Measurements - A comparative study. TRITA LWR Degree Project 04-4, 58 p.

Soupios, P., Papadopoulos, I., Kouli, M., Georgaki, I., Vallianatos, F., Kokkinou, E., (2007) Investigation of waste disposal areas using electrical methods: a case study from Chania, Crete, Greece. Environmental Geology, 51 (7): 1249-1261.

Sumner, J.S., (1976) Principles of induced polarization for geophysical exploration. Elsevier Scientific Publishing. 277 p.

Telford, W.M., Geldart, L.P. & Sheriff, R.E., (1990) Applied Geophysics, Second Edition, Cambridge University Press. 770 p.

Tham, G. & Andreas, L., (2008) Evaluation of full-scale use of ash and other residues in the final coverage of Tveta Recovery. Avfall Sverige Utveckling, Malmö. 84 p.

Tham, G., Andreas, L. & Lagerkvist, A., (2003) Use of ashes in landfill covers. Ninth International Waste Management and Landfill Symposium, Sardinia. CISA, Environmental Sanitary Engineering Centre. 7 p.

Travar, I., Tham, G., Andreas, L., Lagerkvist, A., Lidelöw, S., (2009) Assessing the environmental impact of ashes used in a landfill cover construction. Waste Management 29 (4): 1336-1346.

Travar, I., Tham, G., Andreas, L., Lagerkvist, A., (2007) Environmental impact of ashes used in a landfill cover construction, Eleventh International Waste Management and Landfill Symposium, Sardinia. CISA, Environmental Sanitary Engineering Centre. 9 p.

Travar, I., Andreas, L., Tham, G., Lagerkvist, A., (2005) Field test of landfill covers with secondary construction materials, Tenth International Waste Management and Landfill Symposium, Sardinia. CISA, Environmental Sanitary Engineering Centre. 9 p.

Other references:

Telge AB own sources – received in April 2009 from Igor Travar, employed at Telge Återvinning AB.

APPENDIX I — CONSTRUCTION AND OPERATION OF THE COVERAGE

Prototypes of covering layers have been constructed at the eastern slope of Tveta landfill (Appendix fig. 1). Design and parameters of the testing areas were consulted with Environmental Protection Agency (Fig. 79, 80 and Table 6).

The essential difference between designed prototypes was in the composition of impermeable layer (Fig. 80). Content of vegetation and drain layer were the same in all prototypes while protection and foundation layers differed only in one and two cases respectively (Fig. 79). Economically feasible layers consisted of waste material such as compost, ash or sludge. Coverage became more expensive as the content of clay, sand or bentonite increased.

The eastern slope has been divided into seven parts (Appendix fig. 2). Testing areas 1, 2, 3, 4 consisted of two slopes and a shelf between them (Appendix fig. 3). The upper slope was steeper with gradient (1:3). It was constructed to test critical conditions in geotechnical stability. Conditions with minimum run-off and maximum infiltration were created at the plain area. The shelf has been constructed to test critical hydraulic conditions. Lower slope had a moderate gradient (1:8) which corresponded to standard conditions. Prototypes 6 and 7 were profiled with a very small gradient. Area 5 was constructed with the same materials as area 4 but there has not been installed any measuring devices so area 5 was not included in this thesis.

Water balance measurements were taken to verify if coverage worked properly. Precipitation, amount of water collected above and below impermeable layer were examples of measured parameters. Water balance was based on 600 mm annual precipitation (Appendix fig. 4). The magnitude of water absorbed by the coverage was at least 114 mm.

Water, percolated through the protection layer, was collected along drainage layer and passed into the upper wells (Appendix fig. 5) which acted as catchments of the drainage area. Drainage has been subsequently passed through pipes into the lower wells (Appendix fig. 5). Flow meters were installed at the end of the pipes to measure minimum value of drainage infiltrated through the upper slope and shelf. Areas 1, 2, 3, 4 had own measuring wells while areas 6 and 7 were connected to the same well. Water collected in the lower wells was subsequently treated in the aerated lagoon.

Infiltration rate through the impermeable layer has been measured by lysimeters. Every area contained ten, randomly installed lysimeters at the field of 100 m^2 (Appendix fig. 6, 7, 8). The annual leachate limit was 50 dm^3/m^2 for non-hazardous waste and 5 dm^3/m^2 for hazardous waste. This regulation concerned bottom of the lining, not each particular layer. All of the testing areas had annual leachate well below 50 dm^3/m^2, ranging from 1 dm^3/m^2 to less than 30 dm^3/m^2 (Appendix fig. 9) (Tham & Andreas, 2008).

Appendix fig. 1 Plane view on Tveta landfill. The studied area was marked with red polygon (modified after Tham & Andreas, 2008).

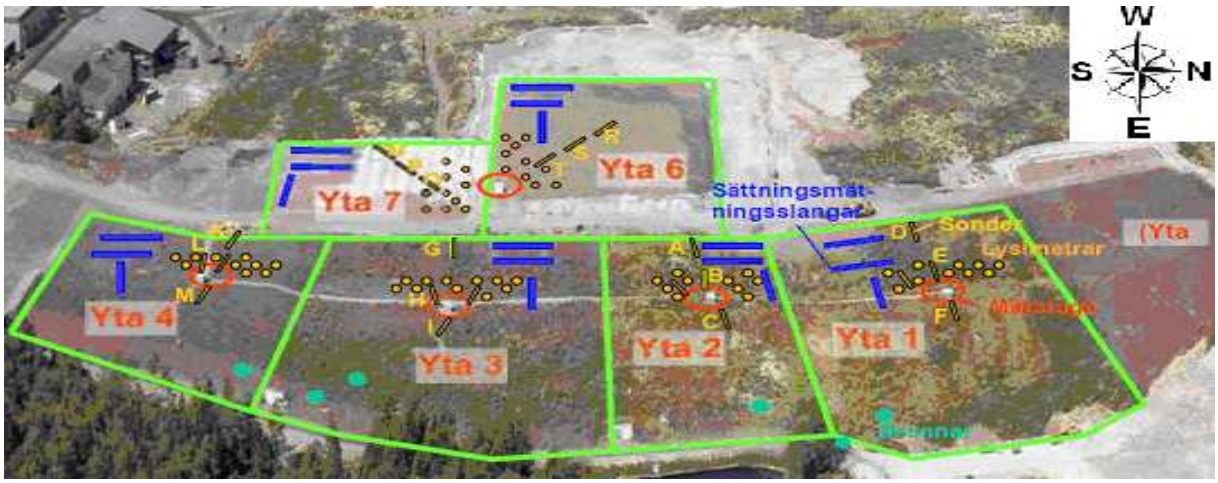

Appendix fig. 2 Division of the east slope into 7 study areas (Tham & Andreas, 2008).

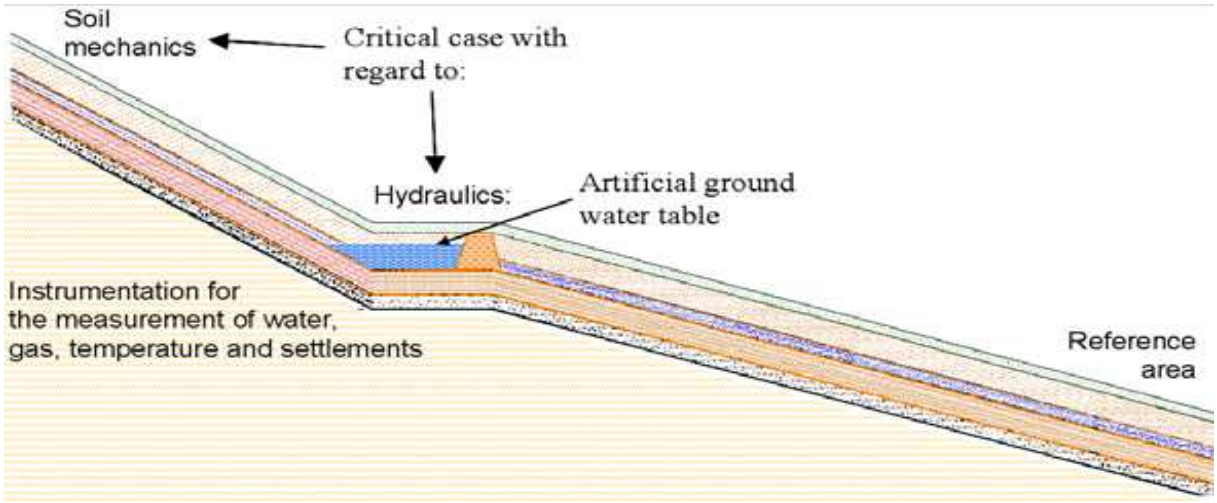

Appendix fig. 3 Cross section of the areas 1, 2, 3, 4 (Tham et al, 2003).

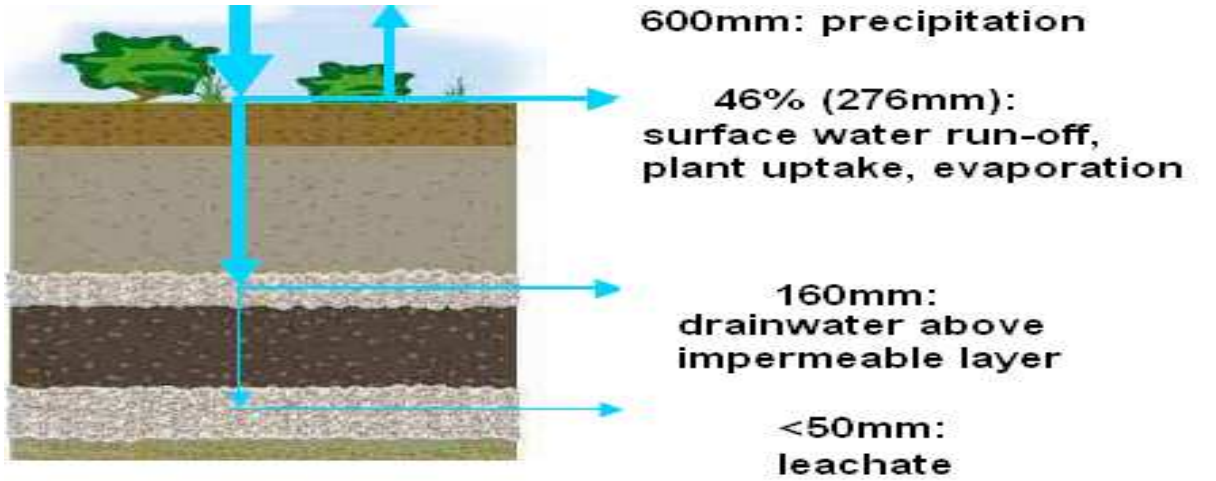

Appendix fig. 4 Water balance based on 600 mm annual precipitation (modified after Tham & Andreas, 2008).

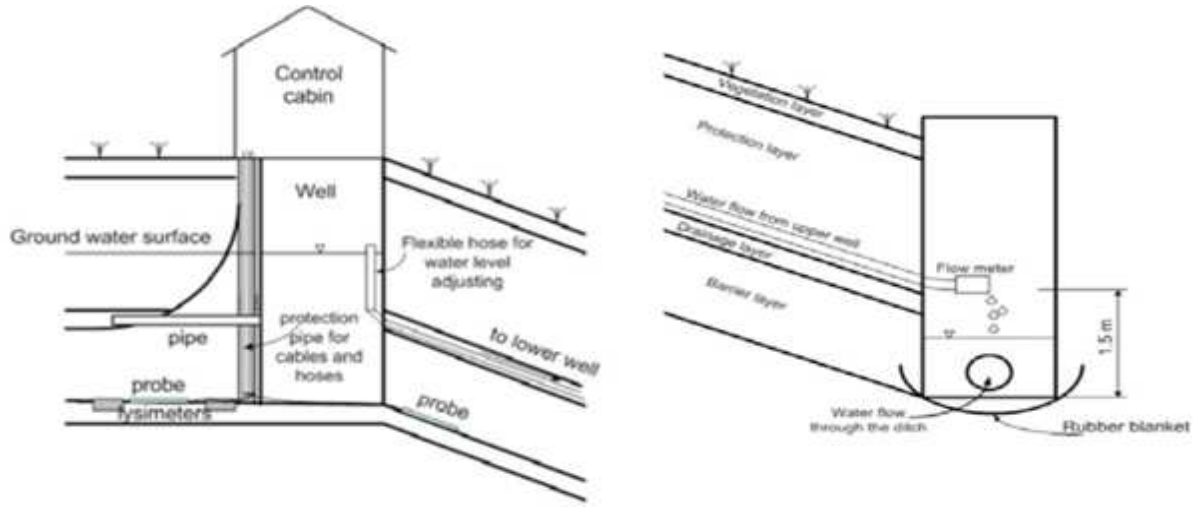

Appendix fig. 5 Cross section of upper (left) and lower (right) well (Travar et al, 2005).

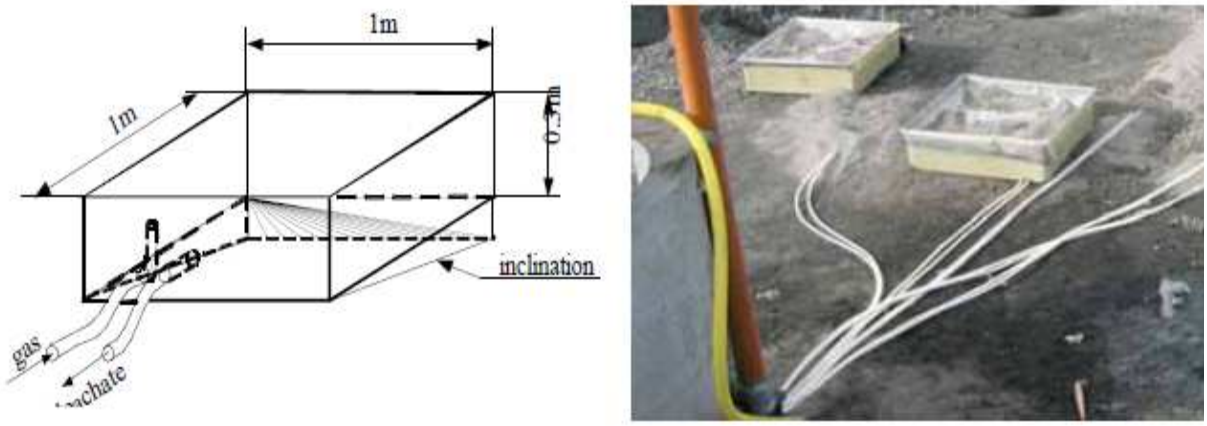

Appendix fig. 6 Lysimeters collecting leachate, placed on the bottom of the impermeable layer (Travar et al, 2005; Tham & Andreas, 2008).

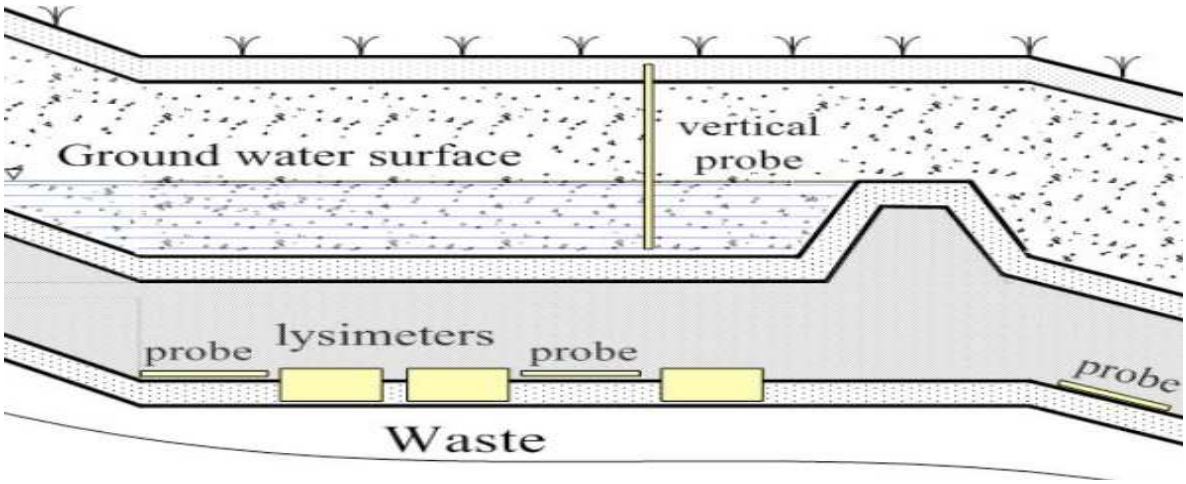

Appendix fig. 7 Cross section of the plain area with installed lysimeters (Travar et al, 2007; Travar et al, 2009).

Appendix fig. 8 Installation of lysimeters (Tham & Andreas, 2008).

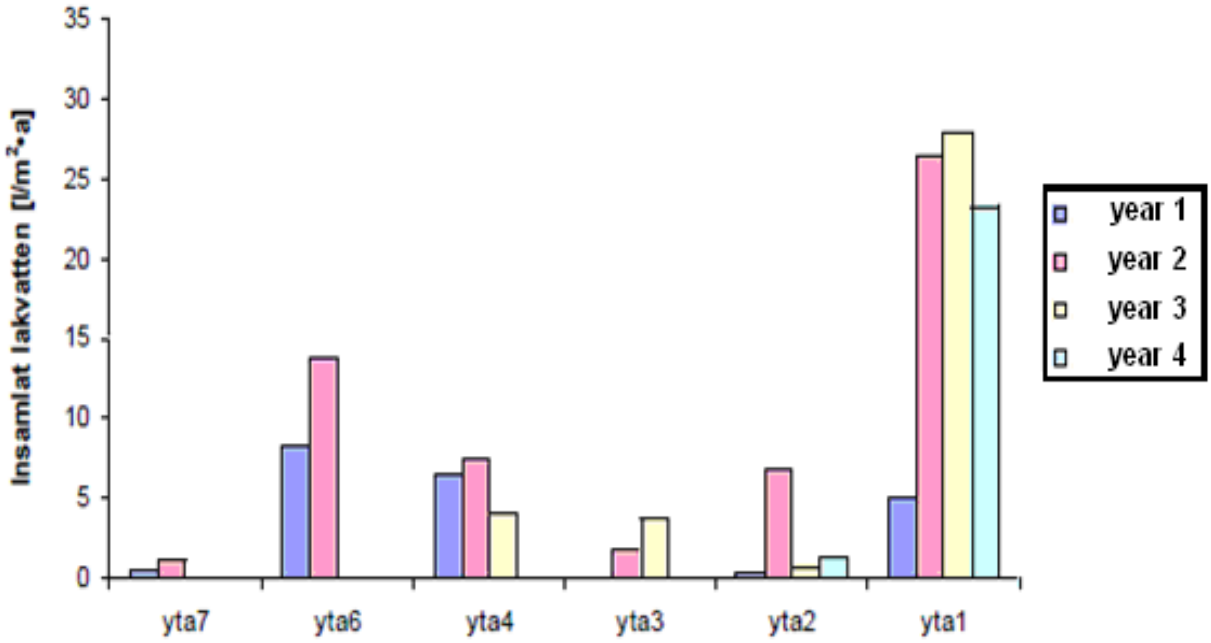

Appendix fig. 9 Water permeability through the test areas during first years after construction [L/m²*year] (Tham & Andreas, 2008).